AEDC-TR-73-162
AFATL-TR-73-188

cy. 2

EXPERIMENTAL MAGNUS CHARACTERISTICS OF BALLISTIC PROJECTILES WITH AND WITHOUT ANTI-MAGNUS VANES AT MACH NUMBERS 1.5 THROUGH 2.5

Leroy M. Jenke

ARO, Inc.

December 1973

Approved for public release; distribution unlimited.

VON KÁRMÁN GAS DYNAMICS FACILITY
ARNOLD ENGINEERING DEVELOPMENT CENTER
AIR FORCE SYSTEMS COMMAND
ARNOLD AIR FORCE STATION, TENNESSEE

NOTICES

EXPERIMENTAL MAGNUS CHARACTERISTICS OF BALLISTIC PROJECTILES WITH AND WITHOUT ANTI-MAGNUS VANES AT MACH NUMBERS 1.5 THROUGH 2.5

Leroy M. Jenke
ARO, Inc.

FOREWORD

The work reported herein was conducted by the Arnold Engineering Development Center (AEDC) for the Naval Weapons Laboratory (NWL) under sponsorship of the Air Force Armament Laboratory (AFATL), Air Force Systems Command (AFSC), under Program Element 62602F, Project 2547. AFATL Project Monitor was Mr. E. Sears.

The results presented herein were obtained by ARO, Inc. (a subsidiary of Sverdrup & Parcel and Associates, Inc.), contract operator of AEDC, AFSC, Arnold Air Force Station, Tennessee. The tests were conducted on May 24 and 25, 1973, under ARO Project No. VA332. The final data package was completed on June 15, 1973, and the manuscript was submitted for publication on June 28, 1973.

This technical report has been reviewed and is approved.

JIMMY W. MULLINS	FRANK J. PASSARELLO
Lt Colonel, USAF	Colonel, USAF
Chief Air Force Test Director, VKF	Director of Test
Directorate of Test	

ABSTRACT

An experimental investigation was conducted to determine static-stability and Magnus characteristics of four spin-stabilized ballistic shell configurations with and without small anti-Magnus vanes on the boattail. The models (slightly larger than full scale) were tested at Mach numbers 1.5, 2.0, and 2.5 over an angle-of-attack range from -2 to 8 deg. The Reynolds number, based on a model diameter of 5.2 in., was 1.7×10^6, and the spin parameter ($pd/2V_\infty$) ranged from 0 to 0.25 radians. Results are presented showing the effects of spin, Mach number, angle of attack, and anti-Magnus vanes. These results show that the vanes were effective in reducing both Magnus force and moment for two of the basic configurations and that the canted (7.2-deg) vanes were generally more effective than the straight vanes.

CONTENTS

TABLES

APPENDIX
ILLUSTRATIONS

NOMENCLATURE

A	Reference area, model maximum cross-sectional area (see Fig. 2), in.^{2}
C_m	Pitching-moment coefficient, pitching moment/$q_\infty Ad$

$C_{m\alpha}$	Pitching-moment coefficient derivative at $\alpha = 0$, $\partial C_m/\partial\alpha$, per deg
C_N	Normal-force coefficient, normal force/$q_\infty A$
$C_{N\alpha}$	Normal-force coefficient derivative at $\alpha = 0$, $\partial C_N/\partial\alpha$, per deg
C_n	Yawing (Magnus)-moment coefficient, yawing moment/$q_\infty Ad$ (see Fig. 2)
C_{n_p}	Magnus-moment spin derivative coefficient for $(pd/2V_\infty) < 0.1$, $\partial C_n/\partial(pd/2V_\infty)$, per radian
$C_{n_{p\alpha}}$	Magnus-moment coefficient derivative at $\alpha = 0$, $\partial^2 C_n/\partial(pd/2V_\infty)\partial\alpha$, per radian^2
C_Y	Side (Magnus)-force coefficient, side force/$q_\infty A$ (see Fig. 2)
C_{Y_p}	Magnus-force spin derivative coefficient for $(pd/2V_\infty) < 0.1$, $\partial C_Y/\partial(pd/2V_\infty)$, per radian
$C_{Y_{p\alpha}}$	Magnus-force coefficient derivative at $\alpha = 0$, $\partial^2 C_Y/\partial(pd/2V_\infty)\partial\alpha$, per radian^2
d	Reference diameter, model maximum diameter (see Fig. 2), in.
M_∞	Free-stream Mach number
p	Model spin rate (positive, clockwise viewing from the base), radians/sec
p_o	Tunnel stilling chamber pressure, psia
$pd/2V_\infty$	Spin parameter, radians
q_∞	Free-stream dynamic pressure, psia
Re	Free-stream unit Reynolds number, ft^{-1}
T_o	Tunnel stilling chamber temperature, °R
V_∞	Free-stream velocity, ft/sec
x_t	Axial distance from the model nose to onset of transition, in.
α	Angle of attack, deg

SECTION I
INTRODUCTION

The present test was conducted as part of a continuing investigation (Refs. 1 and 2) by the Naval Weapons Laboratory (NWL) for development work on ballistic shells. The projectiles are statically unstable and must be spin-stabilized. The spin velocity tends to induce Magnus effects, which can lead to dynamic instabilities. Both of these factors will influence the flight path. This test was initiated to obtain Magnus-force and -moment and static-stability data on four configurations with and without small anti-Magnus vanes (vanes to reduce the Magnus forces). The results will be used in estimating the performance of actual projectiles. Data were obtained at Mach numbers 1.5, 2.0, and 2.5 at a Reynolds number, based on a model diameter of 5.2 in., of 1.7 x 10^6. The angle of attack was varied from -2 to 8 deg, and values of the spin parameter ($pd/2V_\infty$) ranged from 0 to about 0.25 radians.

SECTION II
APPARATUS AND PROCEDURE

2.1 TEST ARTICLES AND TEST MECHANISM

The aluminum models (Figs. 1 and 2, Appendix) were supplied by NWL, and some are the same models tested in Ref. 1. The configurations of these projectiles have not been finalized, but the models are approximately full scale. Two sets of vanes (Fig. 2e) were supplied; one set (eight vanes) had no cant angle, and the other set was canted 7.2 deg; all were attached on the boattail of the models. The knurl pattern on the boattail portion of configuration 0 (Fig. 1c) is used on the actual projectiles to secure a plastic sabot which serves as the spin band to spin the projectile in the gun barrel. The plastic sabot is destroyed in the gun barrel and, therefore, is not included on the test models.

The models were mounted on the Magnus-force test mechanism shown in Fig. 3. Basically, the Magnus-force test mechanism has a sting-mounted, water-jacketed, four-component balance with a shell mounted on ball bearings over the water jacket. A two-stage, air-driven turbine is mounted inside the model mounting shell at a fixed axial position near the forward end of the sting. The turbine is used to spin the model to some desired speed and then is disengaged with an air-operated sliding clutch to allow the model to spin freely on the ball bearings. It is estimated that the turbine will produce a starting torque of 50 in.-lb and a developed torque of approximately 100 in.-lb. The mechanism is designed to operate under normal-force loads up to 500 lb and axial-force loads of 125 lb and for a maximum spin rate of approximately 25,000 rpm.

2.2 TEST FACILITY

Supersonic Wind Tunnel (A) is a continuous, closed-circuit, variable density wind tunnel with an automatically driven flexible-plate-type nozzle and a 40- by 40-in. test section. The tunnel can be operated at Mach numbers from 1.5 to 6 at maximum stagnation

pressures from 29 to 200 psia, respectively, and stagnation temperatures up to 750°R (M_∞ = 6). Minimum operating pressures range from about one-tenth to one-twentieth of the maximum at each Mach number. In most instances, Mach number changes may be made without stopping the tunnel. The model can be injected into the tunnel for a test run and then retracted for model changes without stopping the tunnel flow.

2.3 INSTRUMENTATION

Tunnel A stilling chamber pressure is measured with a 150-psid transducer referenced to a near vacuum and having full-scale calibrated ranges of 10, 50, and 150 psi. Based on periodic comparisons with secondary standards, the precision of this transducer (a band which includes 95 percent of the residuals) is estimated to be within ±0.5 percent of the measured pressure. The stilling chamber temperature is measured with a copper-constantan thermocouple to a precision of ±2°R based on the thermocouple wire manufacturer's specifications.

Model forces and moments were measured with the VKF four-component, moment-type, strain-gage balance shown in Fig. 4. The small outrigger side beams of the balance, with semiconductor strain gages, were used to obtain the sensitivity required to measure small side loads while maintaining adequate balance stiffness for the larger pitch loads. When a yawing moment is imposed on the balance, secondary bending moments are induced in the side beams. Thus, the outrigger beams act as mechanical amplifiers, and a normal-force to side-force capability ratio of 20 was achieved for a 500-lb normal-force loading. Before testing, static loads in each plane and combined static loads were applied to the balance, simulating the range of model loads anticipated for the test. The uncertainties shown in Table I represent the bands for 95 percent of the measurement residuals based on differences between the applied loads and the corresponding values calculated from the final data reduction equations.

TABLE I
BALANCE UNCERTAINTY

Balance Component	Design Load	Range of Static Loads	Measurement Uncertainty
Normal force, lb	500	±100	0.20
Pitching moment*, in.-lb	2500	±200	0.50
Side force, lb	25	± 16	0.07
Yawing moment*, in.-lb	125	± 50	0.10

*About balance forward moment bridge.

The transfer distance to the model moment reference was measured with a precision of ±0.005 in.

The rotational speed of the model was computed from the electrical pulses produced by a ring with reflective surfaces passing an internally mounted infrared-emitting diode and phototransistor. This tachometer system could measure spin rates from 0 to 30,000 rpm.

2.4 TEST PROCEDURE

The test procedure was to prespin the model to the desired spin rate, disengage the clutch, and record data as the model spin rate decayed. For the models with canted vanes, some additional data were obtained by holding the model with the brake, releasing the brake, and taking data as the model spin rate increased. Model spin rates were monitored using the internally mounted tachometer described in Section 2.3.

SECTION III
TEST CONDITIONS AND DATA PRECISION

3.1 TEST CONDITIONS

A summary of the configurations tested is presented below in Table II, and the nominal wind tunnel test parameters at which the data were obtained are presented in Table III. The "x" in Table II indicates that Magnus data were obtained for α = -2 to 8 deg.

TABLE II
TEST SUMMARY

Configuration	Number of Vanes	Vane Cant Angle, deg	M_∞ 1.5	M_∞ 2.0	M_∞ 2.5
0	0	—	x	x	x
0	8	0		x	x
0	8	7.2	x	x	x
2	0	—	x	x	x
2	8	0	x	x	x
2	8	7.2	x	x	x
3	0	—	x	x	x
4	0	—	x	x	x

TABLE III
WIND TUNNEL TEST PARAMETERS

M_∞	p_o, psia	T_o, °R	q_∞, psia	V_∞, ft/sec	Re x 10^{-6}, ft^{-1}
1.50	13.6	560	5.84	1444	3.95
2.00	16.5	560	5.91	1729	4.02
2.50	21.0	560	5.38	1933	4.02

3.2 DATA PRECISION

Uncertainties (bands which include 95 percent of the calibration data) in the basic tunnel parameters, p_o, T_o, and M_∞, were estimated from repeat calibrations of the instrumentation and from the repeatability and uniformity of the test section flow during tunnel calibrations. These uncertainties were then used to estimate uncertainties in other free-stream properties, using the Taylor series method of error propagation. Listed in Table IV are the uncertainties in the basic wind tunnel parameters at which the data were obtained.

TABLE IV
WIND TUNNEL PARAMETER PRECISION

	Uncertainty, percent					
M_∞	M_∞	p_o	T_o	q_∞	V_∞	Re
1.5	±0.7	±0.50	±0.36	±0.52	±0.51	±0.73
2.0	±0.5	±0.50	±0.36	±0.75	±0.33	±0.83
2.5	±0.3	±0.50	±0.36	±0.78	±0.23	±0.83

Measurements of the model attitude in pitch including the model-balance deflection are precise within ±0.05 deg, based on repeat calibrations. The rpm precision is estimated to be ±5 rpm.

The basic uncertainties listed in Section 2.3 were combined with uncertainties in the tunnel parameters (Table IV), assuming a Taylor series error propagation, to estimate the precision of the aerodynamic coefficients. The uncertainties shown in Tables V and VI are those that were computed for the test conditions at which most of the data were obtained and are near the maximum aerodynamic loads. The uncertainties near the minimum loads were somewhat smaller.

TABLE V
AERODYNAMIC COEFFICIENT PRECISION

	Uncertainty				
M_∞	C_N	C_m	C_Y	C_n	$pd/2V_\infty$*, percent
1.5	±0.0023	±0.0031	±0.0006	±0.0004	±0.51
2.0	±0.0034	±0.0036	±0.0006	±0.0004	±0.33
2.5	±0.0037	±0.0035	±0.0006	±0.0004	±0.23

*For spin rates > 4000 rpm.

TABLE VI
DERIVATIVE COEFFICIENT PRECISION

M_∞	C_{N_α},deg^{-1}	C_{m_α},deg^{-1}	C_{Y_p},rad^{-1}	C_{n_p},rad^{-1}	$C_{Y_{p_\alpha}}$,rad^{-2}	$C_{n_{p_\alpha}}$,rad^{-2}
1.5	±0.0011	±0.0015	±0.006	±0.004	±0.12	±0.10
2.0	±0.0017	±0.0018	±0.006	±0.004	±0.12	±0.10
2.5	±0.0018	±0.0017	±0.006	±0.004	±0.12	±0.10

It should be noted that data repeatability, which is a measure of the random-type errors. was generally well within the maximum propagated uncertainties quoted.

SECTION IV
RESULTS AND DISCUSSION

These tests were conducted primarily to determine the change in the Magnus force and moment produced by small vanes on the boattail of ballistic shell configurations at supersonic Mach numbers. Data were obtained at Mach numbers 1.5, 2.0, and 2.5 for angles of attack from -2 to 8 deg. The spin rate parameter ($pd/2V_\infty$) ranged from 0 to 0.25 radians.

The variations of normal force (C_N) and pitching moment (C_m) with angle of attack are presented in Figs. 5 through 8. Since gun-launched projectiles are spin-stabilized, they are all statically unstable, as expected. Both C_N and C_m are esentially linear functions of angle of attack for angles up to 6 deg. Figure 9 shows the variations of C_{N_α} and C_{m_α} with Mach number for the present investigation as well as some results from a previous test (Ref. 1). As the Mach number increased, C_{N_α} increased and C_{m_α} decreased for all configurations except configuration 3, for which C_{m_α} increased at the lower Mach numbers ($M_\infty < 1.2$). As expected, the vanes increased C_{N_α} and decreased C_{m_α}, and the cant angle had no effect on either parameter.

Figure 10 presents the typical variation of C_Y and C_n with $pd/2V_\infty$ for configuration 0 without vanes and with canted vanes at $M_\infty = 1.5$. The data typify the type of data, the amount of scatter, and the number of points that were obtained as the model spin rate changed. The data presented hereafter in this report show a computer fairing through the data points (a third-degree, least-squares curve fit) instead of a symbol for each data point. The complete C_Y and C_n versus $pd/2V_\infty$ results are presented in Figs. 11 through 18. The results generally indicate that both C_Y and C_n are nonlinear with $pd/2V_\infty$ at the higher angles of attack ($\alpha > 4$ deg) and higher spin rates ($pd/2V_\infty > 0.15$). In addition, the usual negative C_Y and positive C_n for positive values of $pd/2V_\infty$ and α were obtained for all configurations, with the exception of configuration 2 at $M_\infty = 2.5$ (Figs. 14c, 15c, and 16c). This exception at $M_\infty = 2.5$ will be discussed below.

To examine the effects of angle of attack, the linear portion of the data (slopes of C_Y and C_n versus $pd/2V_\infty$ for $pd/2V_\infty < 0.1$) will be used. These variations of C_{Y_p} and C_{n_p} with angle of attack are presented in Figs. 19 through 22. The results indicate

that the magnitudes of both C_{Y_p} and C_{n_p} generally increase continuously with angle of attack and are linear up to about 2 deg, except for configurations 0 and 2 at $M_\infty = 2.5$ (Figs. 19a and 20). The unusual variation in C_{Y_p} and C_{n_p} at the small angles of attack ($-2 < \alpha < 2$ deg) at $M_\infty = 2.5$ may be the result of transition being near the base of the model. If the tests at $M_\infty = 2.5$ had been conducted at a higher Reynolds number, C_{Y_p} and C_{n_p} versus α might have been linear at the small angles. It should be noted that this unusual slope of C_{Y_p} and C_{n_p} with α is strictly localized at $\alpha = 0$ and that for $\alpha > 2$ deg both C_{Y_p} and C_{n_p} recover to their more normal trends. Figure 23 presents the variation of $C_{Y_{p_\alpha}}$ and $C_{n_{p_\alpha}}$ with Mach number for the present and previous investigations. The data for configurations 0 and 2 (Figs. 23a and b) show a peak in both $C_{Y_{p_\alpha}}$ and $C_{n_{p_\alpha}}$ near $M_\infty = 1$ and are nearly constant at the supersonic Mach numbers with the exception of configuration 2 at $M_\infty = 2.5$. In addition, the results show excellent agreement with results from Ref. 1. The effectiveness of the vanes in decreasing the Magnus components on configurations 0 and 2 is clearly shown, with the canted vanes generally being the most effective. The vanes apparently reduce the body Magnus force by changing the flow pattern on the boattail. In addition, the axial force on the canted vanes produces a negative yawing moment at positive angles of attack (Ref. 2). For both configurations 3 and 4, $C_{Y_{p_\alpha}}$ was constant at the supersonic Mach number ($M_\infty > 1.5$). For configuration 4, $C_{n_{p_\alpha}}$ was also constant, but for configuration 3, $C_{n_{p_\alpha}}$ decreased with increasing Mach number for $M_\infty > 1.5$.

Platou (Ref. 3) has shown that body Magnus characteristics are dependent on flow conditions in the boundary layer, and Pate and Schueler (Ref. 4) have shown that transition location is dominated by the aerodynamic noise present in wind tunnels and is a function of tunnel size, with smaller tunnels having a shorter distance to transition from the model nose for a given unit Reynolds number and Mach number. Since the location of transition is a possible factor affecting Magnus characteristics on spinning models, the estimated location of transition on the model leeward side (from Tunnel A shadowgraph photographs) is presented in Fig. 24. Although these data are not complete, they may be of benefit in the future in comparing the present data with those from other test facilities. A typical shadowgraph photograph showing the flow patterns at $M_\infty = 2$ is presented in Fig. 25.

SECTION V
CONCLUDING REMARKS

An investigation was conducted to determine the static-stability and Magnus characteristics of several Naval Weapons Laboratory ballistic shell configurations with and without anti-Magnus vanes. The tests were conducted at Mach numbers 1.5, 2.0, and 2.5 for an angle-of-attack range from -2 to 8 deg. Results were obtained at spin parameter ($pd/2V_\infty$) values up to 0.25 radians. The test results are summarized as follows:

1. For the Mach number range tested, C_{N_α} increased and C_{m_α} decreased with increasing Mach number for all configurations except configuration 3, for which C_{m_α} increased between $0.9 < M_\infty < 1.2$.

2. The vanes increased C_{N_α} and decreased C_{m_α}.

3. Both C_Y and C_n were nonlinear with $pd/2V_\infty$ at the higher angles of attack ($\alpha > 4$ deg) and $pd/2V_\infty$ values ($pd/2V_\infty > 0.15$).

4. Generally, for positive values of $pd/2V_\infty$ and α, C_Y was negative and C_n was positive.

5. The magnitudes of C_{Y_p} and C_{n_p} increased with α and were linear up to about 2 deg except at $M_\infty = 2.5$ for configuration 2.

6. At the supersonic Mach numbers ($M_\infty \geqslant 1.5$) $C_{Y_{p_\alpha}}$ and $C_{n_{p_\alpha}}$ were nearly constant. Two exceptions were configuration 2 at $M_\infty = 2.5$, where both parameters decreased, and configuration 3, where $C_{n_{p_\alpha}}$ decreased with increasing Mach number.

7. The vanes generally decreased the Magnus force and moment on configurations 0 and 2.

8. The canted vanes were generally more effective in reducing the Magnus force and moment than were the straight vanes.

REFERENCES

1. Jenke, Leroy M. and Carman, Jack B. "Experimental Magnus Characteristics of Ballistic Projectiles with Anti-Magnus Vanes at Mach Numbers 0.7 through 2.5." AEDC-TR-73-126.

2. Benton, Edward R. "Supersonic Magnus Effect on a Finned Missile." AIAA Journal, Vol. 2, No. 1, January 1964, pp. 153-155.

3. Platou, A.S. "The Magnus Force on a Short Body at Supersonic Speeds." BRL Report No. 1062 (AD212064), January 1959.

4. Pate, S.R. and Schueler, C.J. "Effects of Radiated Aerodynamic Noise on Model Boundary-Layer Transition in Supersonic and Hypersonic Wind Tunnels." AEDC-TR-67-236 (AD666644), March 1968. Also AIAA Journal, Vol. 7, No. 3, March 1969, pp. 450-457.

APPENDIX
ILLUSTRATIONS

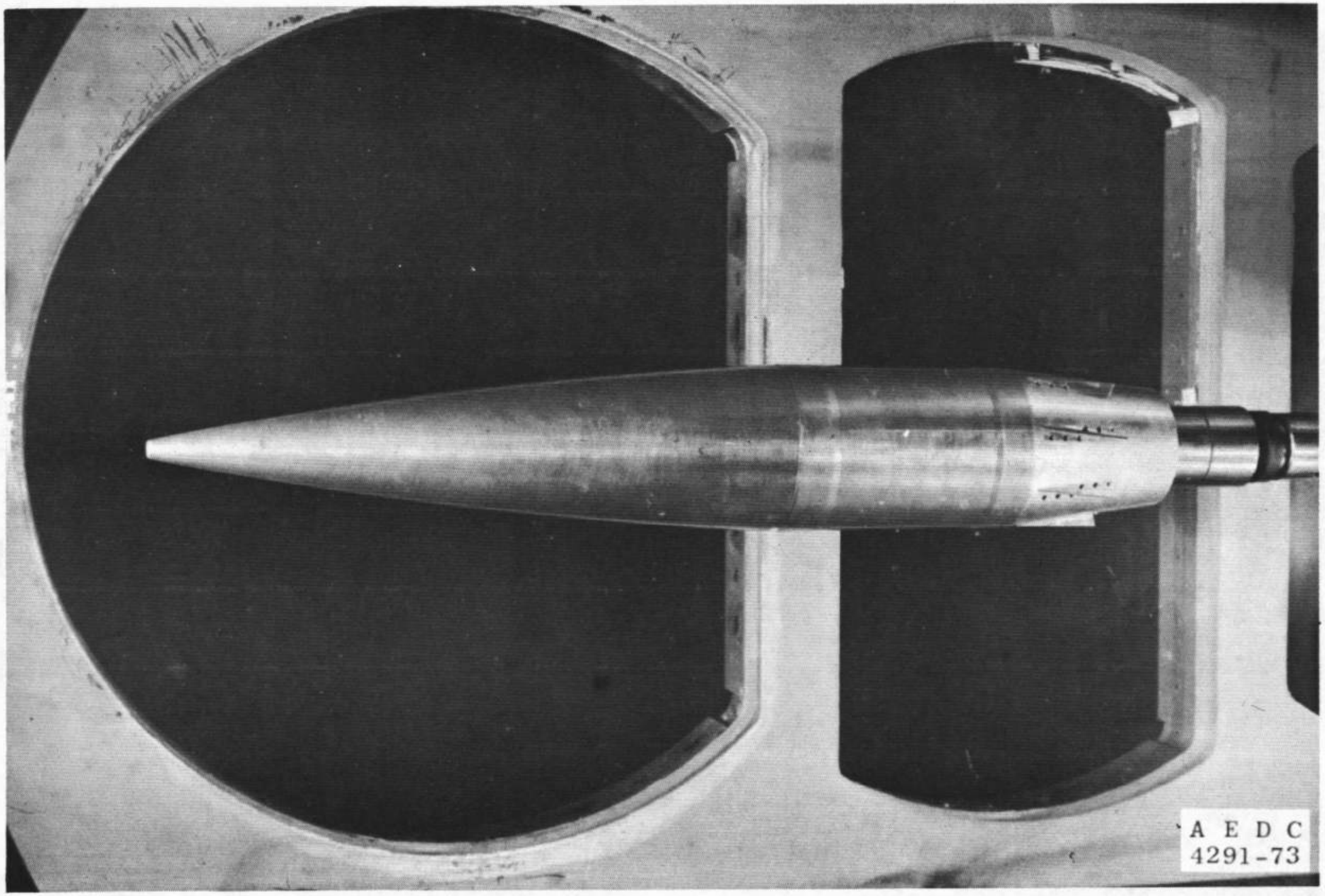

a. Tunnel A Installation (Configuration 2)
Fig. 1 Model Photographs

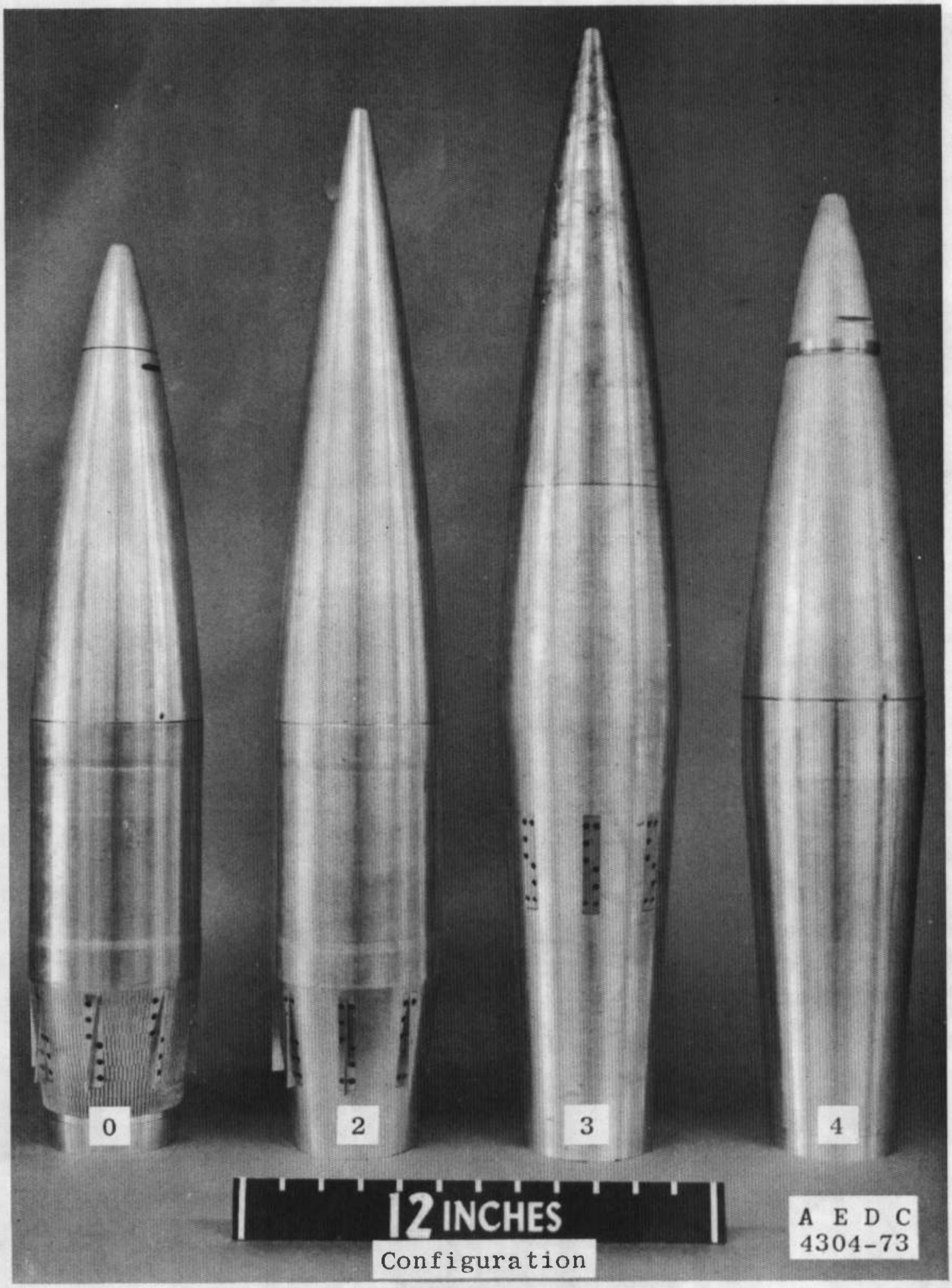

b. Complete Configurations
Fig. 1 Continued

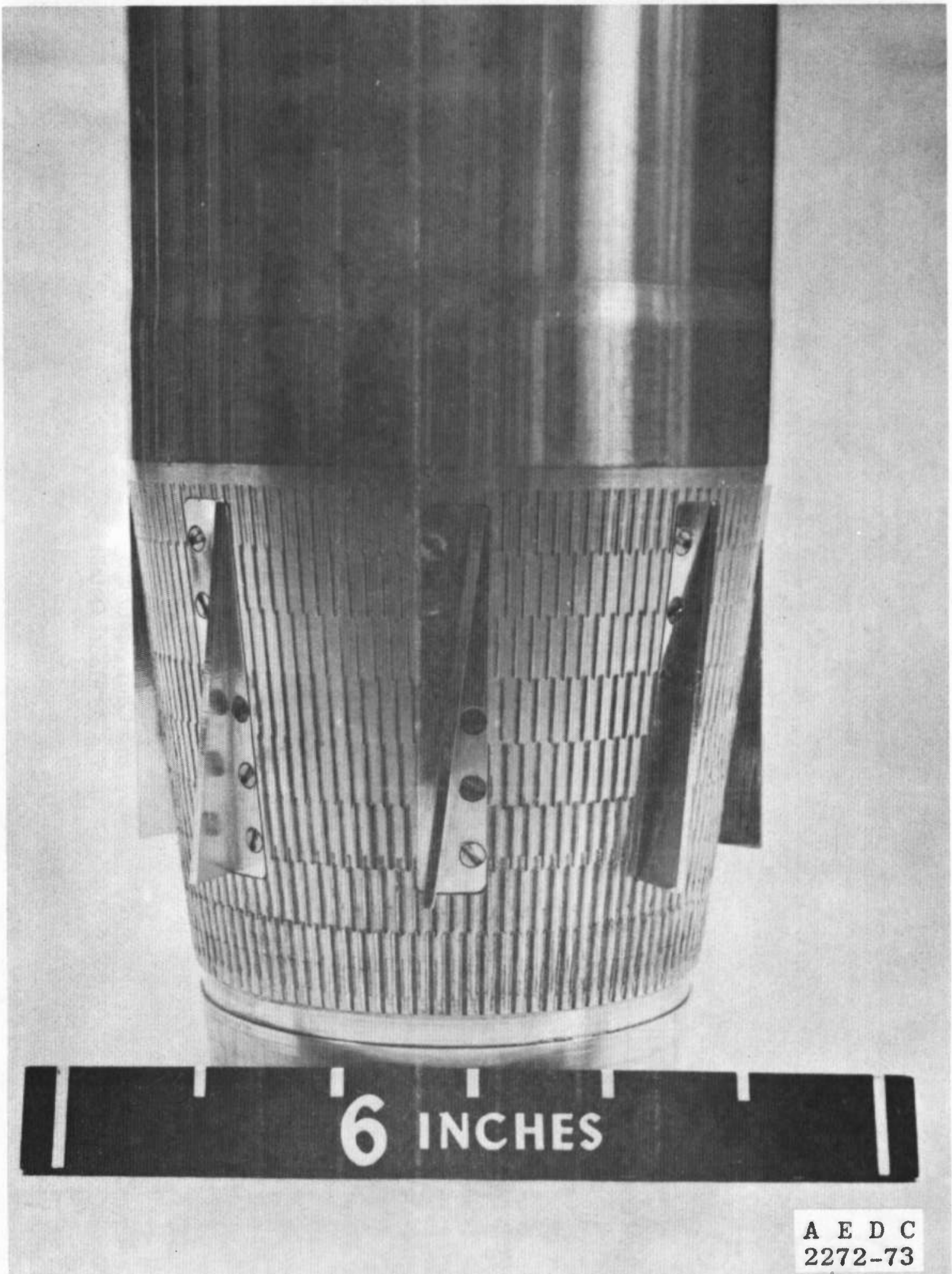

c. Knurl Pattern
Fig. 1 Concluded

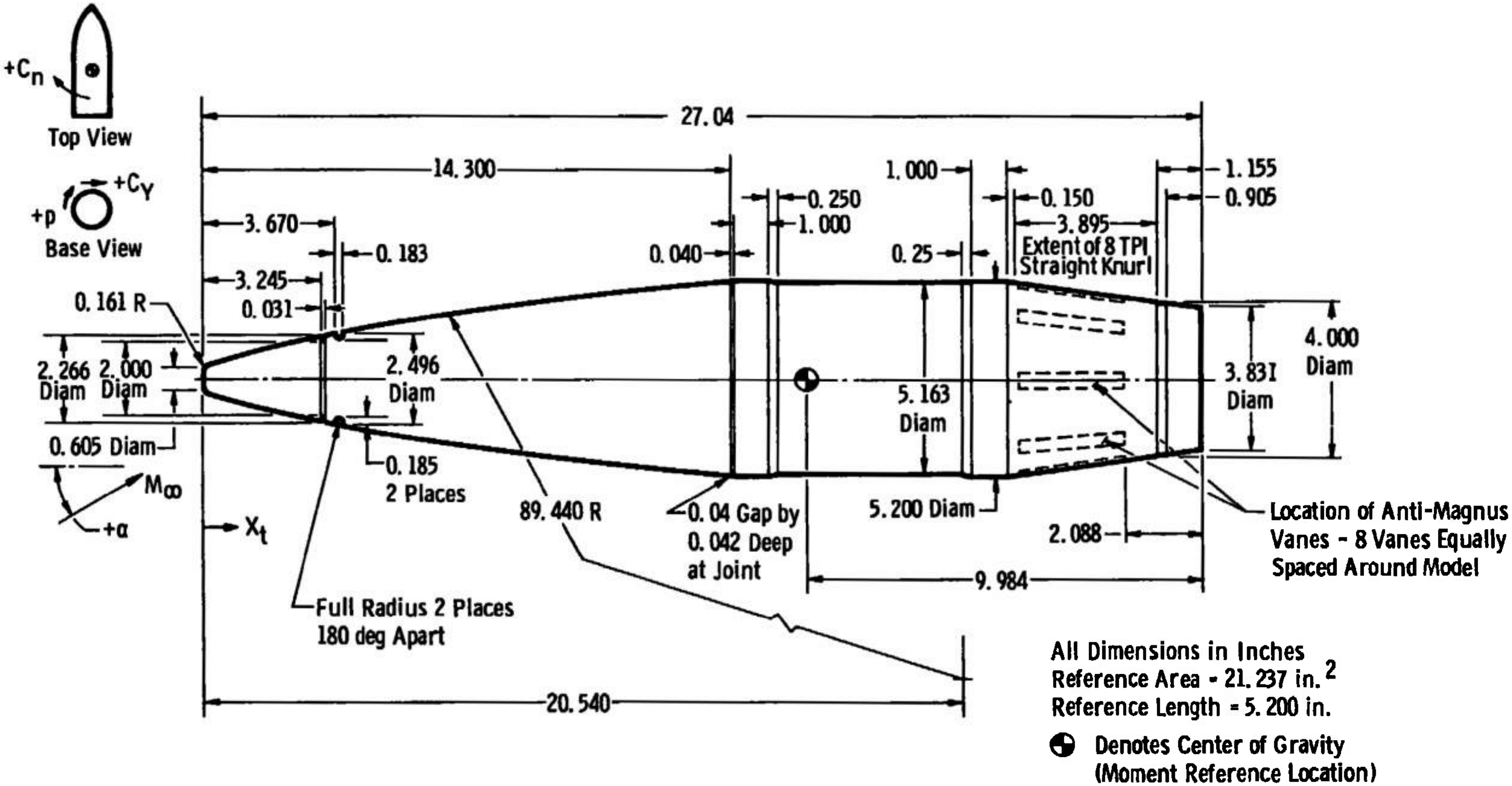

a. Configuration 0

Fig. 2 Model Details

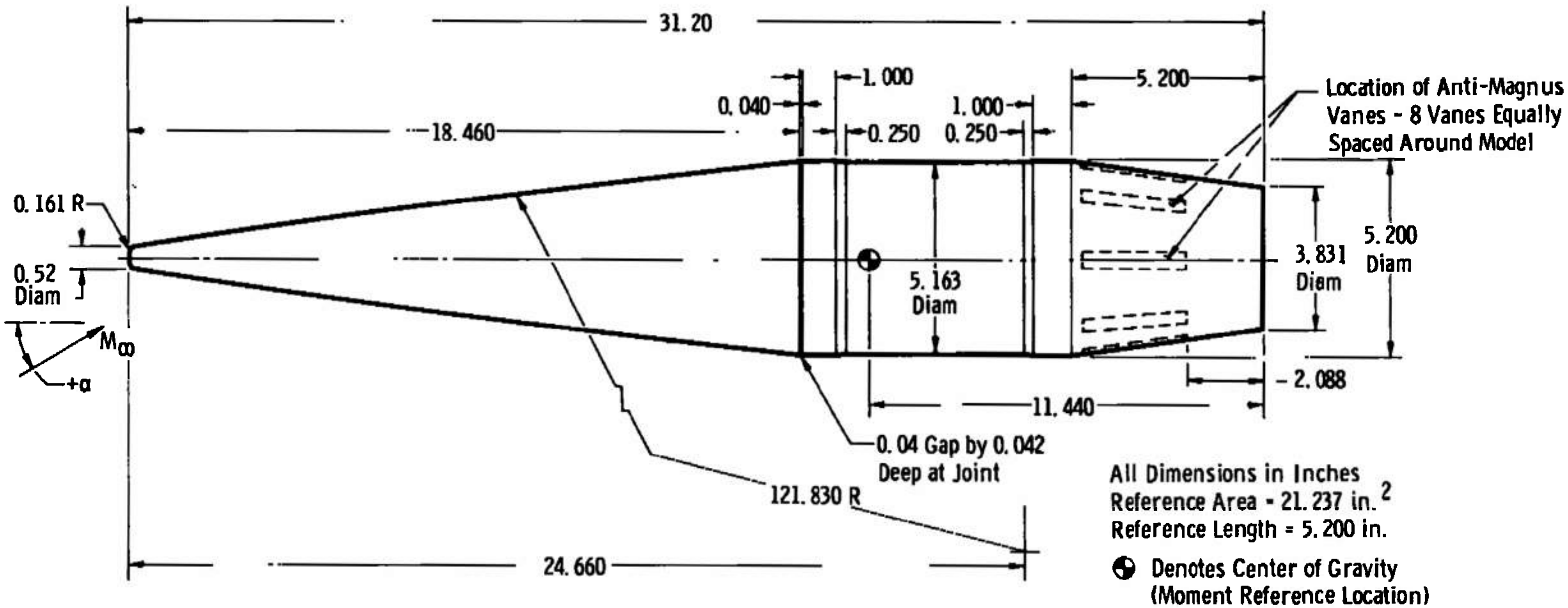

b. Configuration 2
Fig. 2 Continued

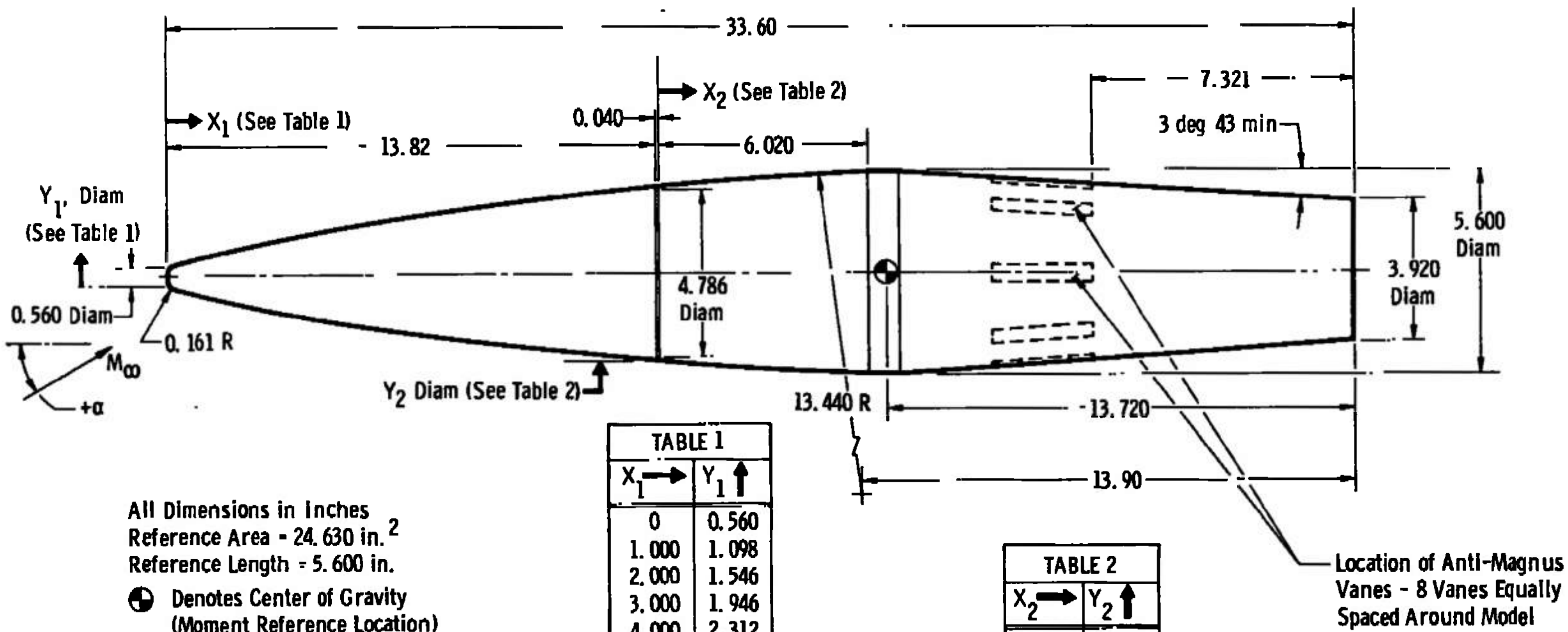

All Dimensions in Inches
Reference Area = 24.630 in.^{2}
Reference Length = 5.600 in.
⊕ Denotes Center of Gravity
(Moment Reference Location)

TABLE 1

X_1 →	Y_1 ↑
0	0.560
1.000	1.098
2.000	1.546
3.000	1.946
4.000	2.312
5.000	2.650
6.000	2.966
7.000	3.264
8.000	3.542
9.000	3.804
10.000	4.050
11.000	4.281
12.000	4.500
13.000	4.702
13.820	4.856

TABLE 2

X_2 →	Y_2 ↑
0	4.860
0.140	4.890
1.140	5.060
2.140	5.216
3.140	5.352
4.140	5.468
5.140	5.556
6.020	5.600

c. Configuration 3
Fig. 2 Continued

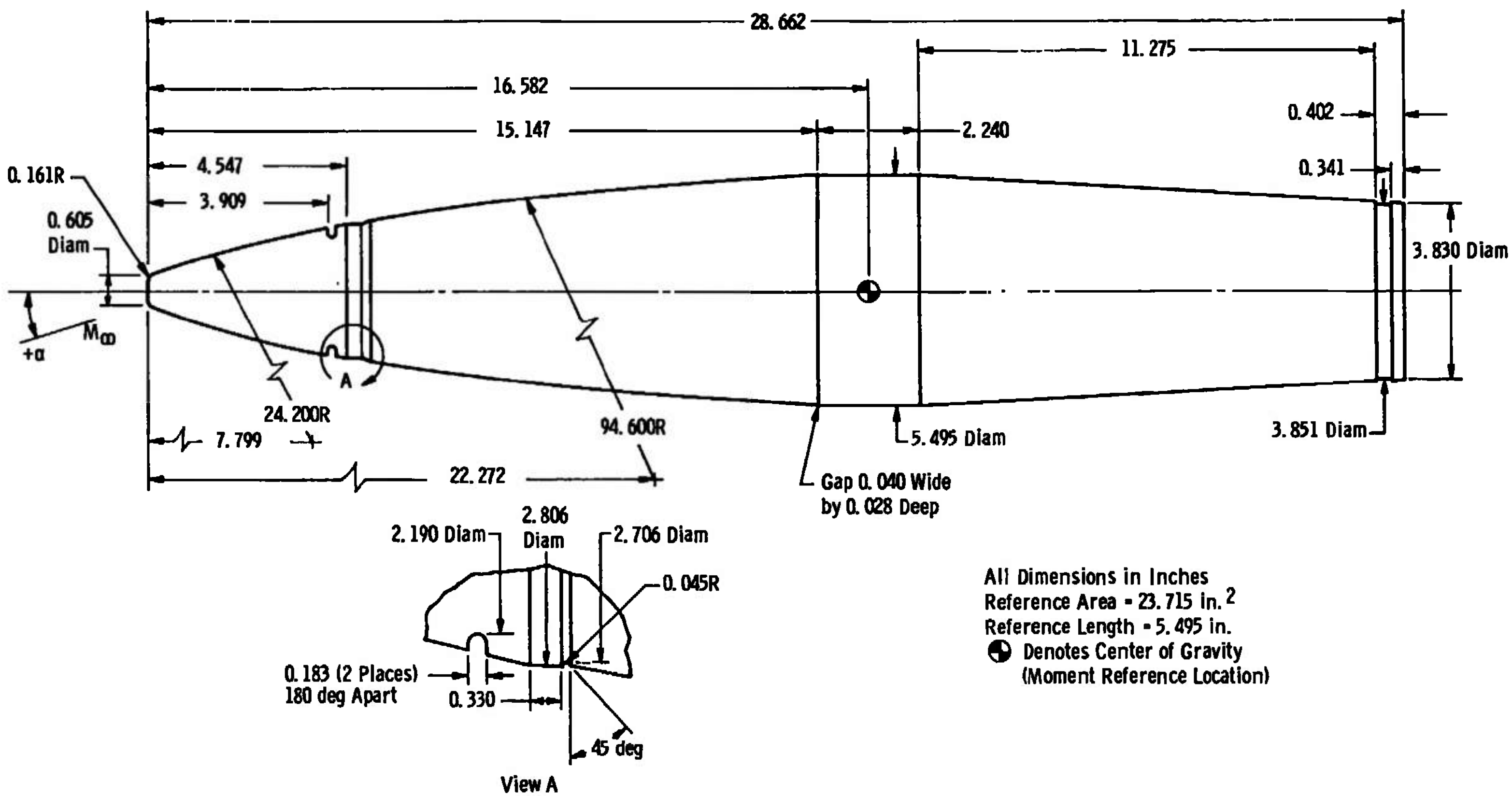

d. Configuration 4
Fig. 2 Continued

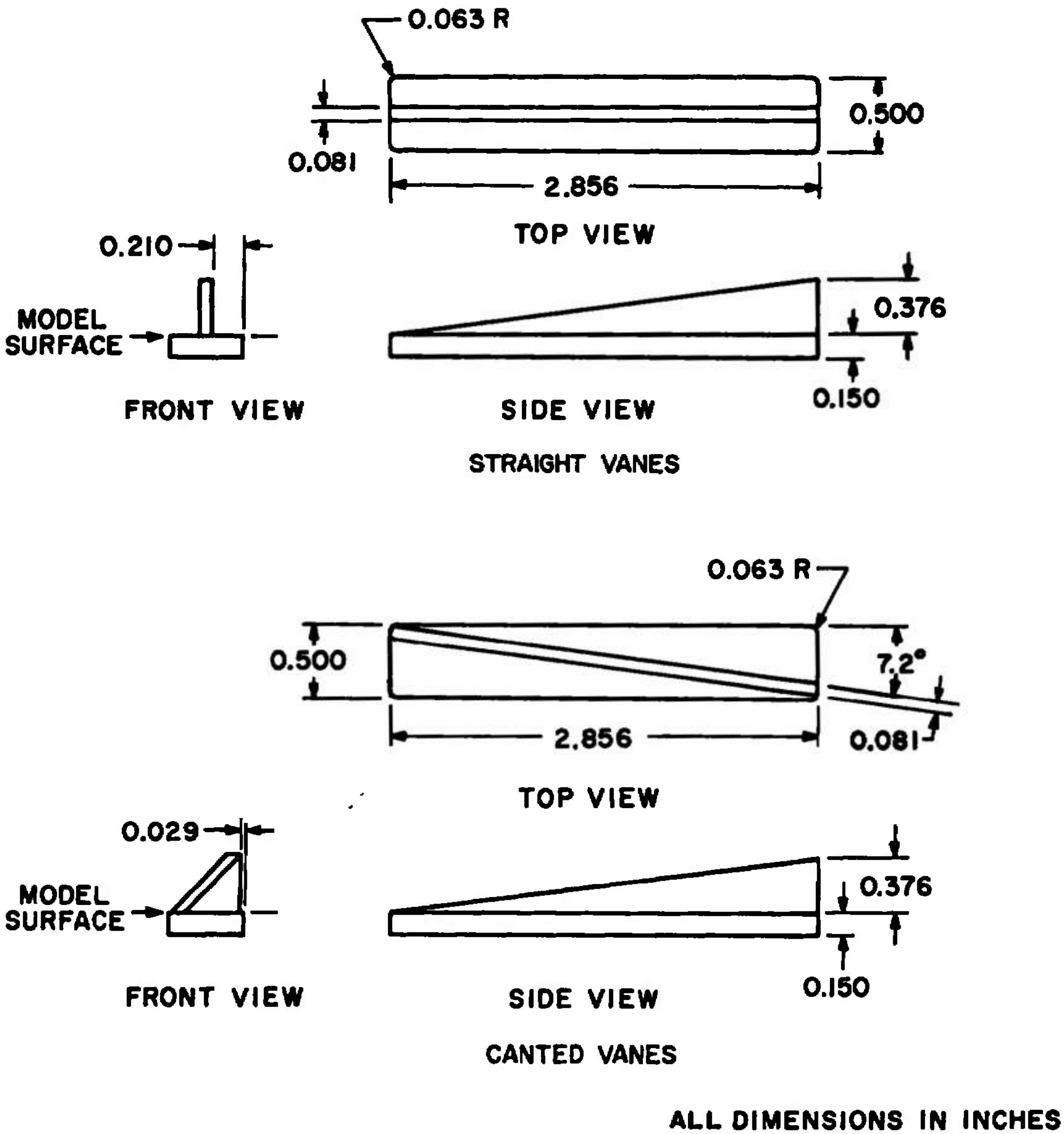

e. Anti-Magnus Vanes
Fig. 2 Concluded

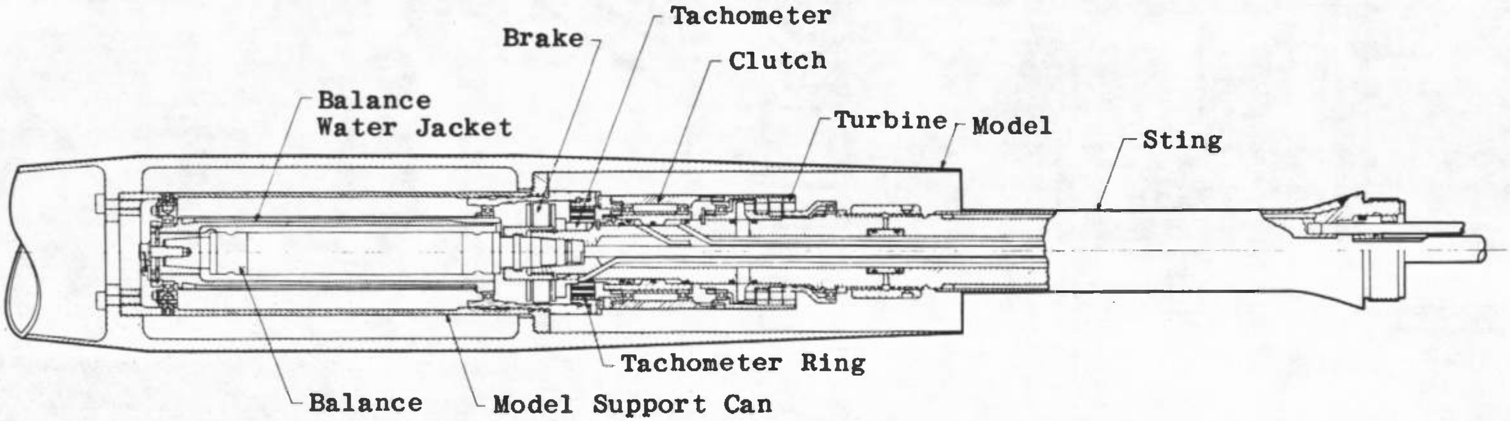

Fig. 3 Magnus-Force Test Mechanism

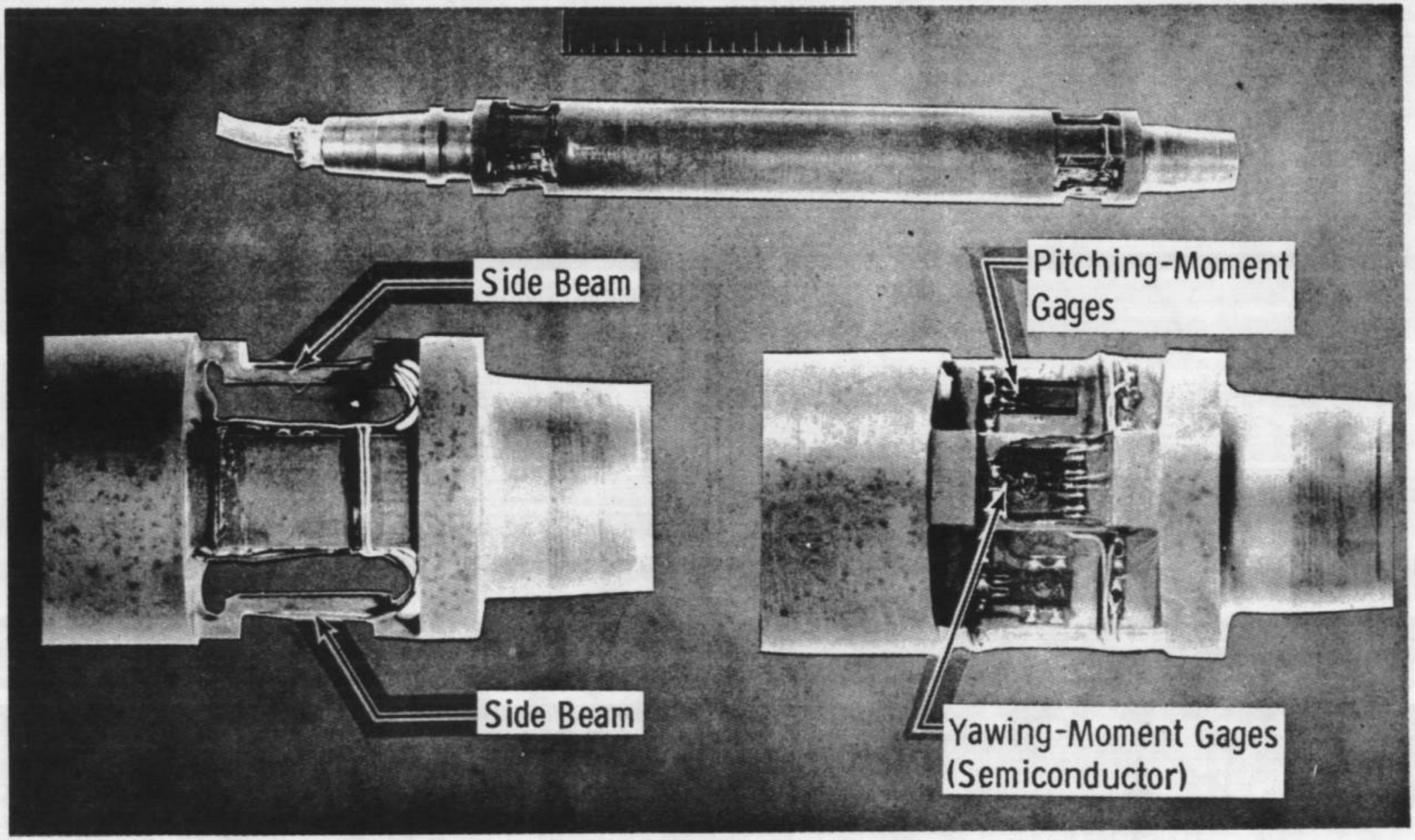

Fig. 4 Balance Details

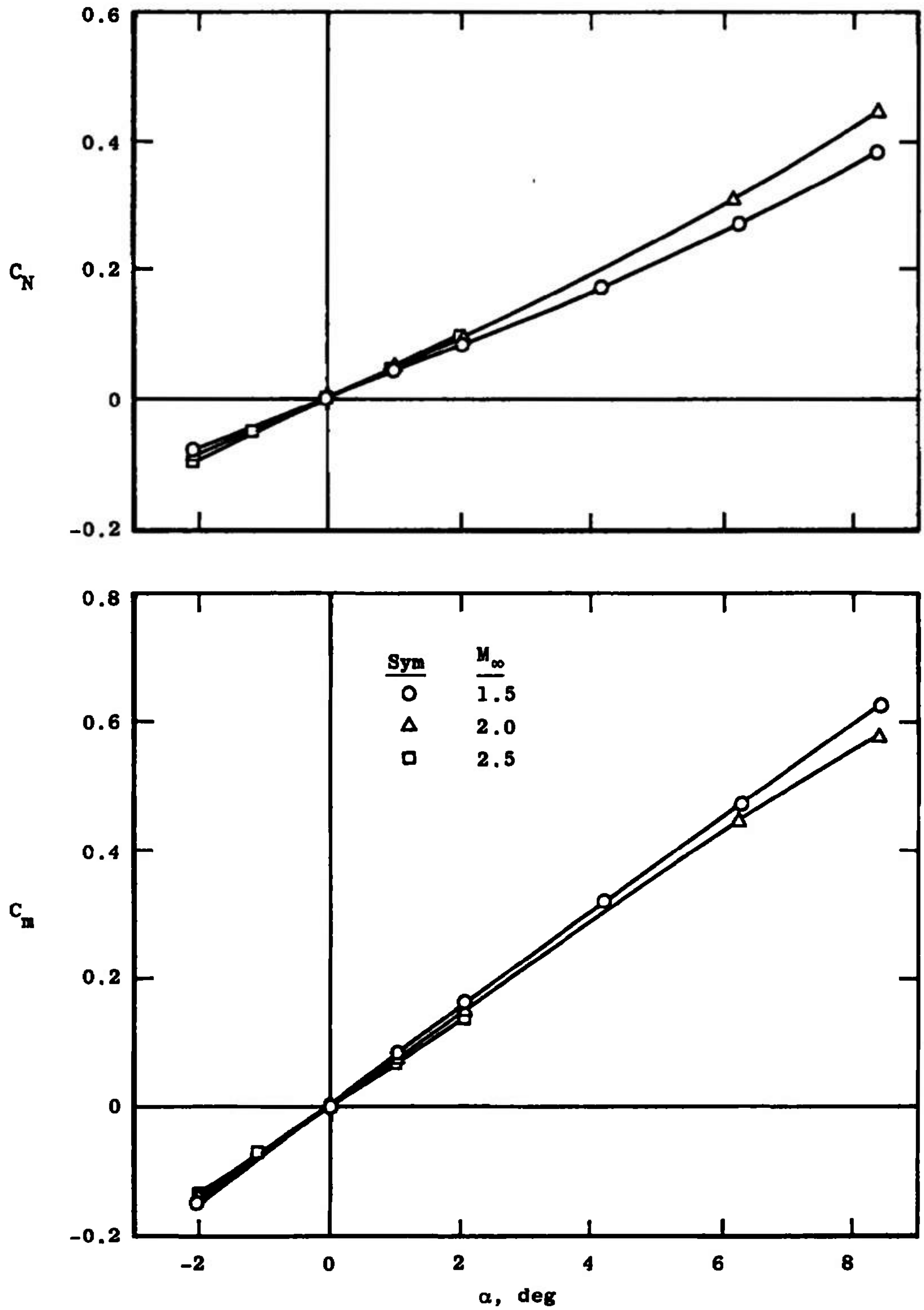

a. Without Vanes

Fig. 5 Variation of C_N and C_m with Angle of Attack, Configuration 0

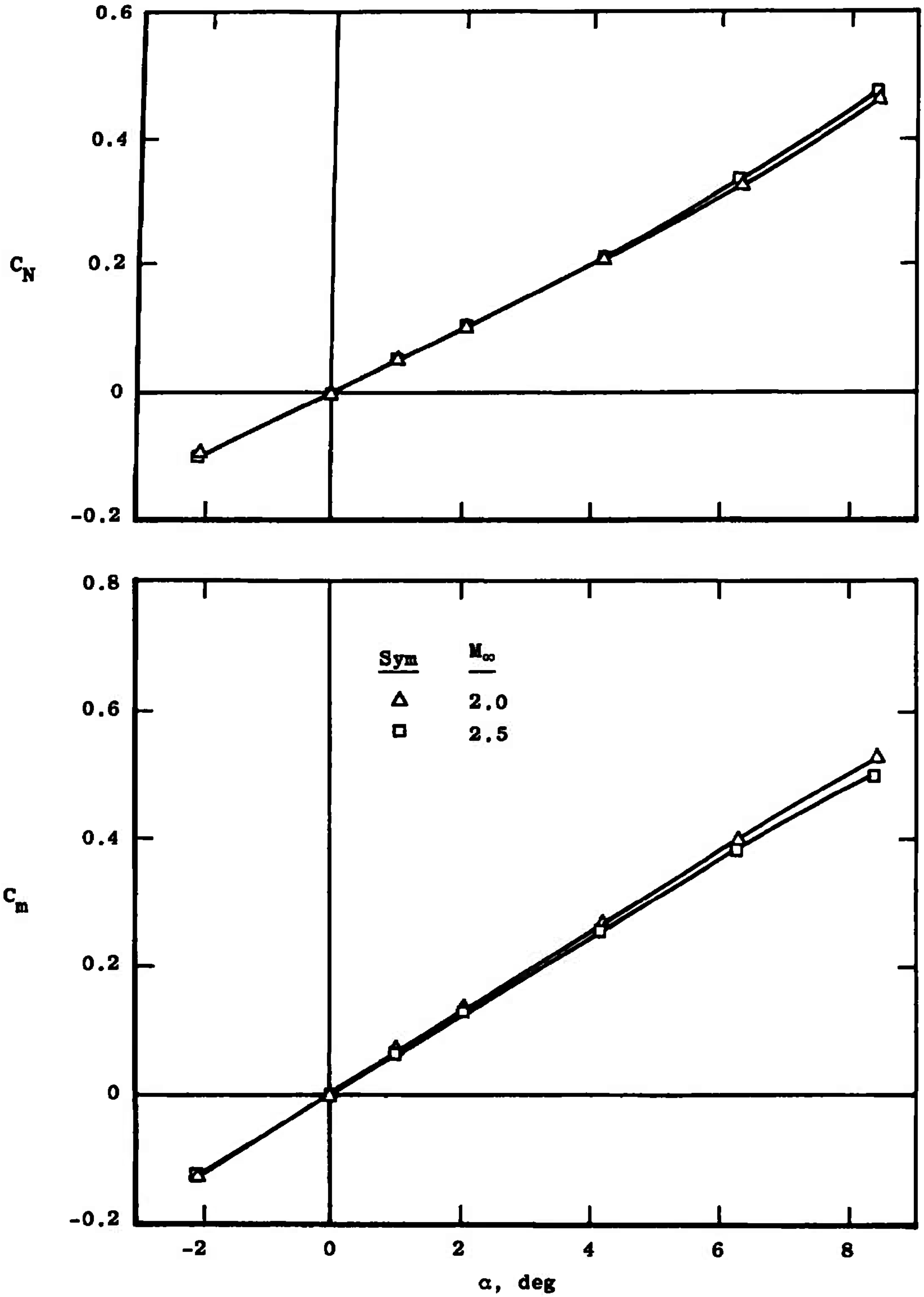

b. With Straight Vanes
Fig. 5 Continued

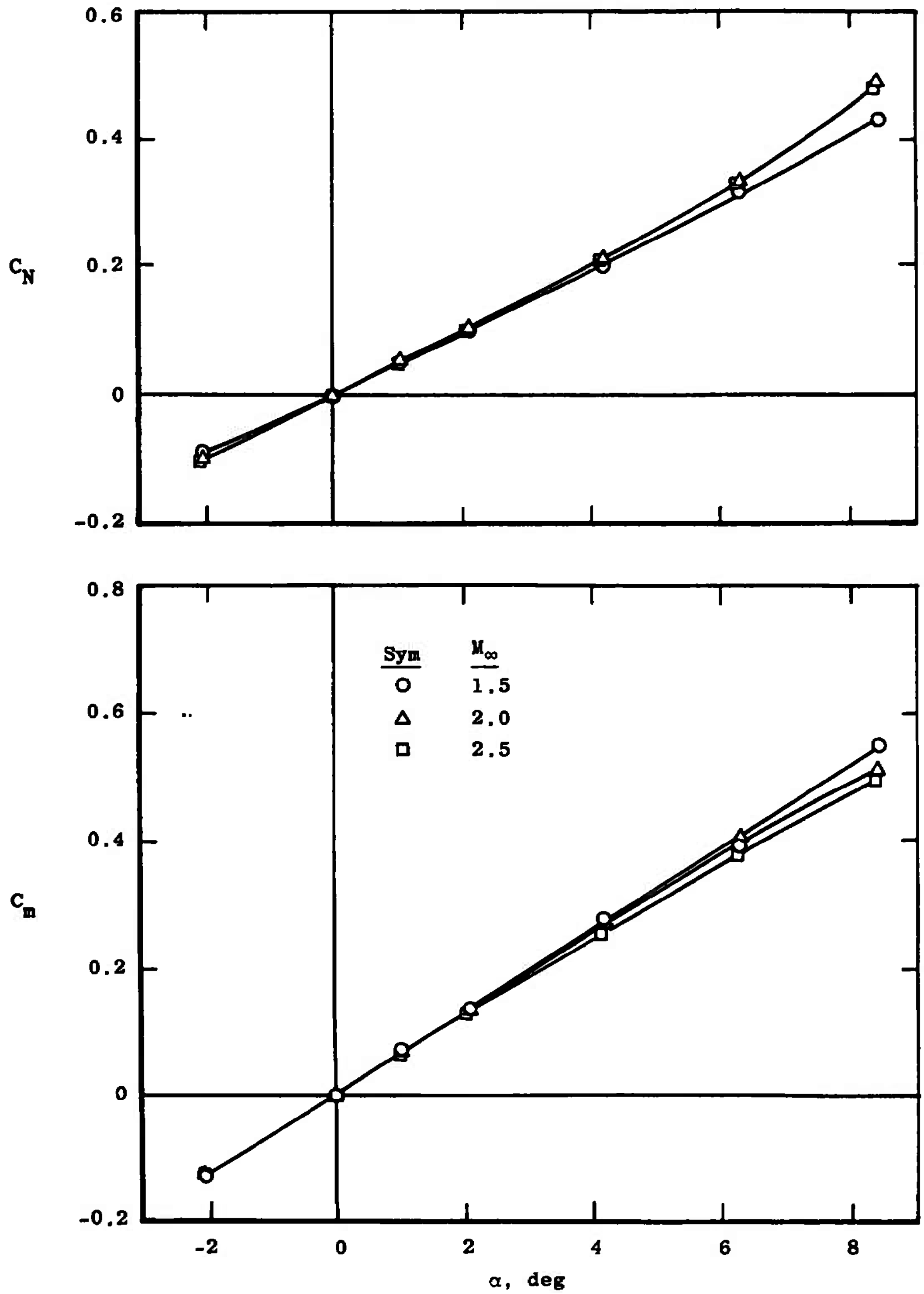

c. With Canted Vanes
Fig. 5 Concluded

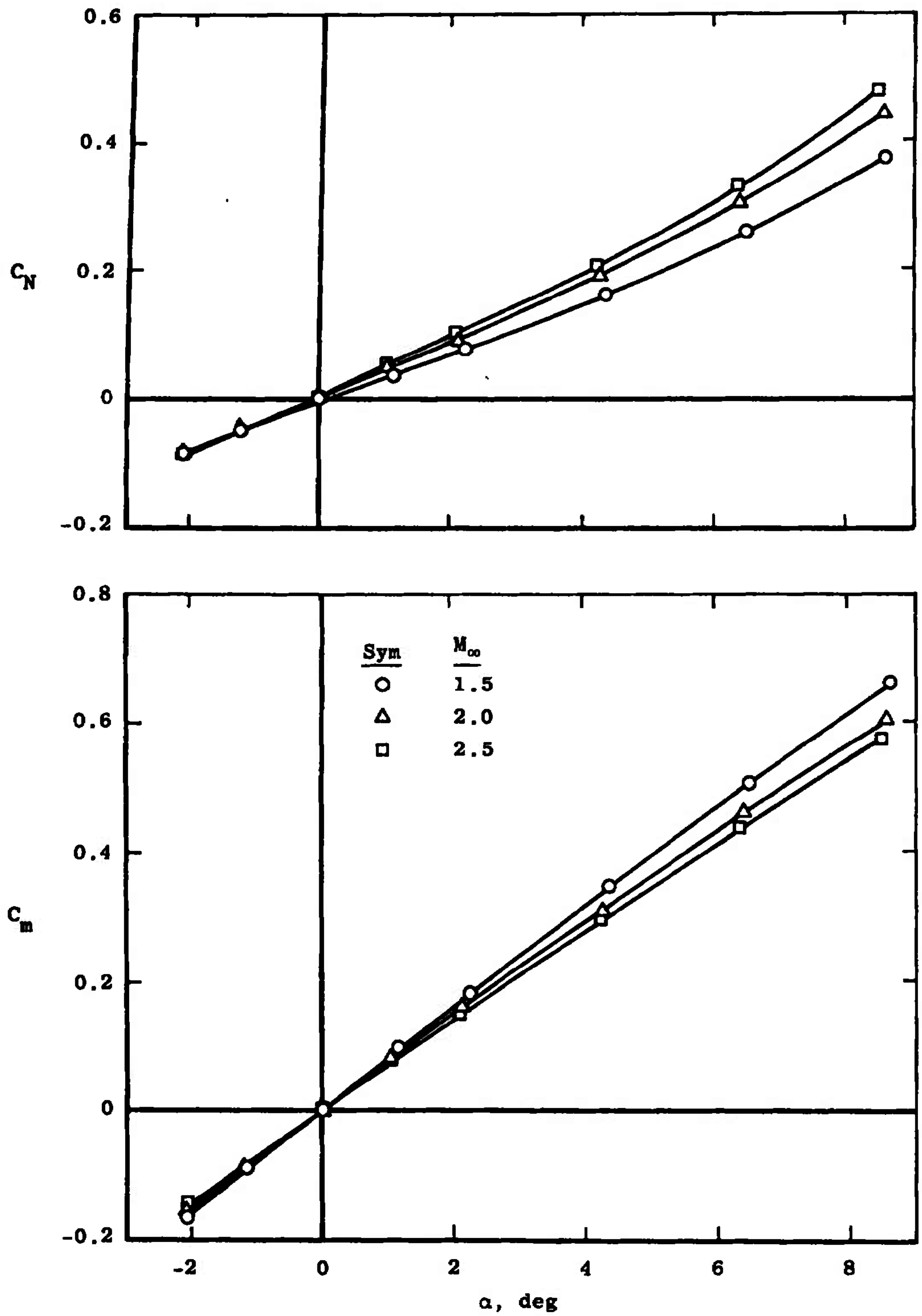

a. Without Vanes

Fig. 6 Variation of C_N and C_m with Angle of Attack, Configuration 2

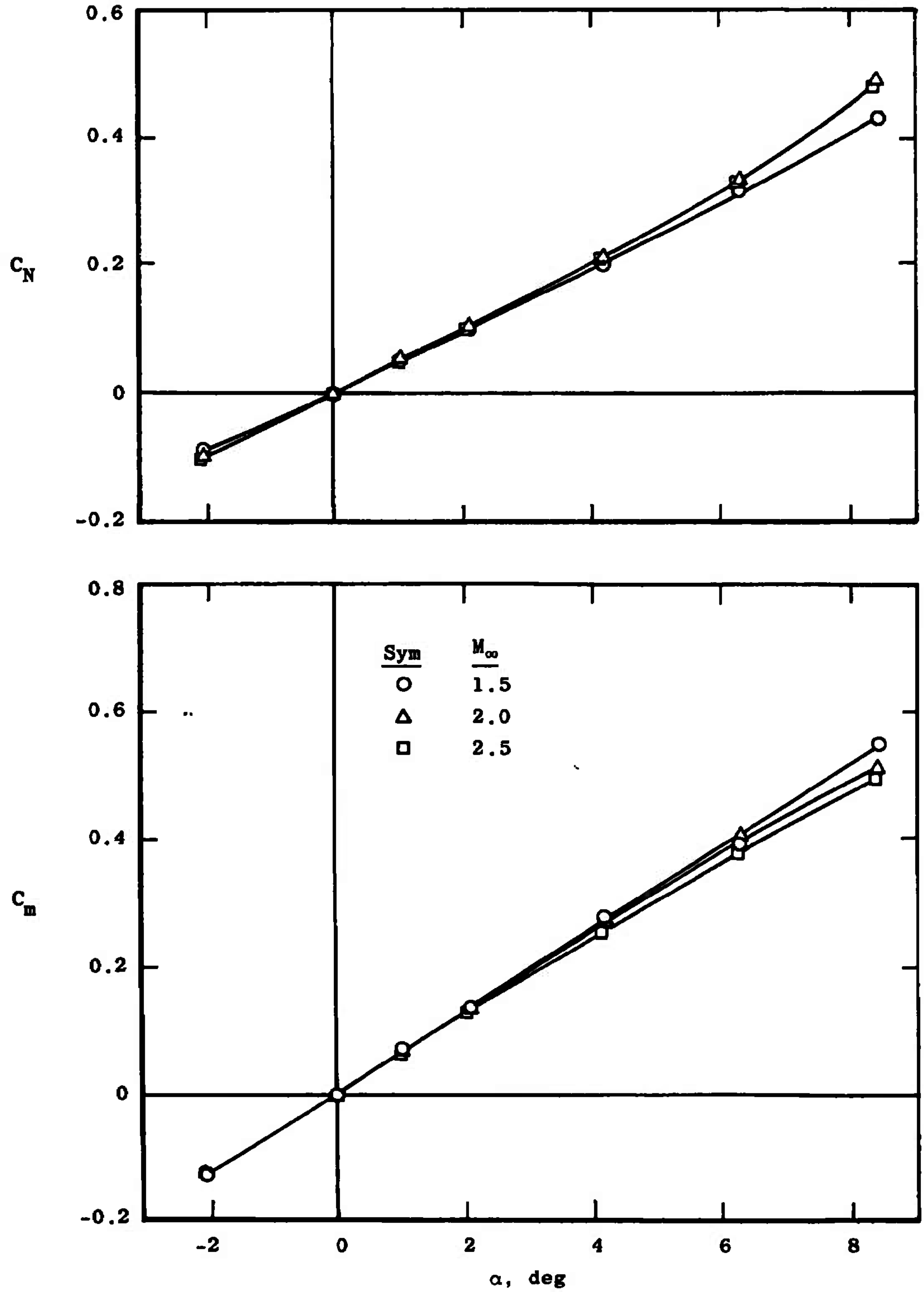

c. With Canted Vanes
Fig. 5 Concluded

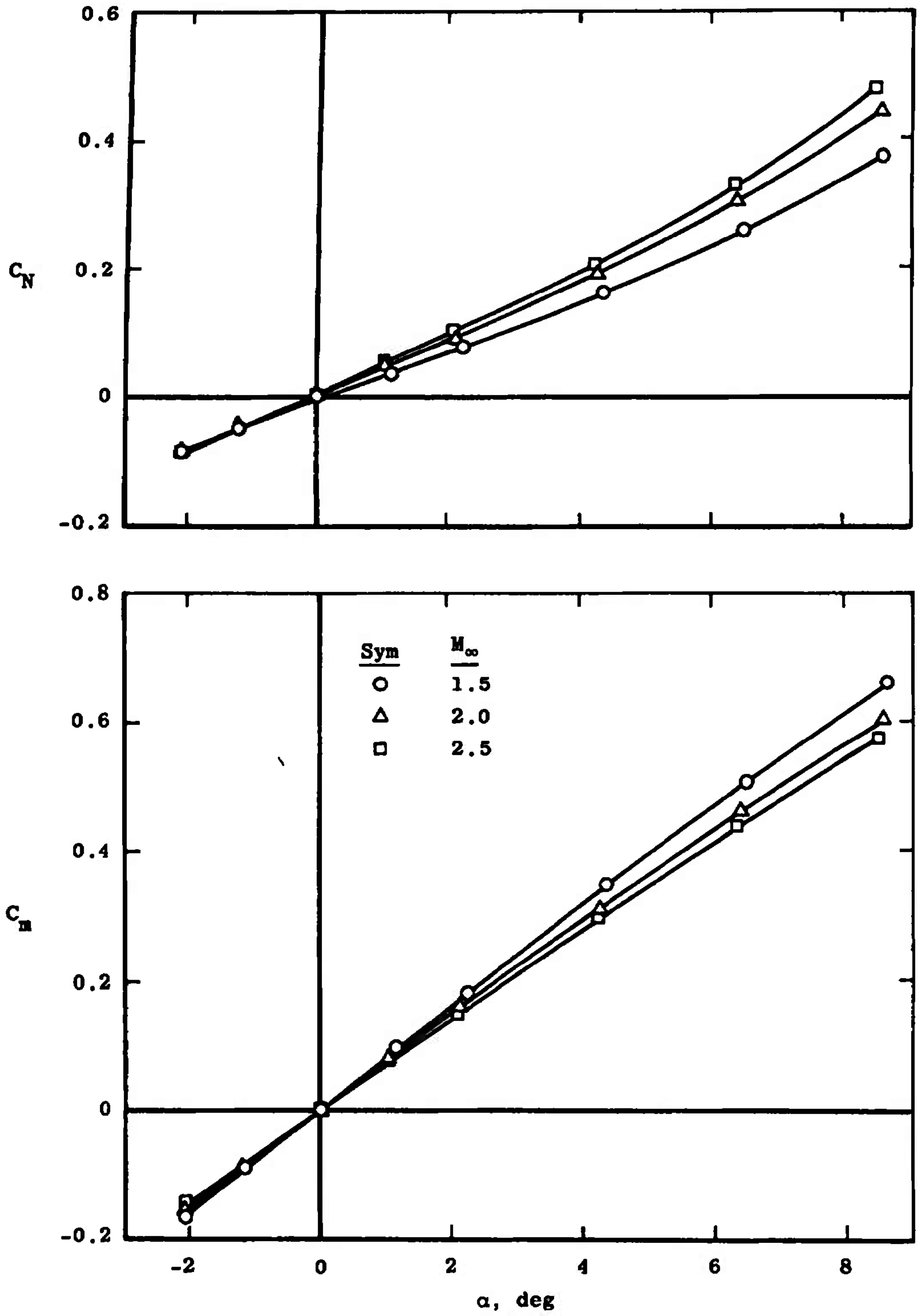

a. Without Vanes

Fig. 6 Variation of C_N and C_m with Angle of Attack, Configuration 2

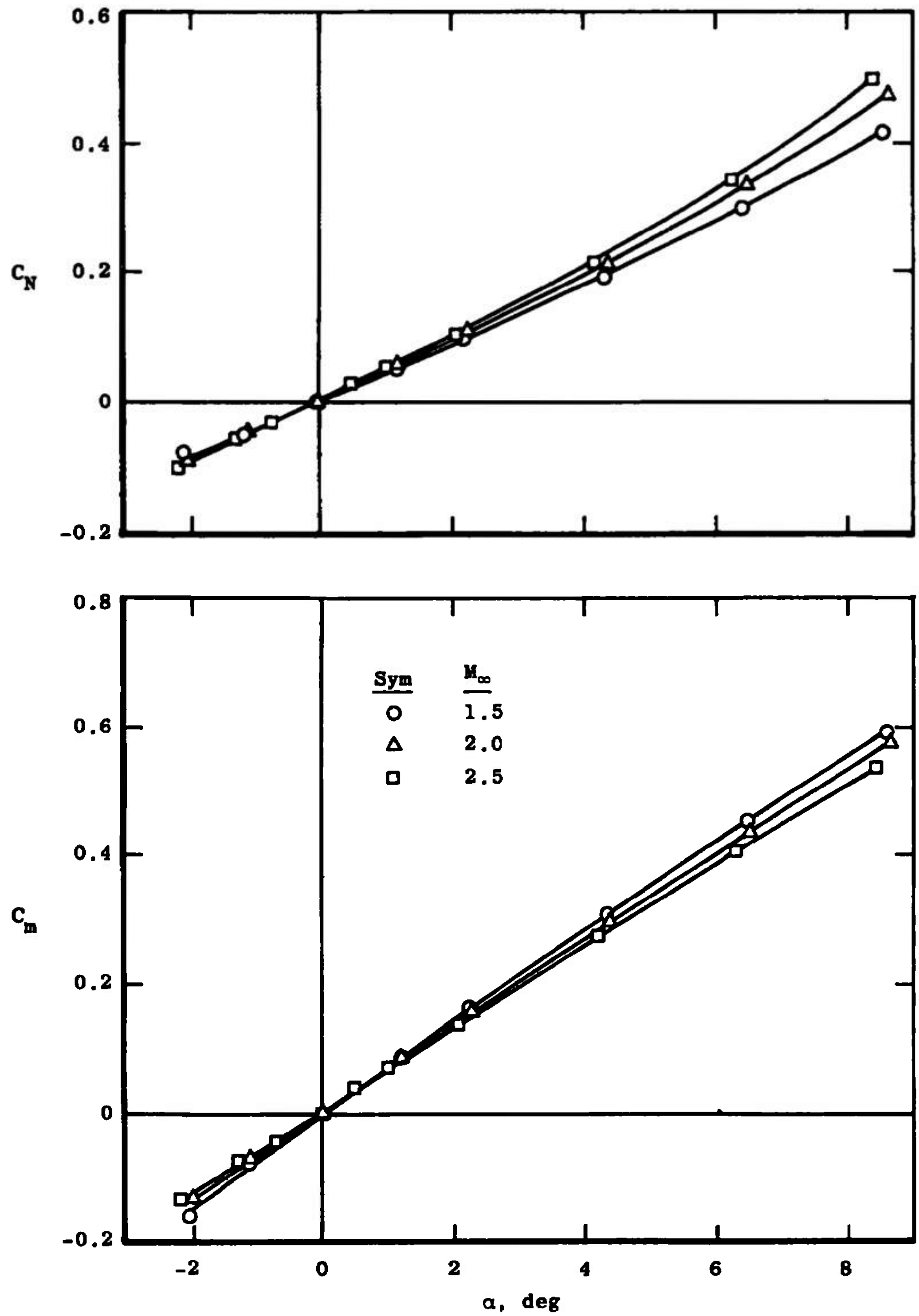

b. With Straight Vanes
Fig. 6 Continued

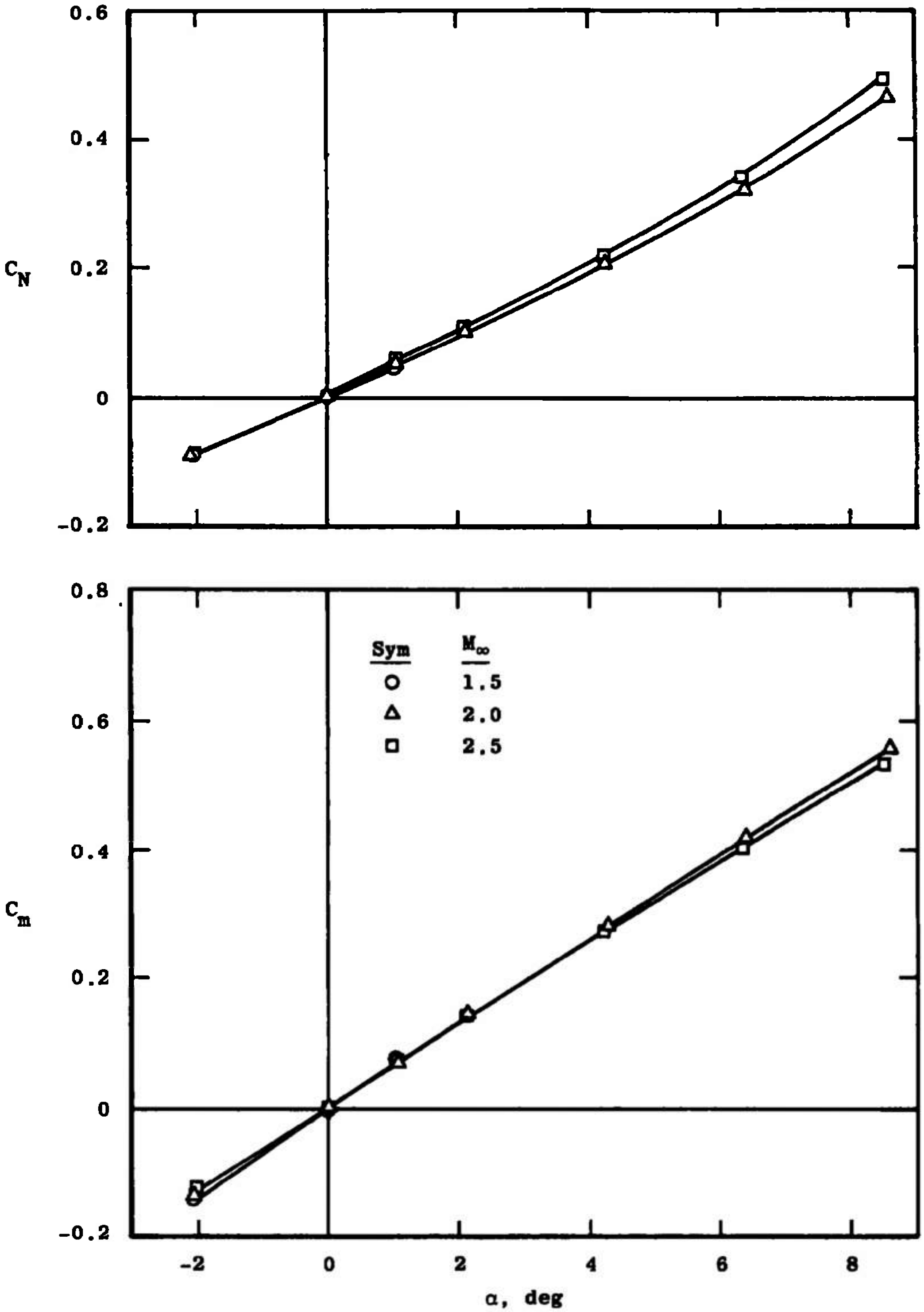

c. With Canted Vanes
Fig. 6 Concluded

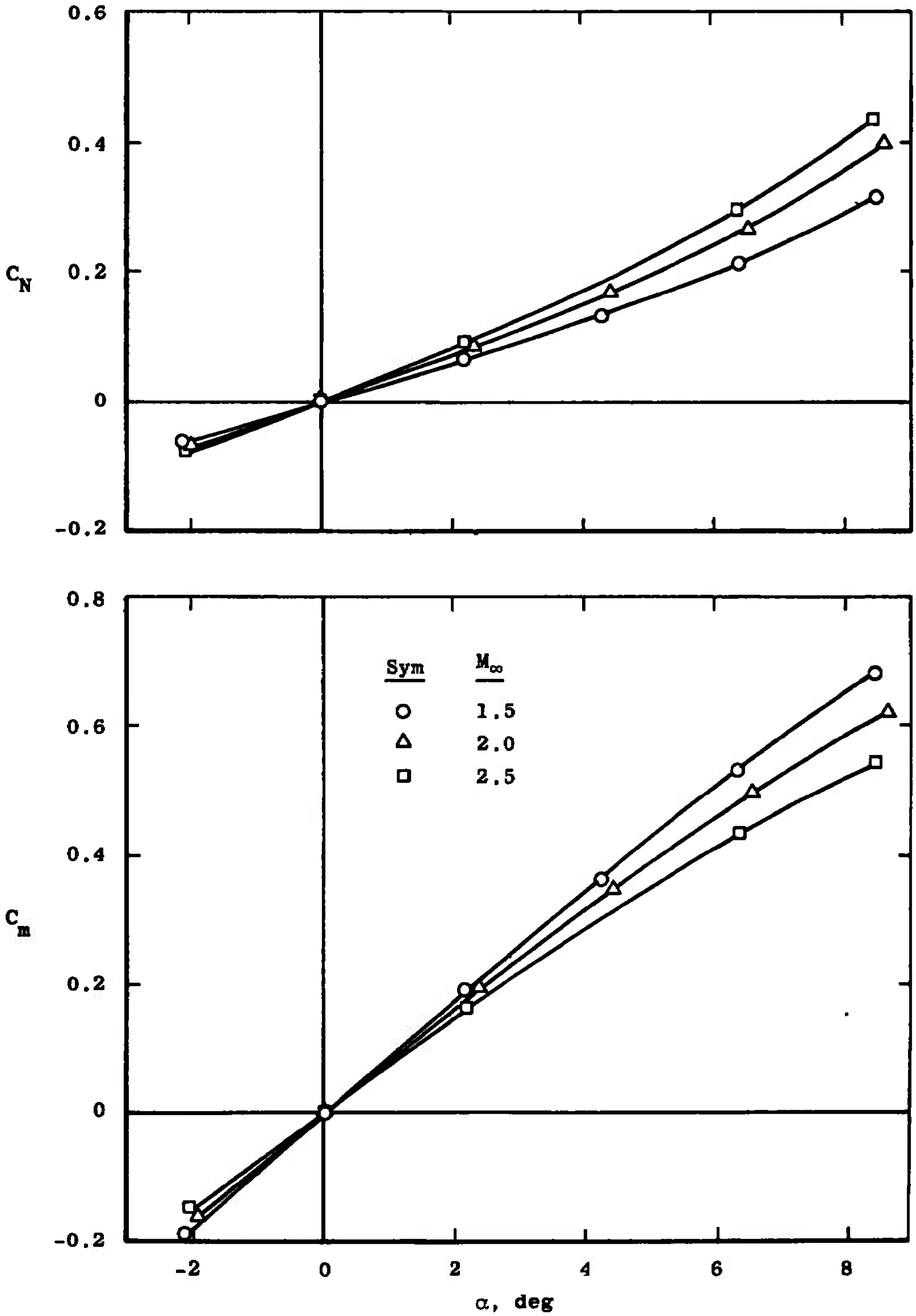

Fig. 7 Variation of C_N and C_m with Angle of Attack, Configuration 3, without Vanes

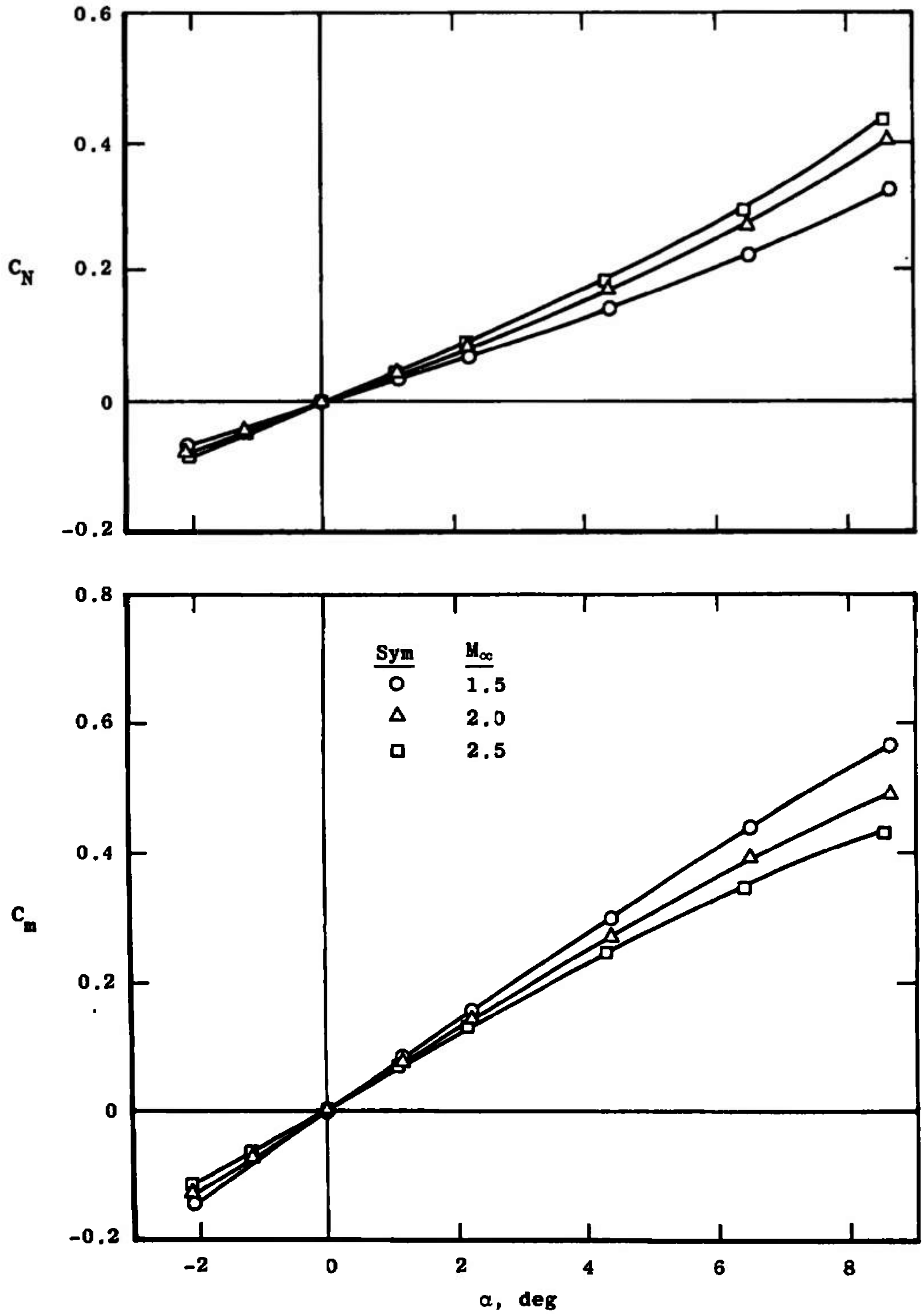

Fig. 8 Variation of C_N and C_m with Angle of Attack, Configuration 4, without Vanes

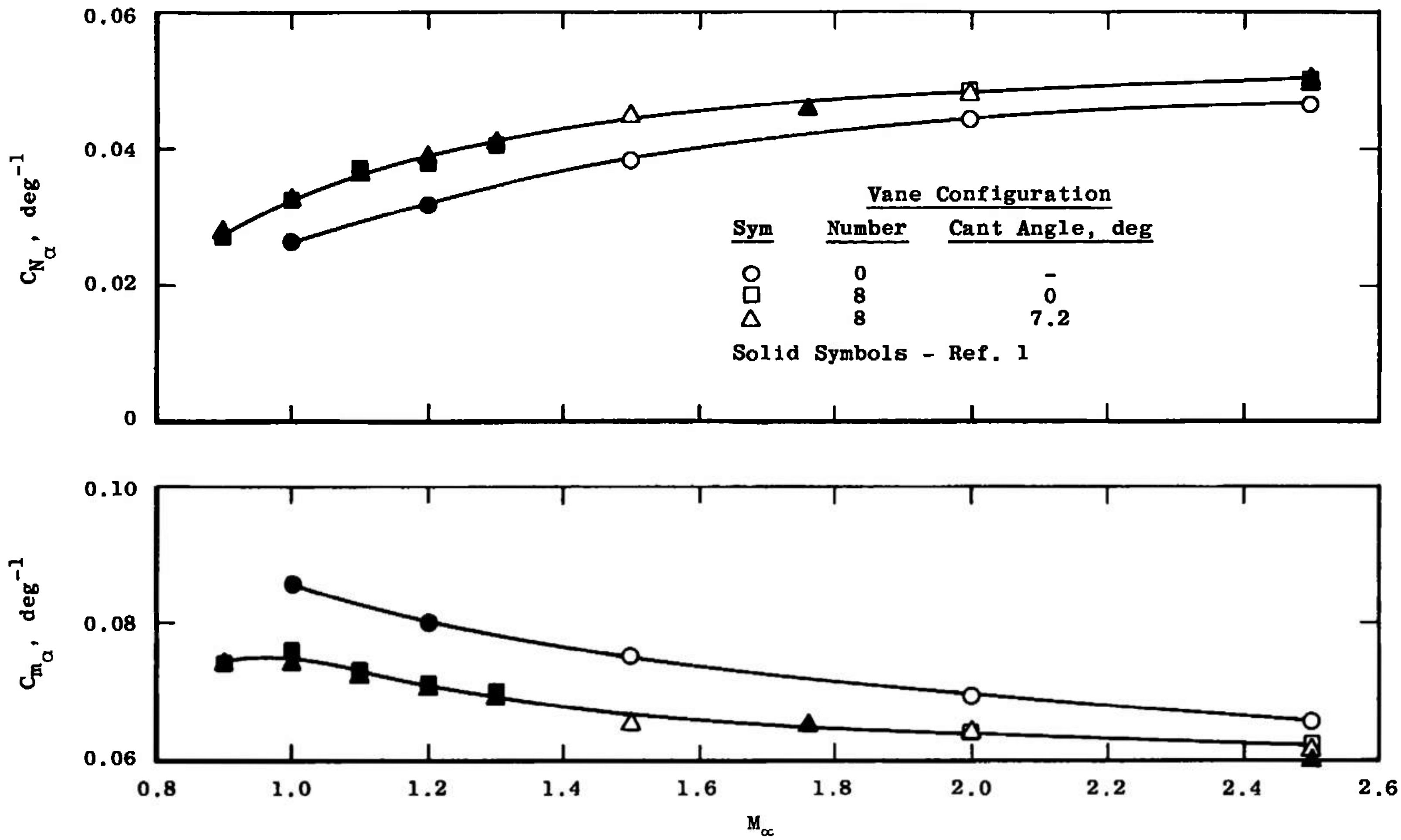

a. Configuration 0

Fig. 9 Variation of $C_{N\alpha}$ and $C_{m\alpha}$ with Mach Number

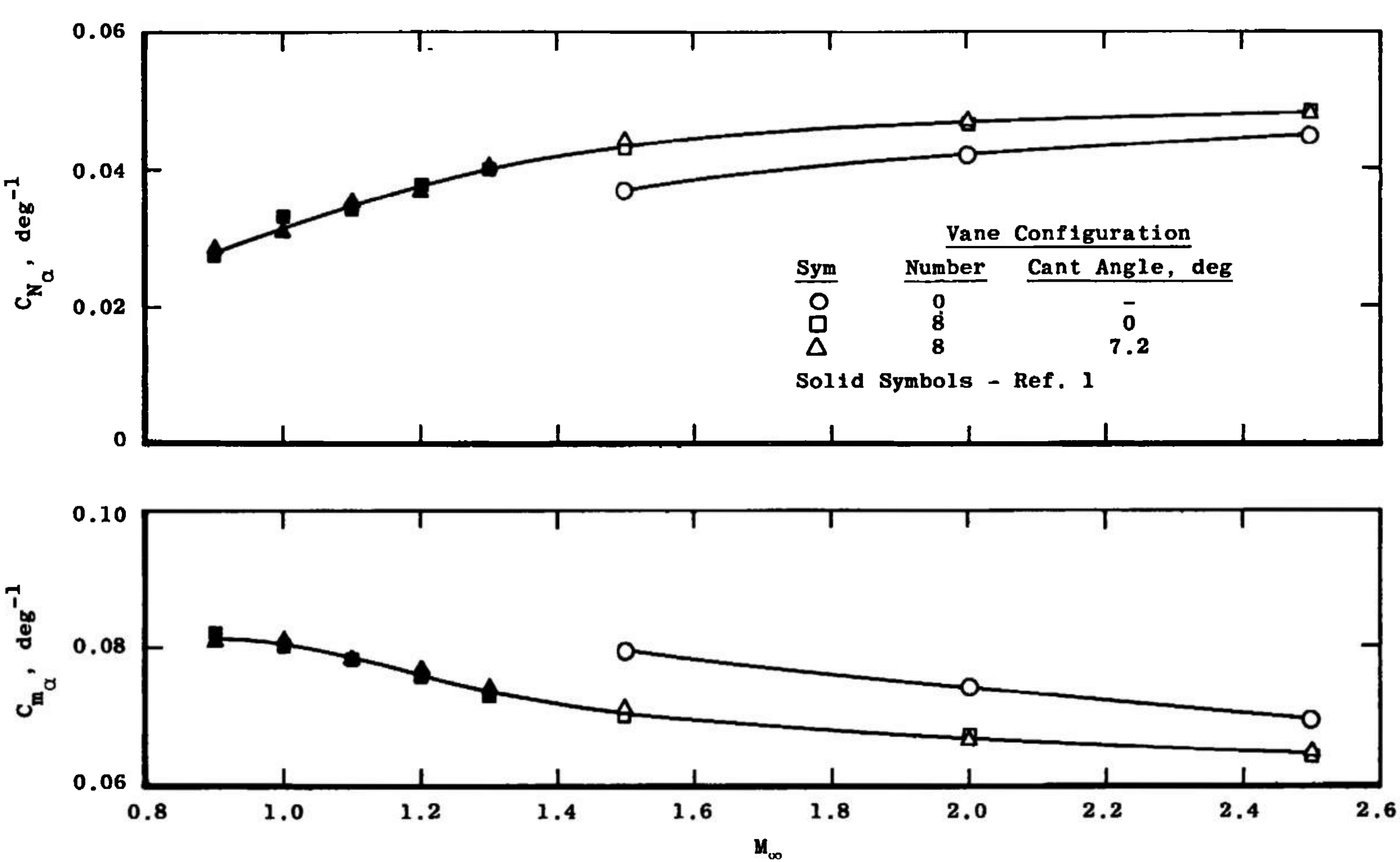

b. Configuration 2
Fig. 9 Continued

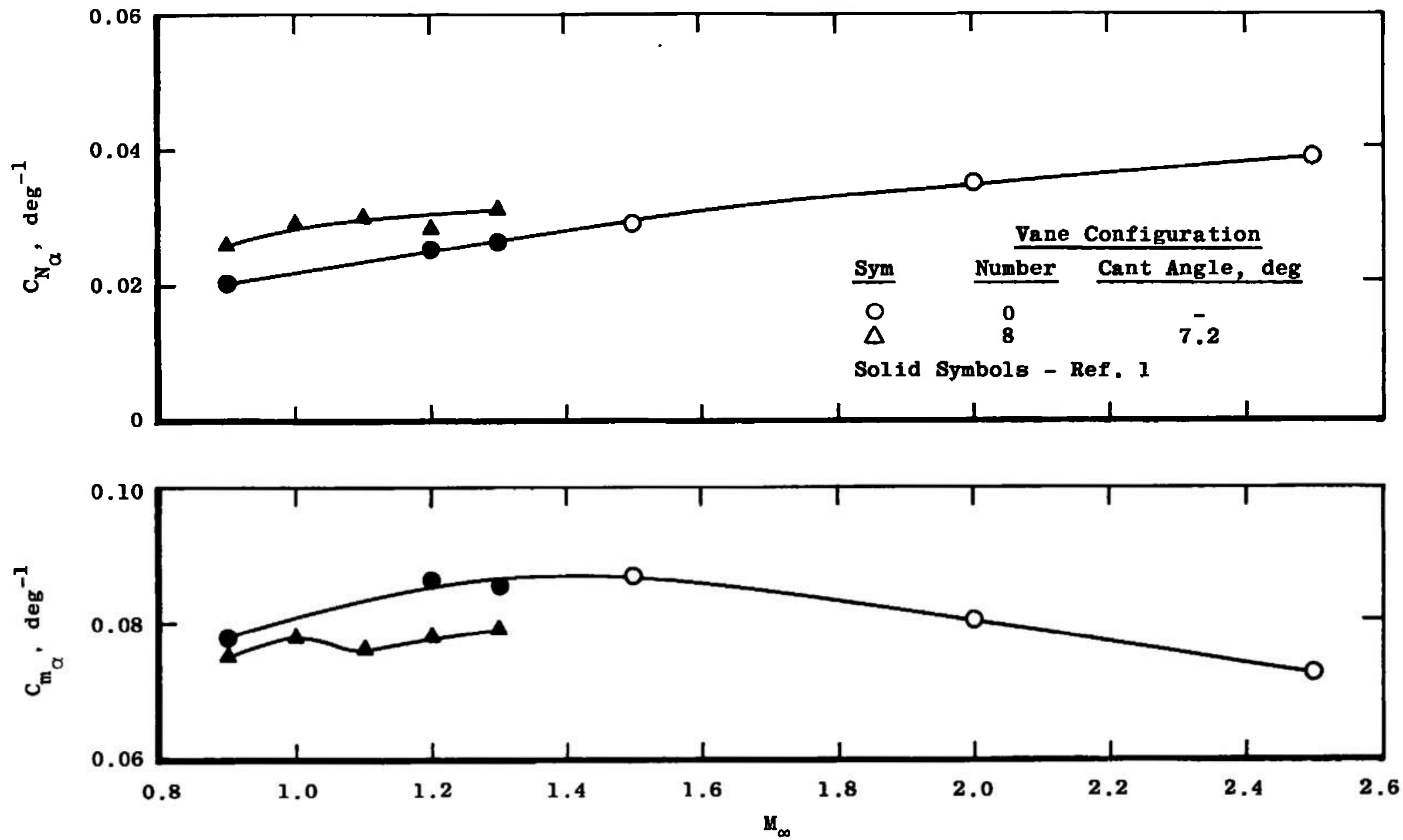

c. Configuration 3
Fig. 9 Continued

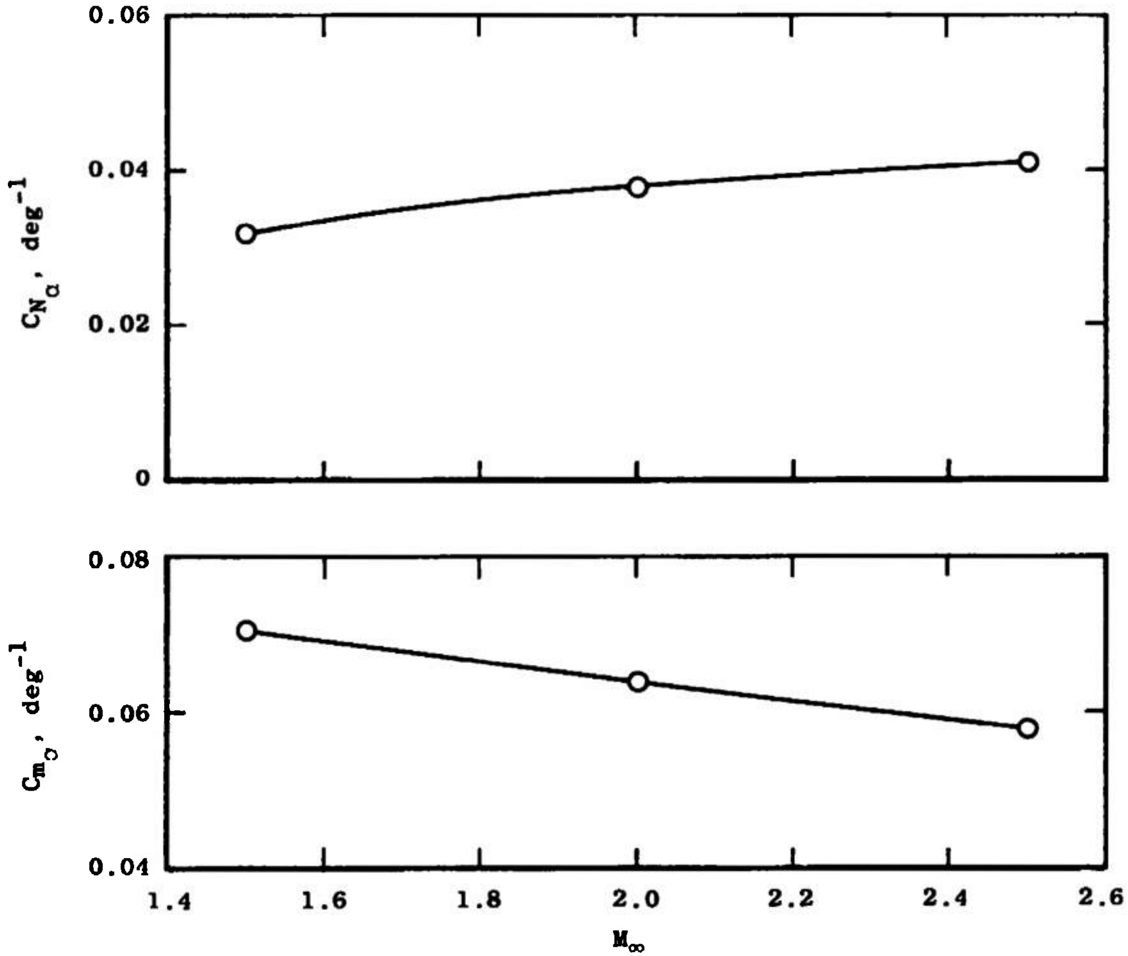

d. Configuration 4
Fig. 9 Concluded

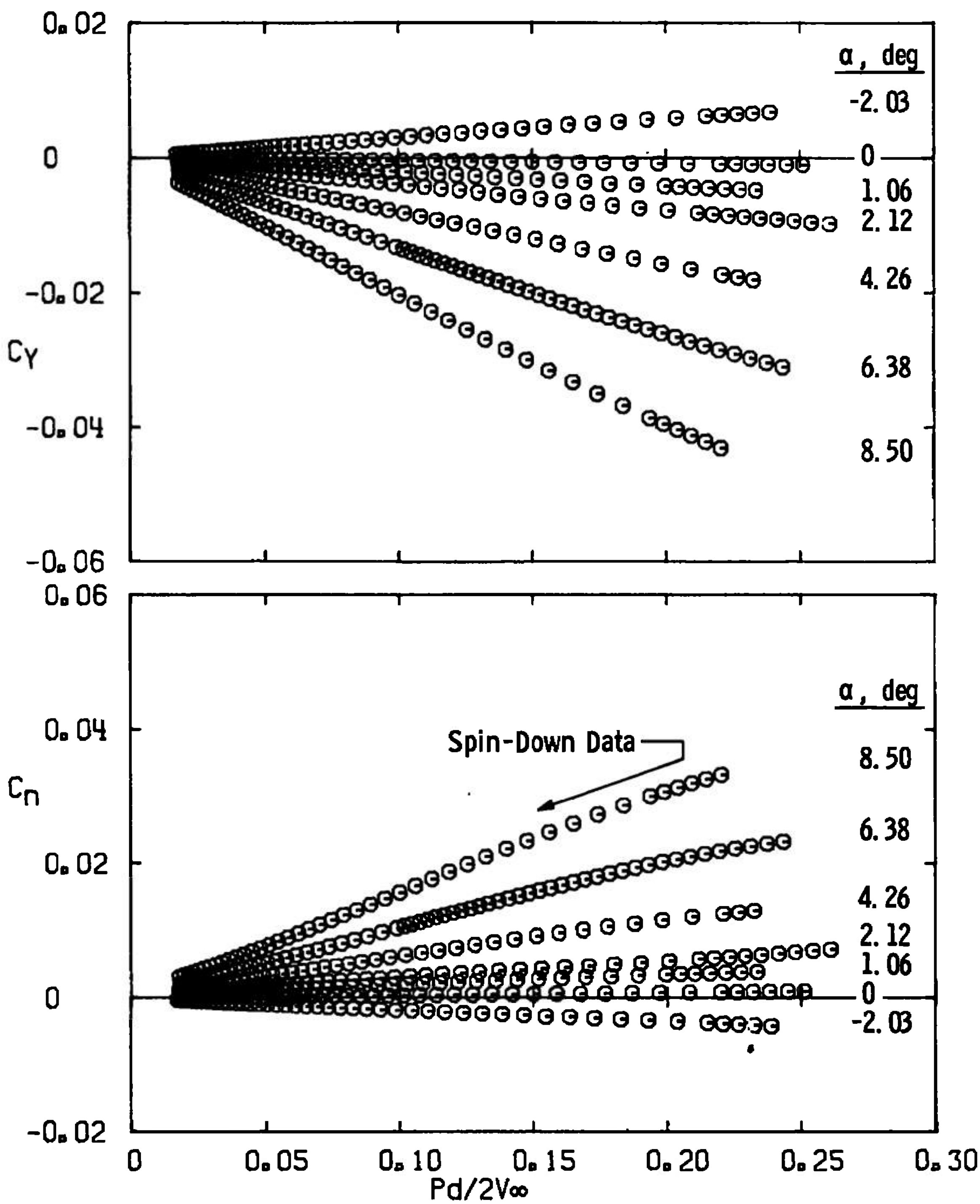

a. Without Vanes

Fig. 10 Typical Variation of C_Y and C_n with $pd/2V_\infty$, Configuration 0, $M_\infty = 1.5$

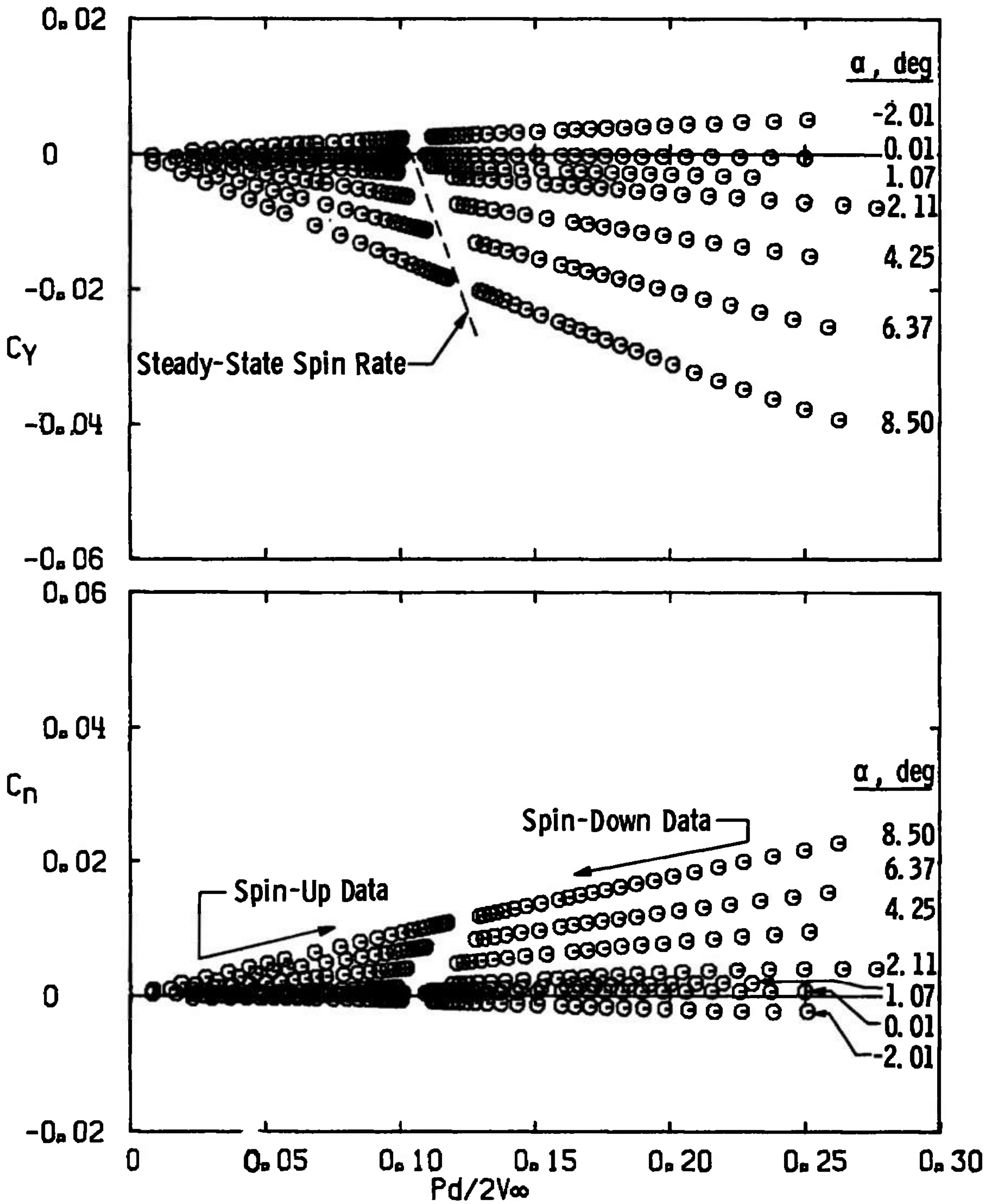

b. With Canted Vanes
Fig. 10 Concluded

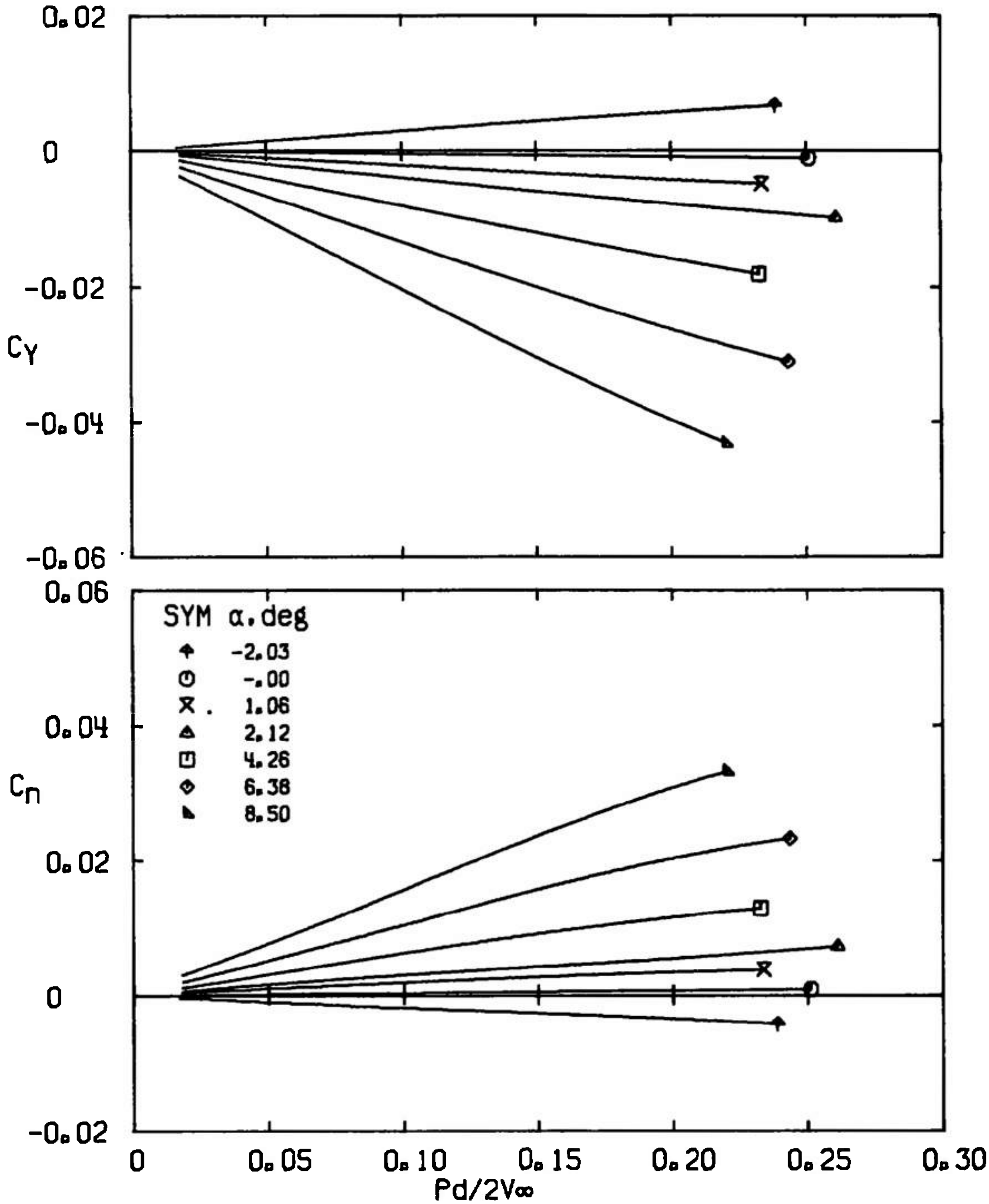

a. $M_\infty = 1.5$

Fig. 11 Variation of C_Y and C_n with $pd/2V_\infty$ for Configuration 0 without Vanes

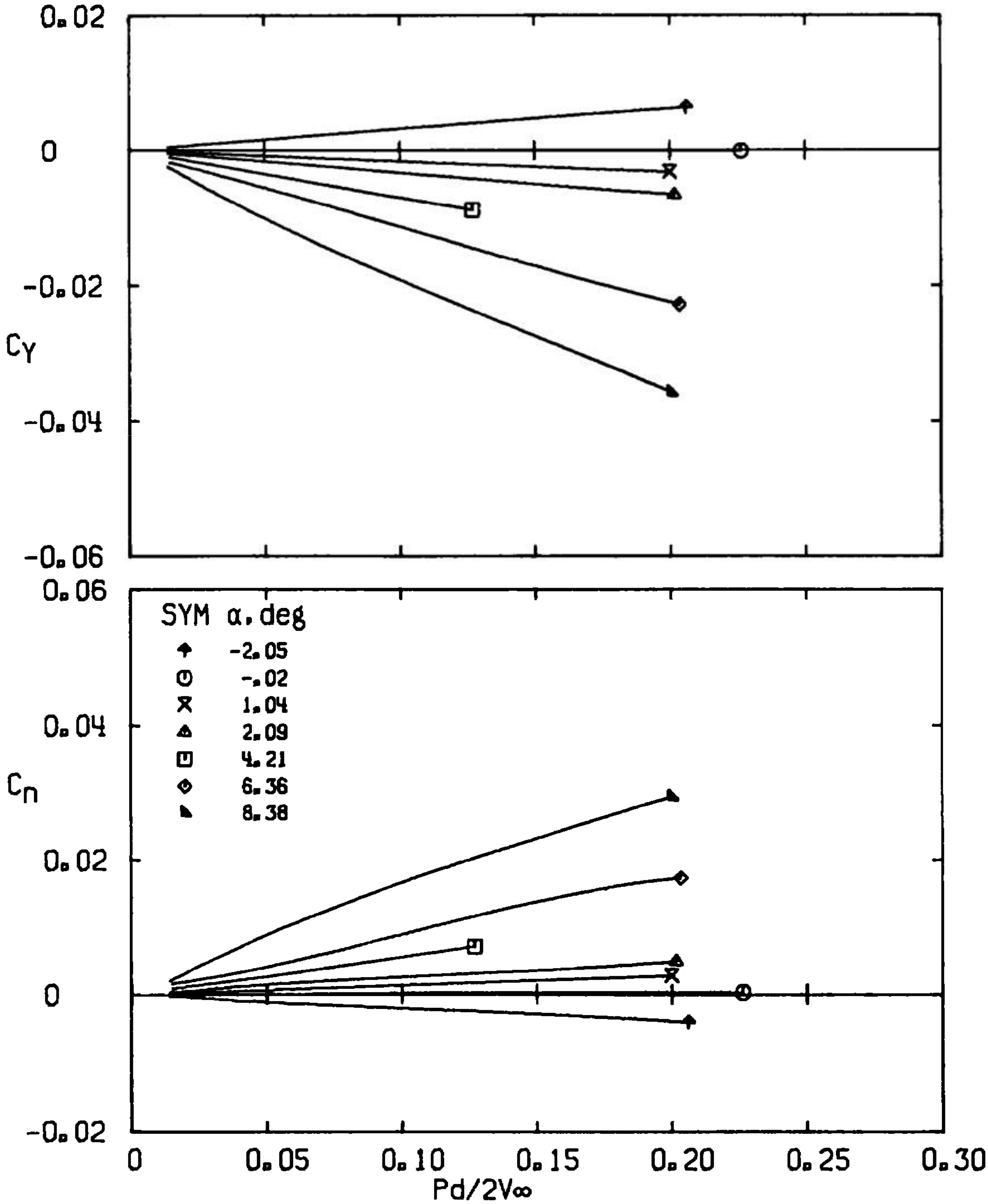

b. M_∞ = 2.0
Fig. 11 Continued

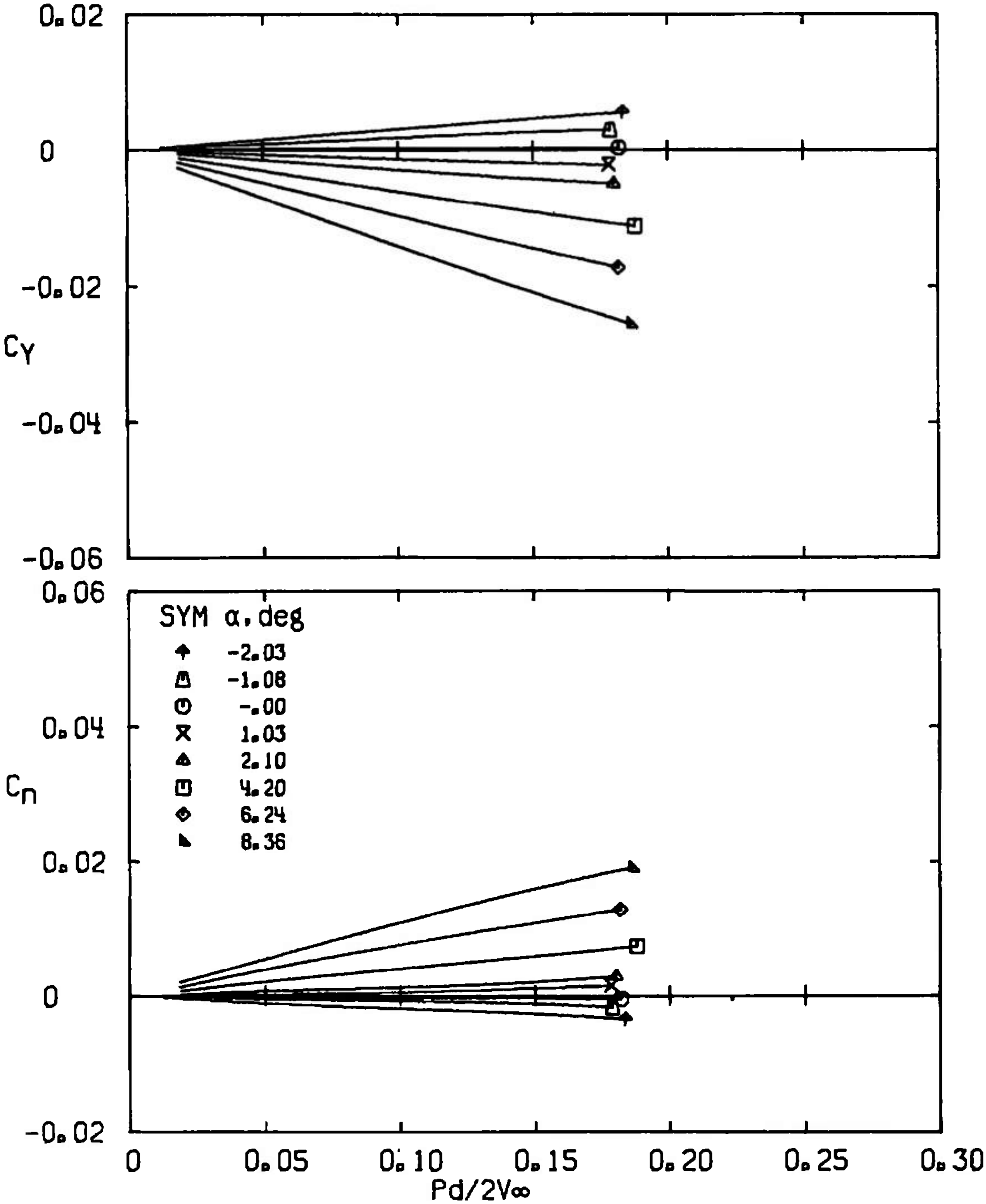

c. $M_\infty = 2.5$
Fig. 11 Concluded

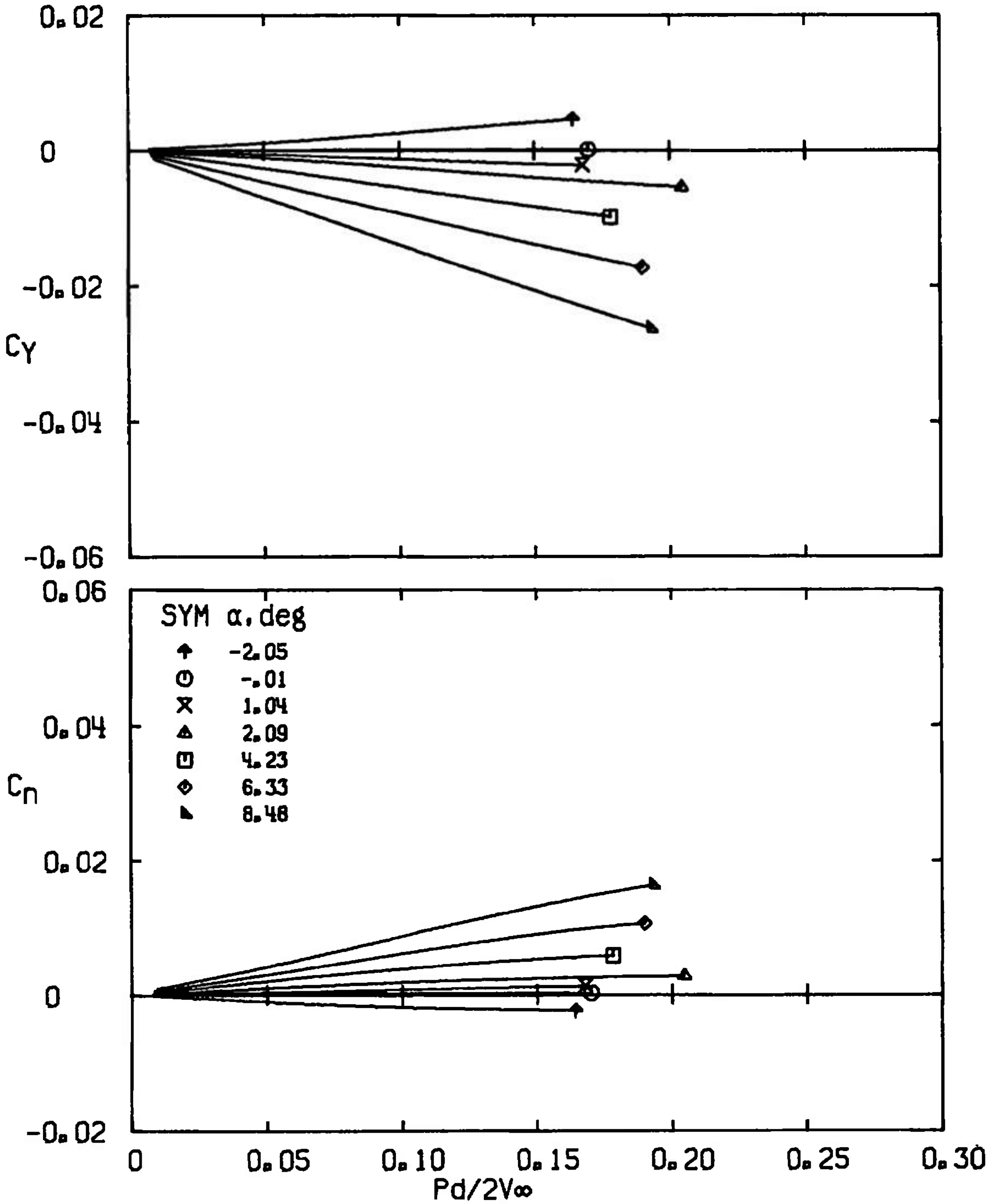

a. $M_\infty = 2.0$

Fig. 12 Variation of C_Y and C_n with $pd/2V_\infty$ for Configuration 0 with Straight Vanes

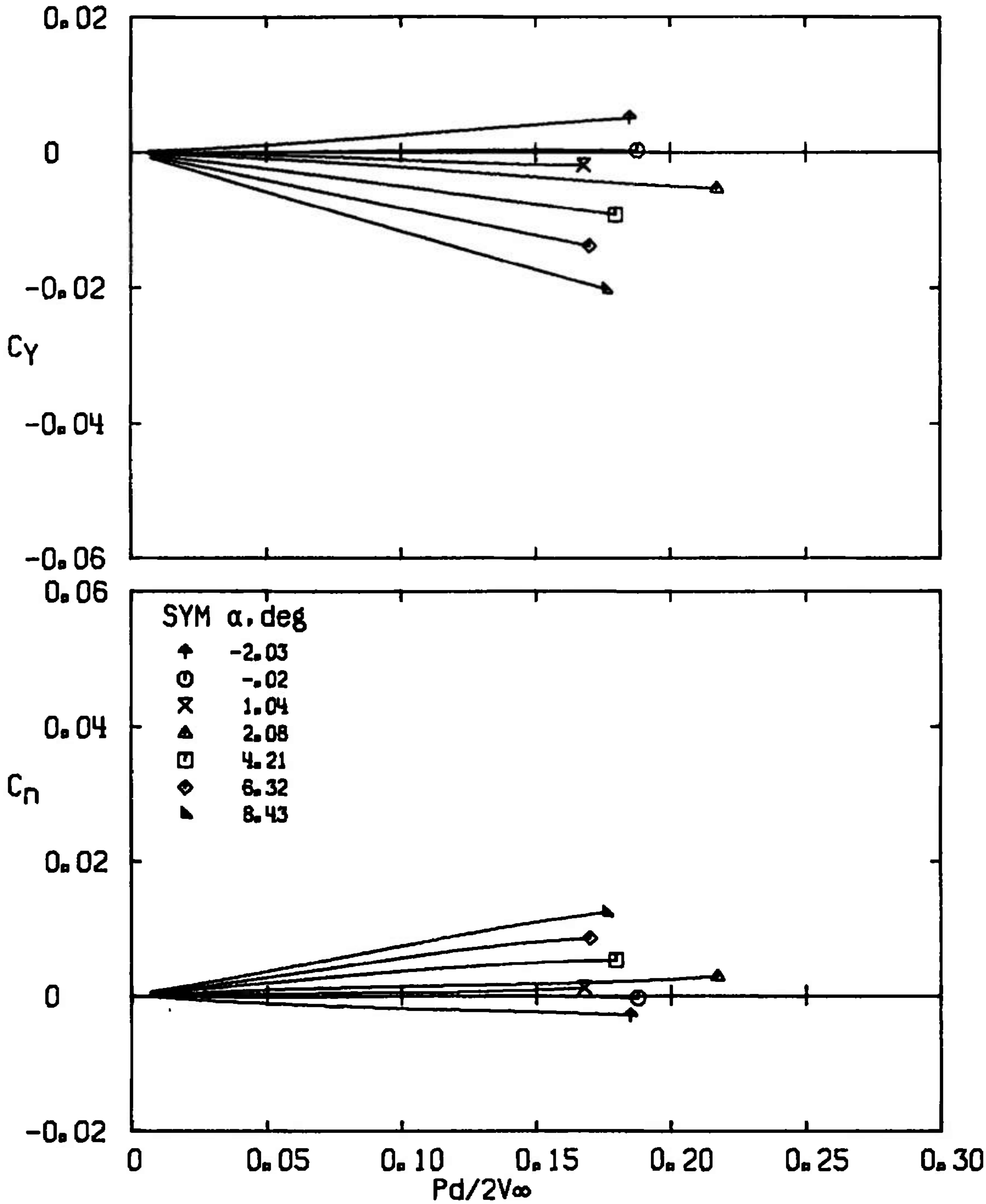

b. $M_\infty = 2.5$
Fig. 12 Concluded

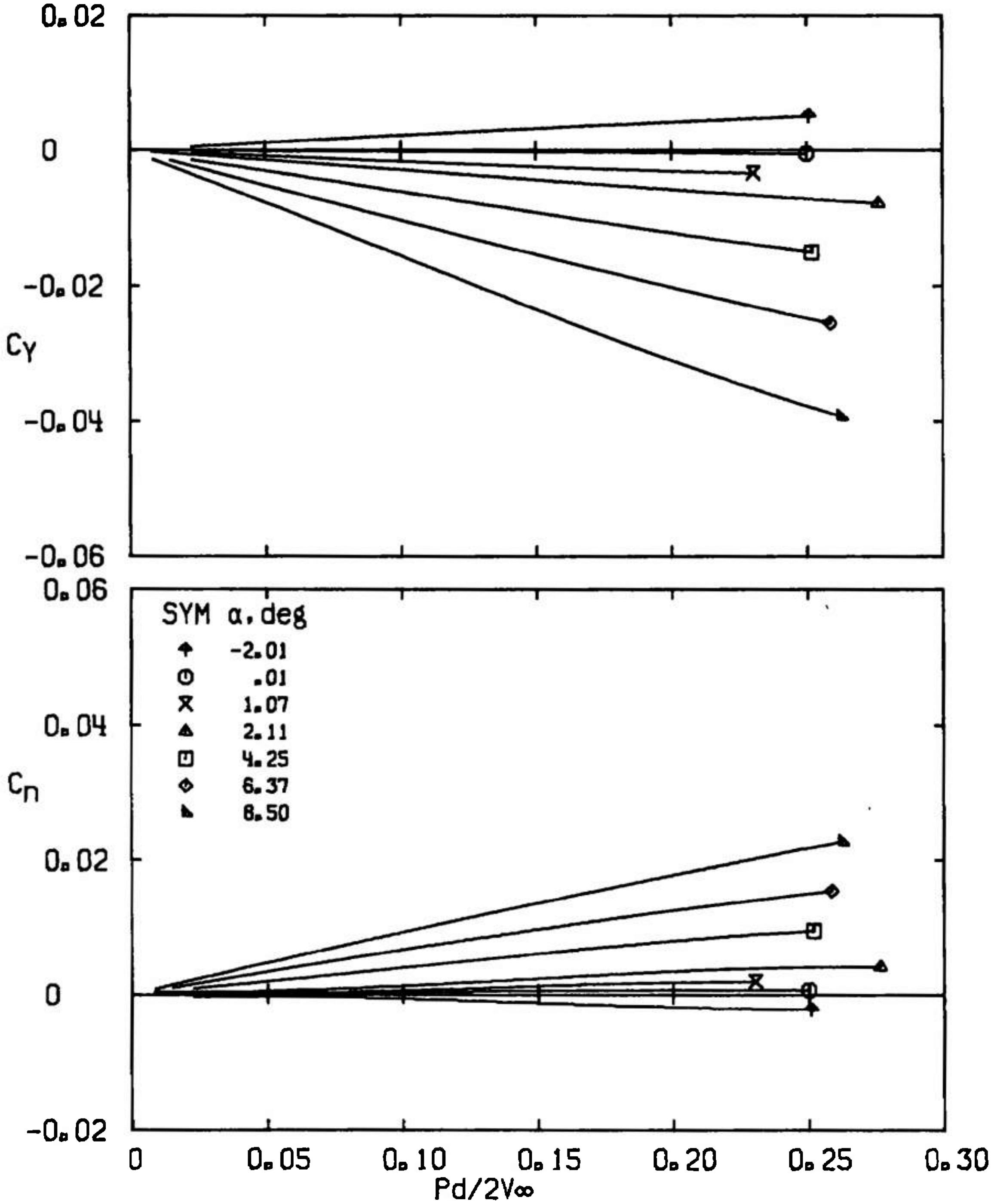

a. $M_\infty = 1.5$

Fig. 13 Variation of C_Y and C_n with $pd/2V_\infty$ for Configuration 0 with Canted Vanes

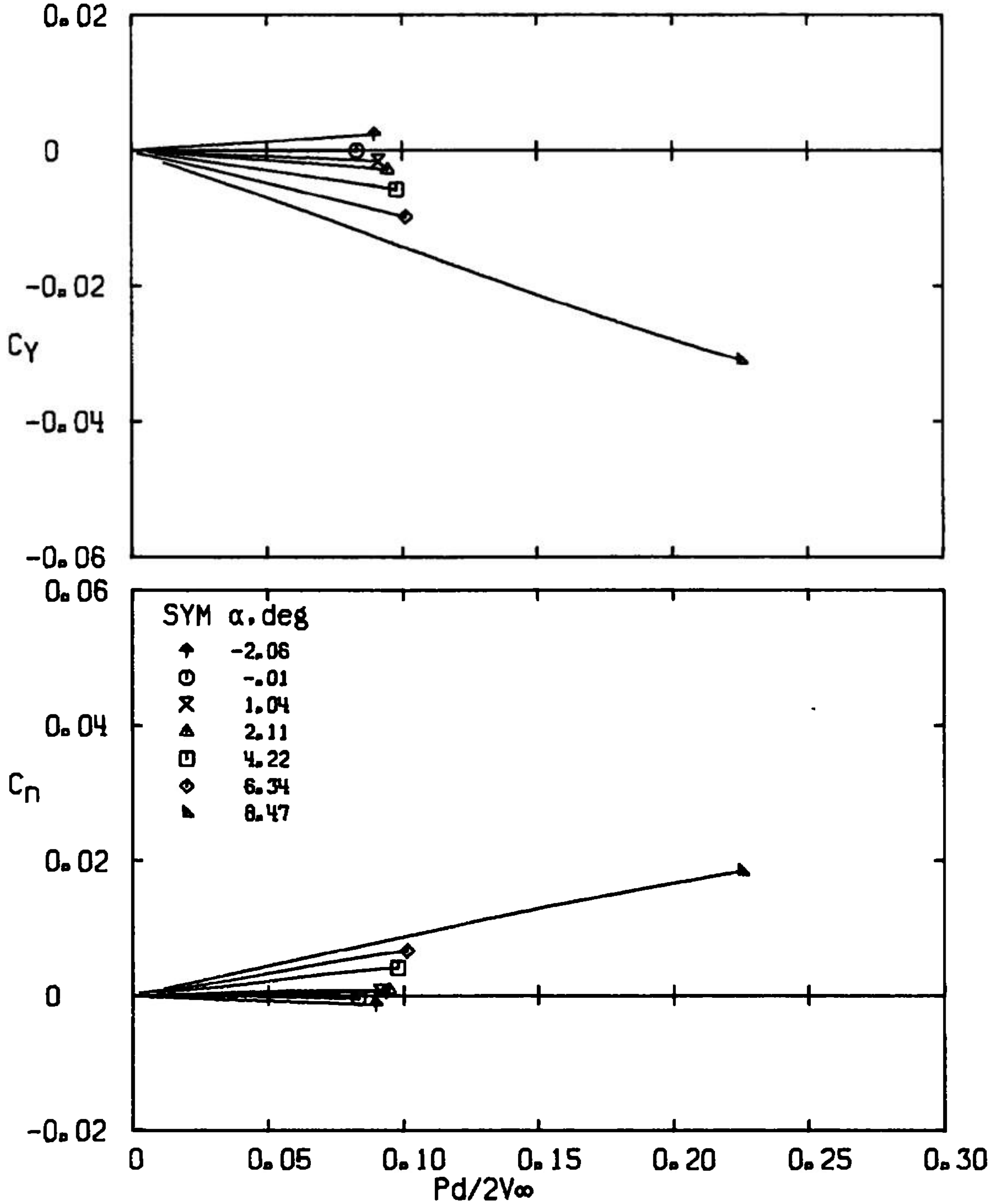

b. $M_\infty = 2.0$
Fig. 13 Continued

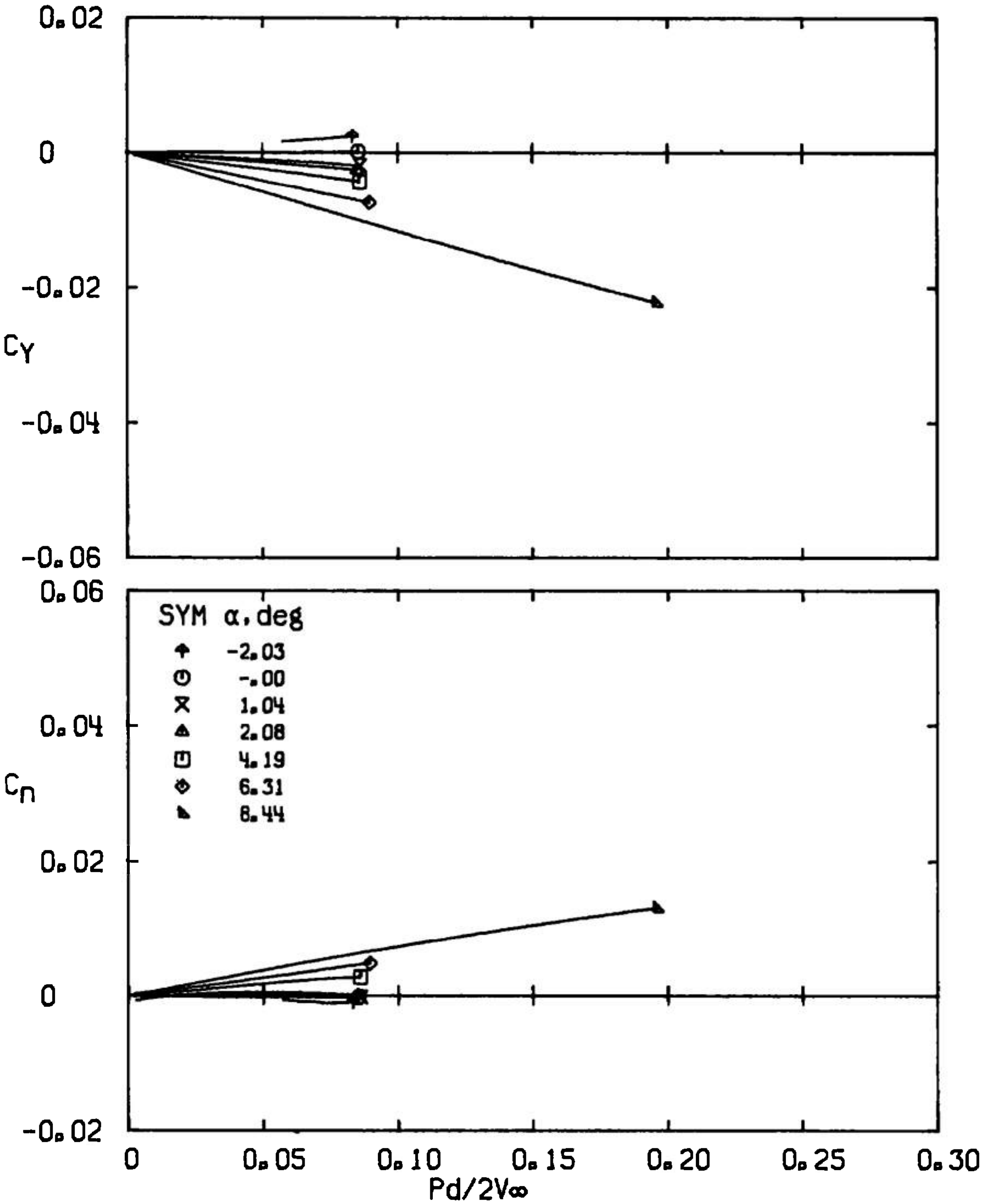

c. M_∞ = 2.5
Fig. 13 Concluded

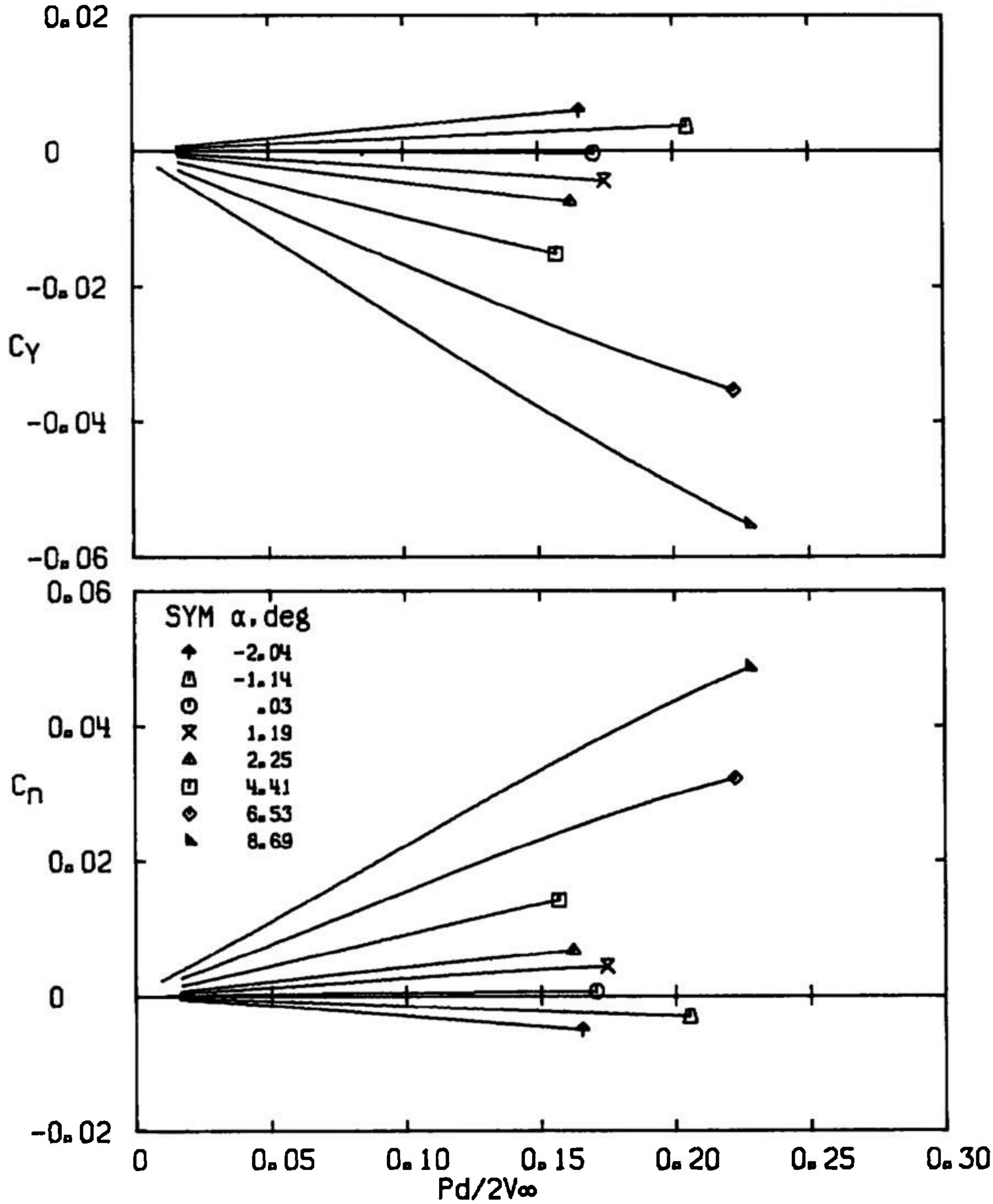

a. $M_\infty = 1.5$

Fig. 14 Variation of C_Y and C_n with $pd/2V_\infty$ for Configuration 2 without Vanes

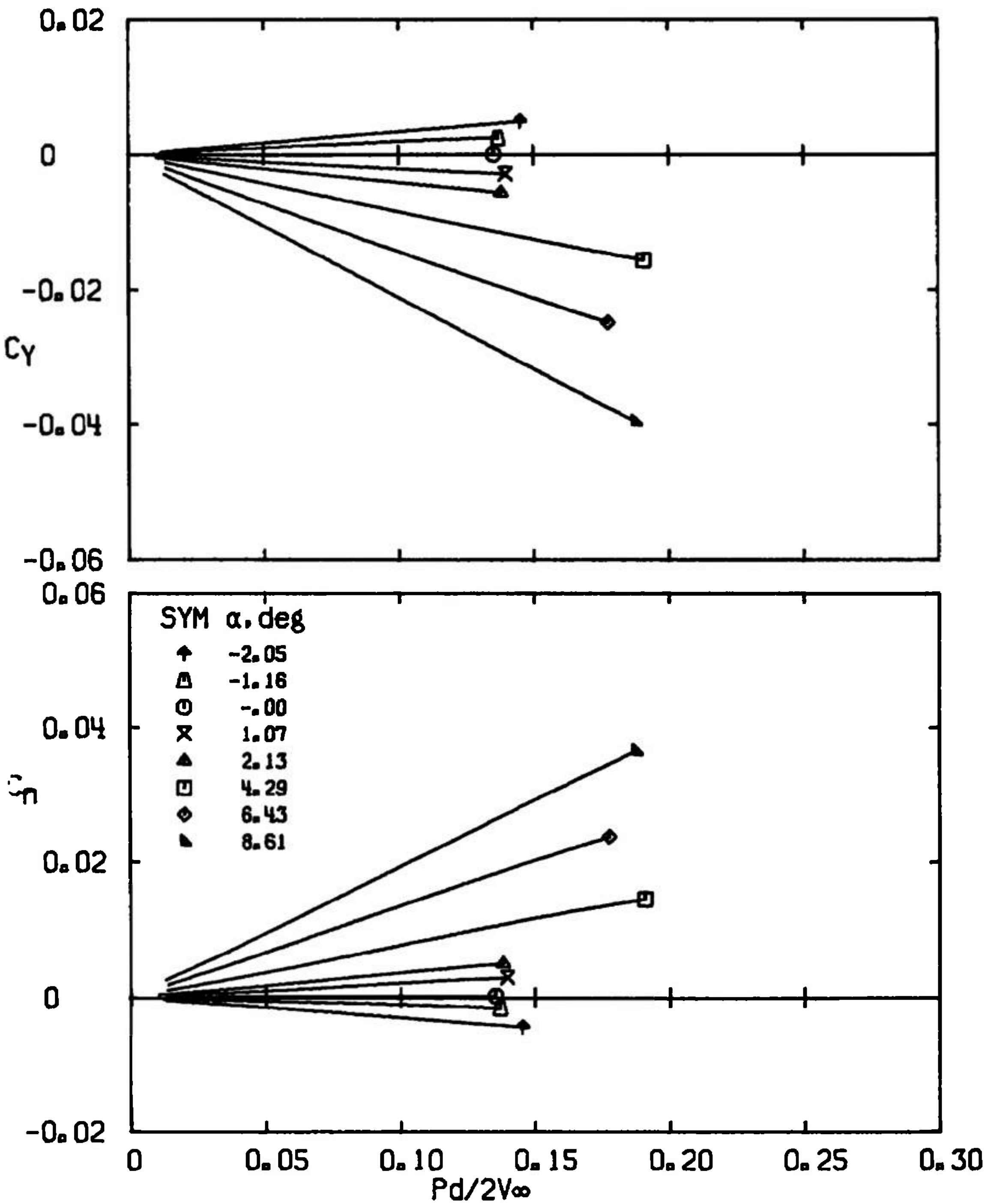

b. $M_\infty = 2.0$
Fig. 14 Continued

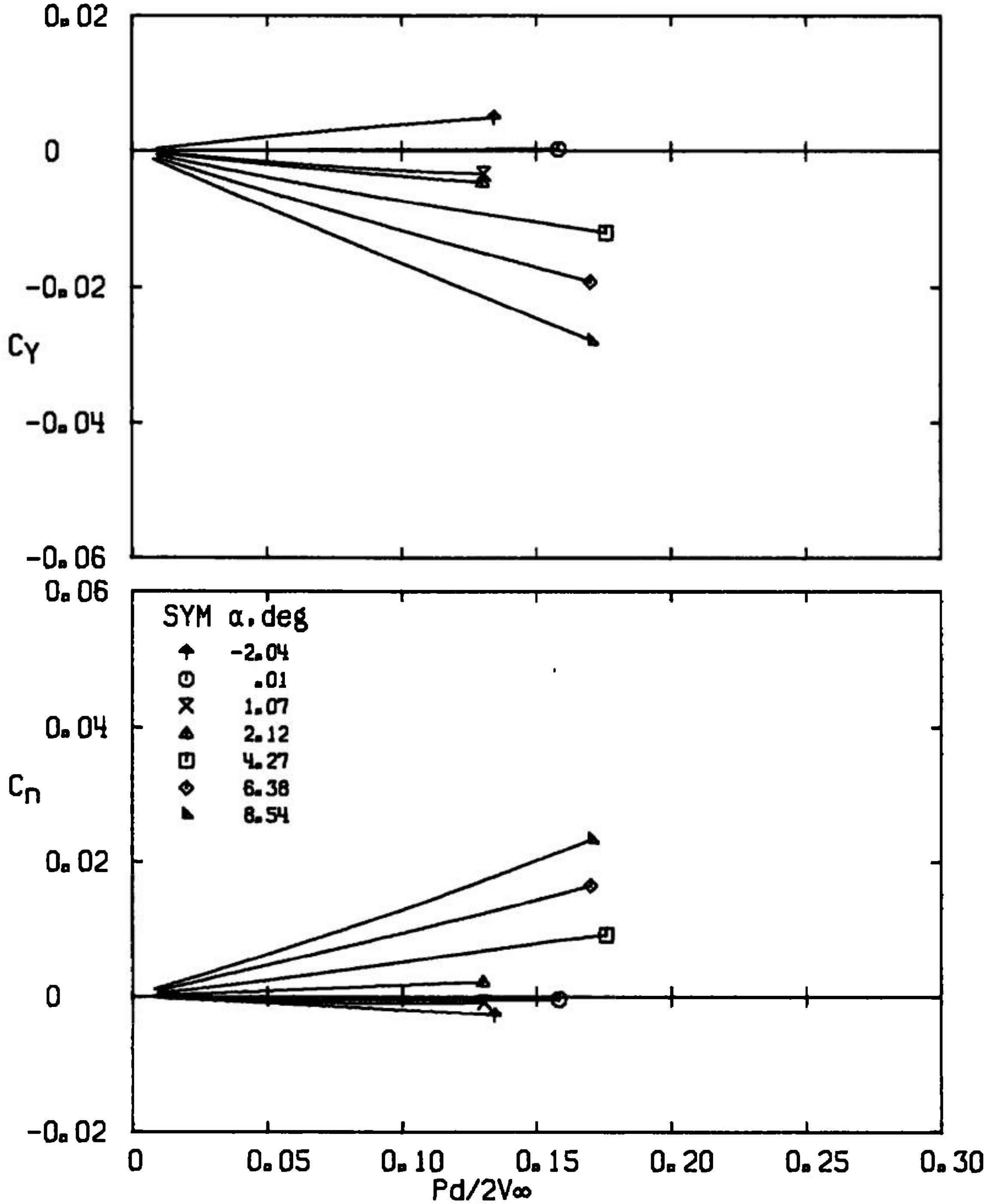

c. $M_\infty = 2.5$
Fig. 14 Concluded

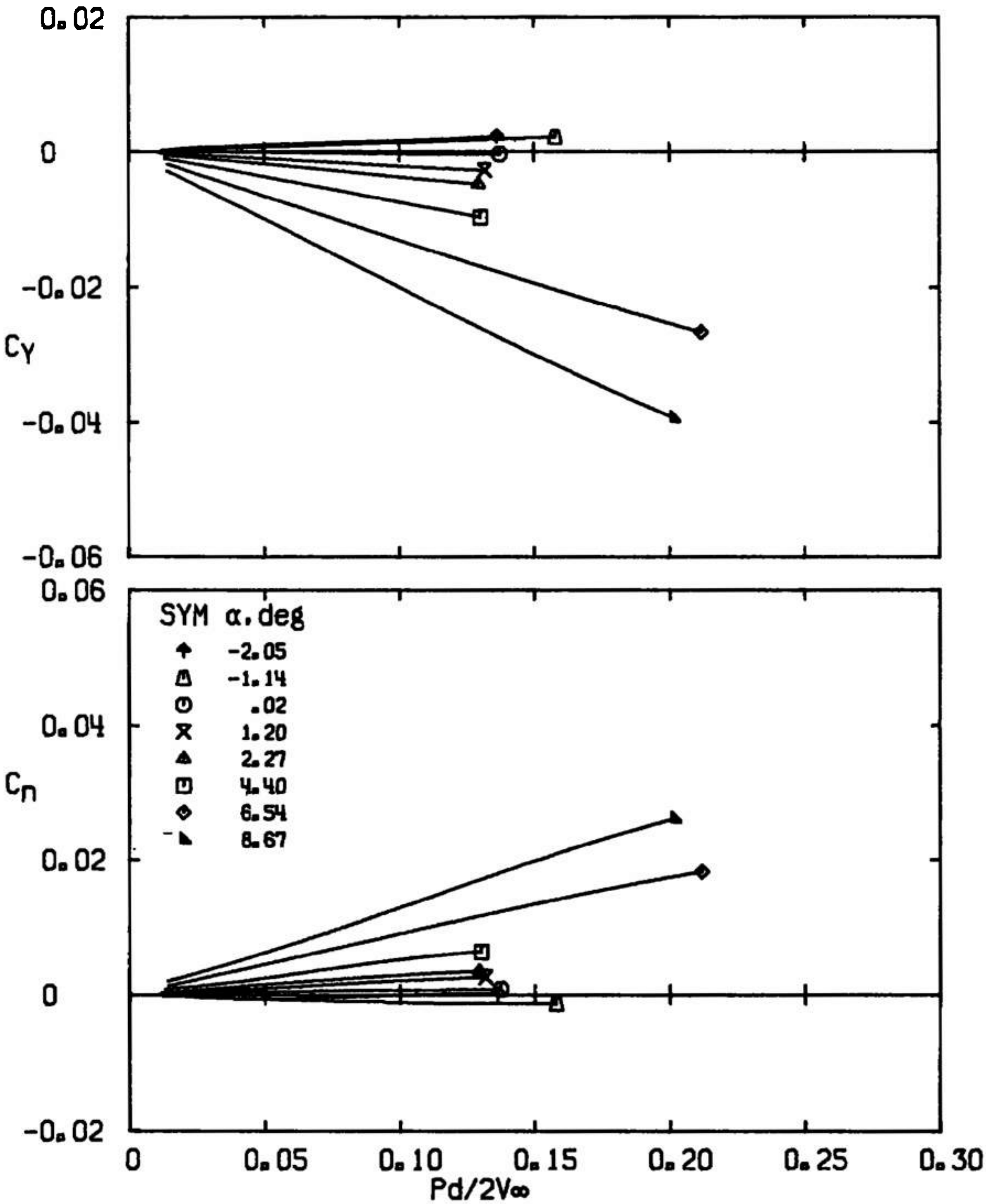

a. $M_\infty = 1.5$

Fig. 15 Variation of C_Y and C_n with $pd/2V_\infty$ for Configuration 2 with Straight Vanes

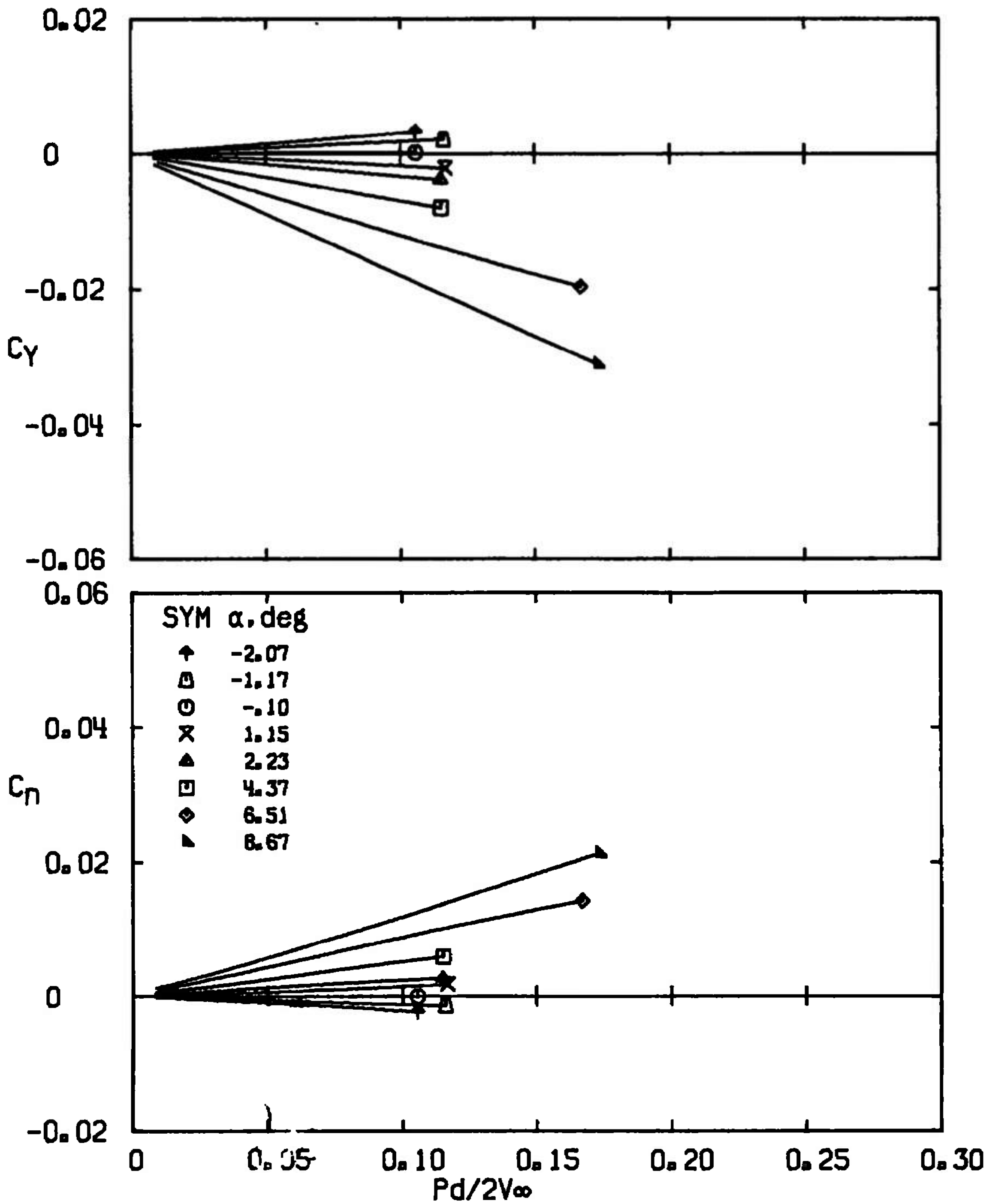

b. $M_\infty = 2.0$
Fig. 15 Continued

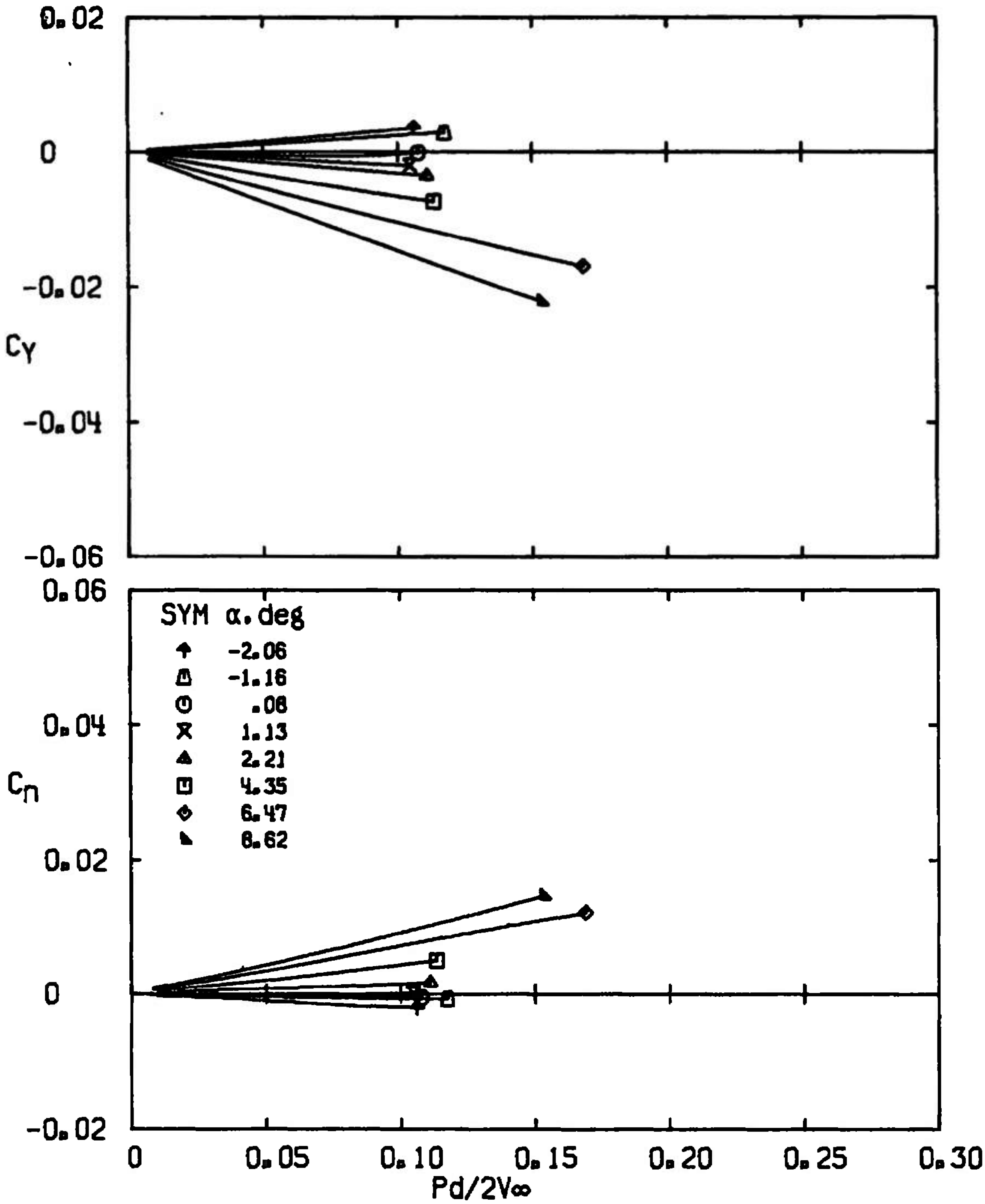

c. $M_\infty = 2.5$
Fig. 15 Concluded

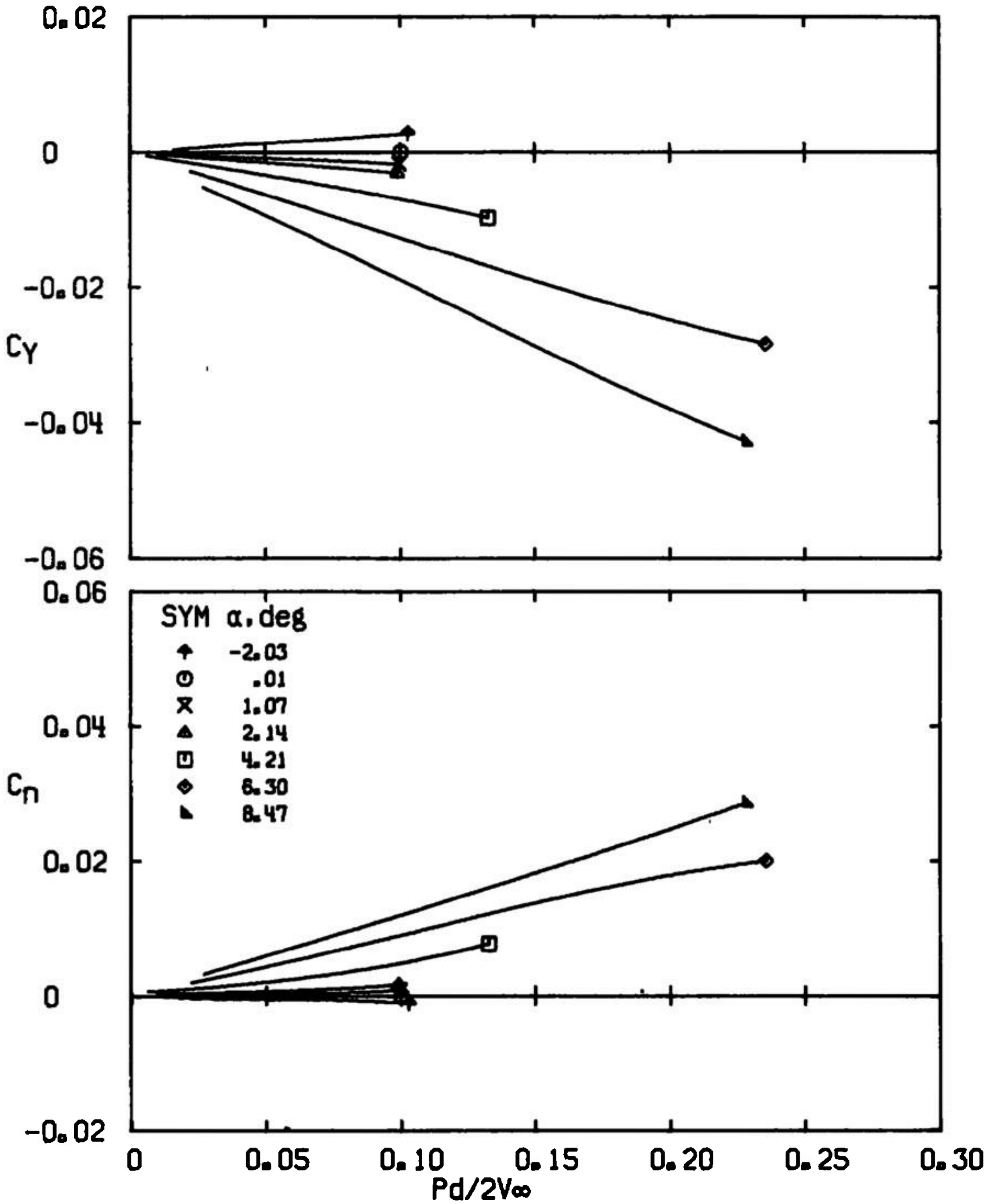

a. $M_\infty = 1.5$

Fig. 16 Variation of C_Y and C_n with $pd/2V_\infty$ for Configuration 2 with Canted Vanes

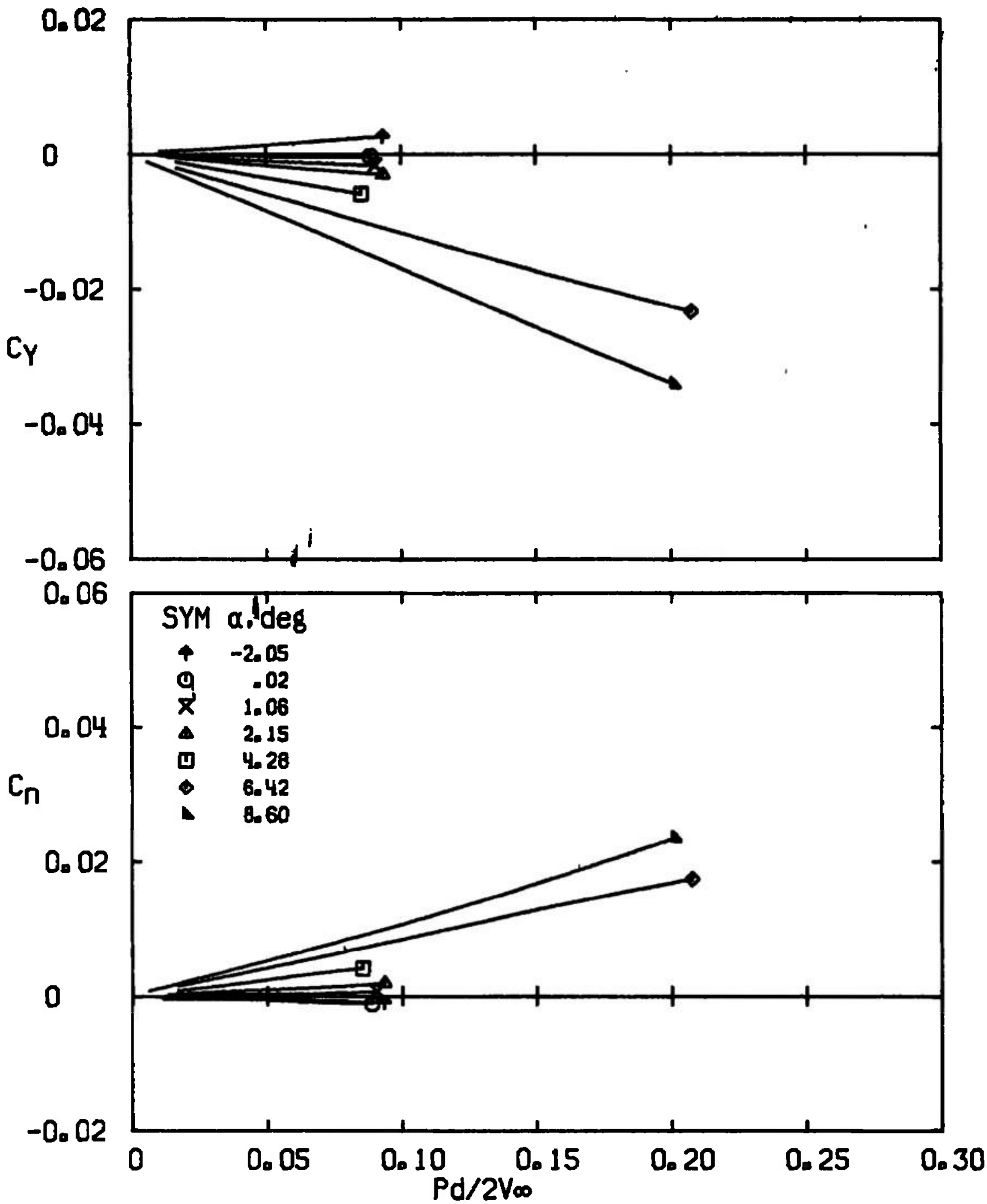

b. M_∞ = 2.0
Fig. 16 Continued

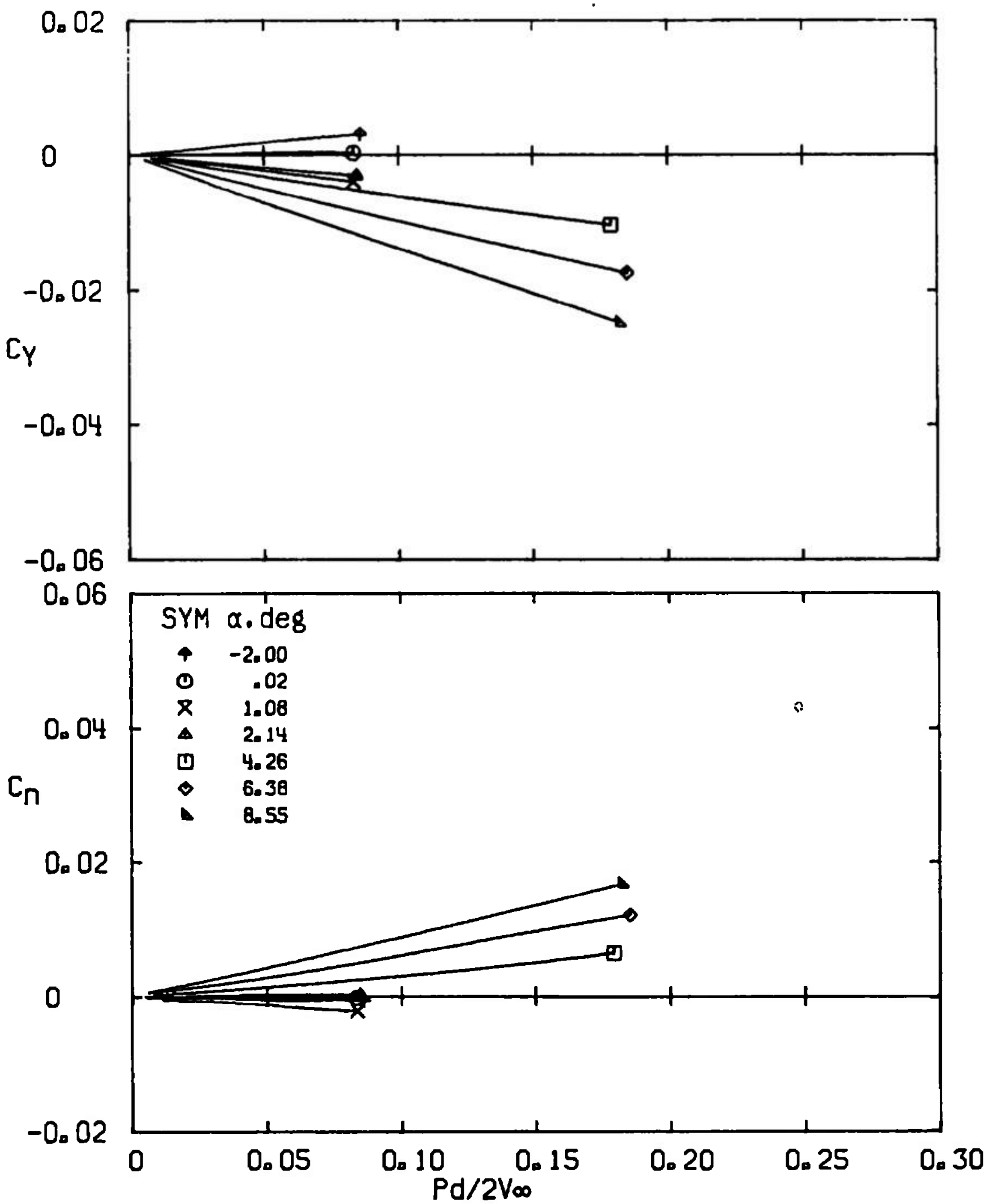

c. $M_\infty = 2.5$
Fig. 16 Concluded

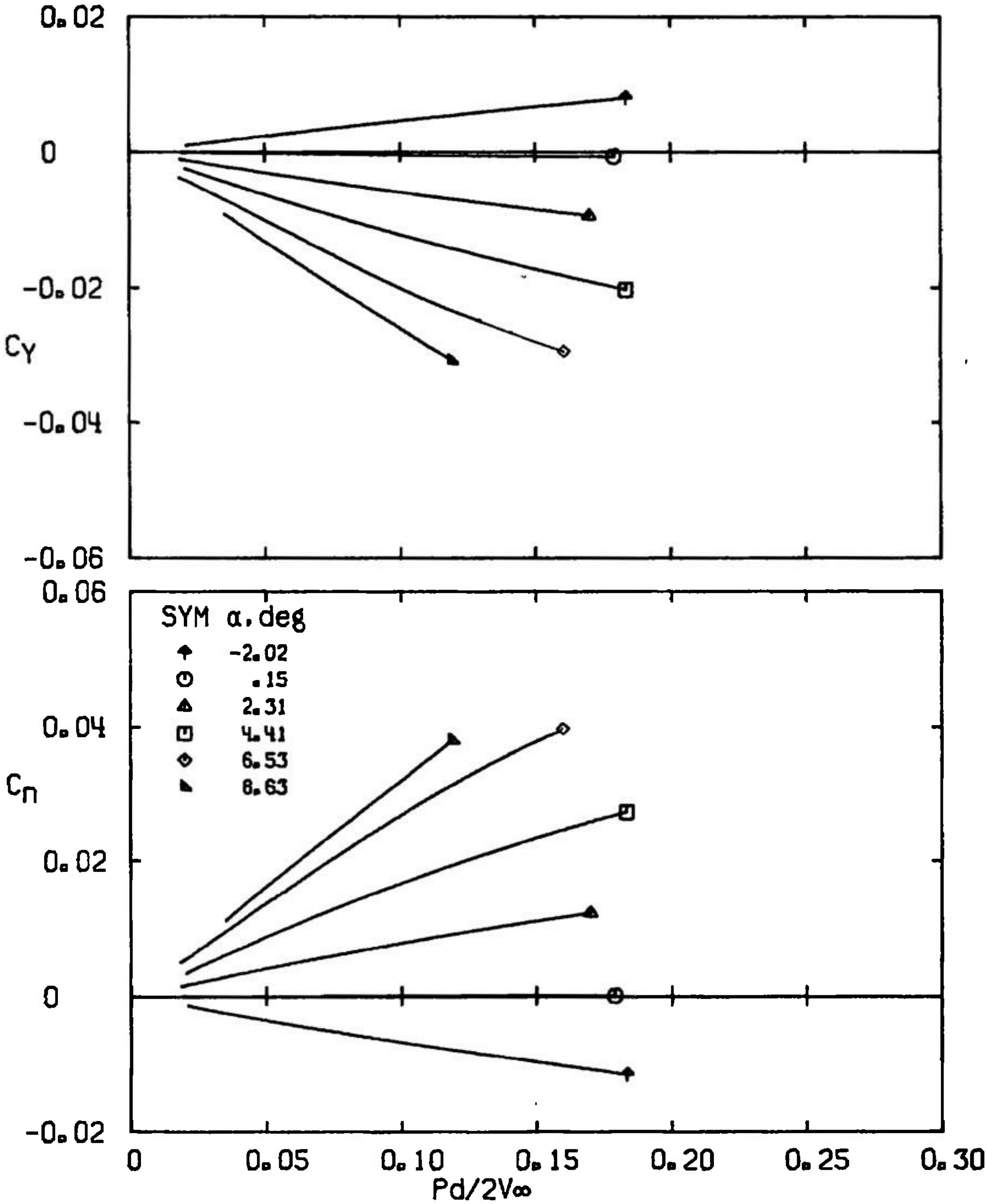

a. $M_\infty = 1.5$

Fig. 17 Variation of C_Y and C_n with $pd/2V_\infty$ for Configuration 3 without Vanes

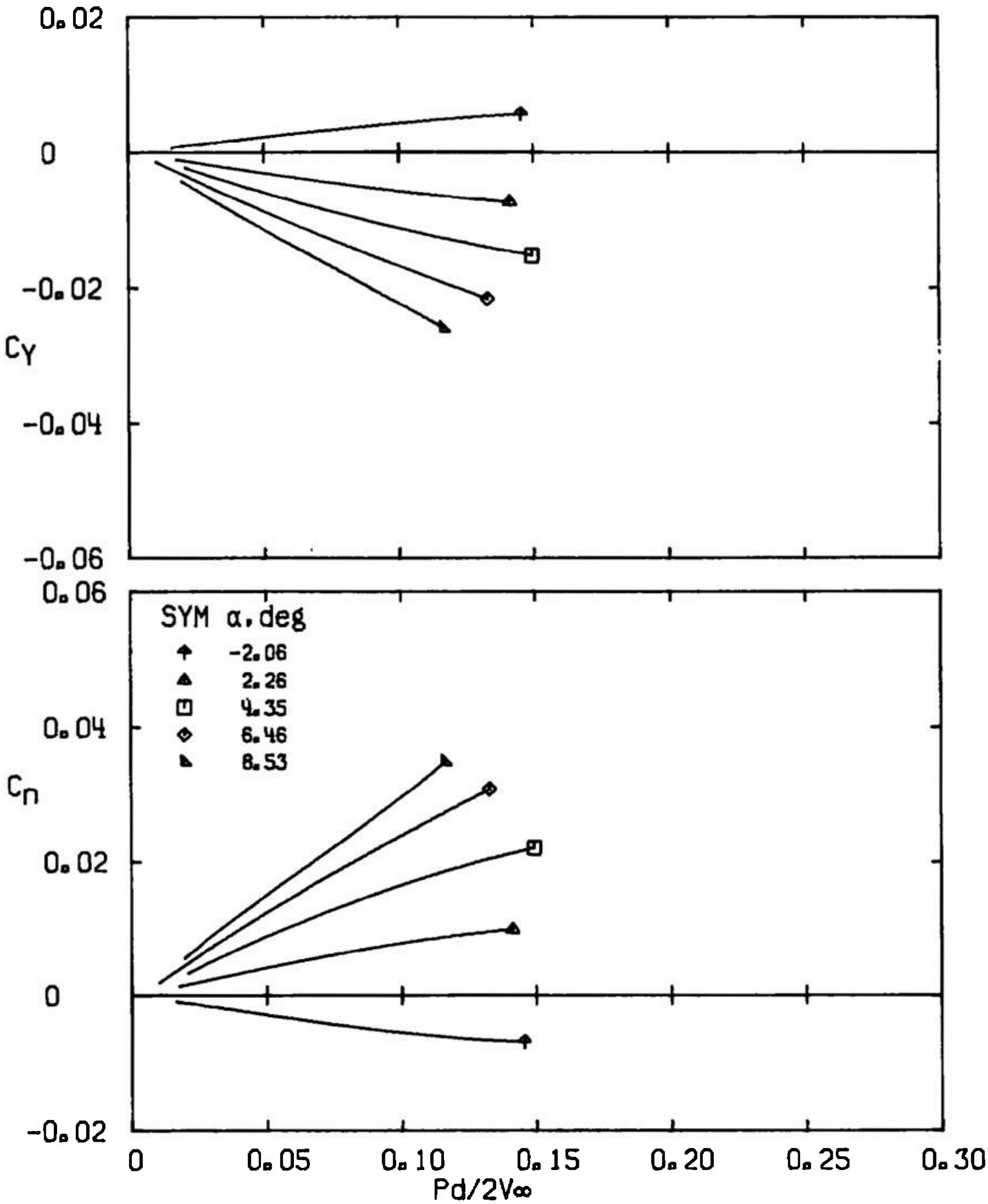

b. $M_\infty = 2.0$
Fig. 17 Continued

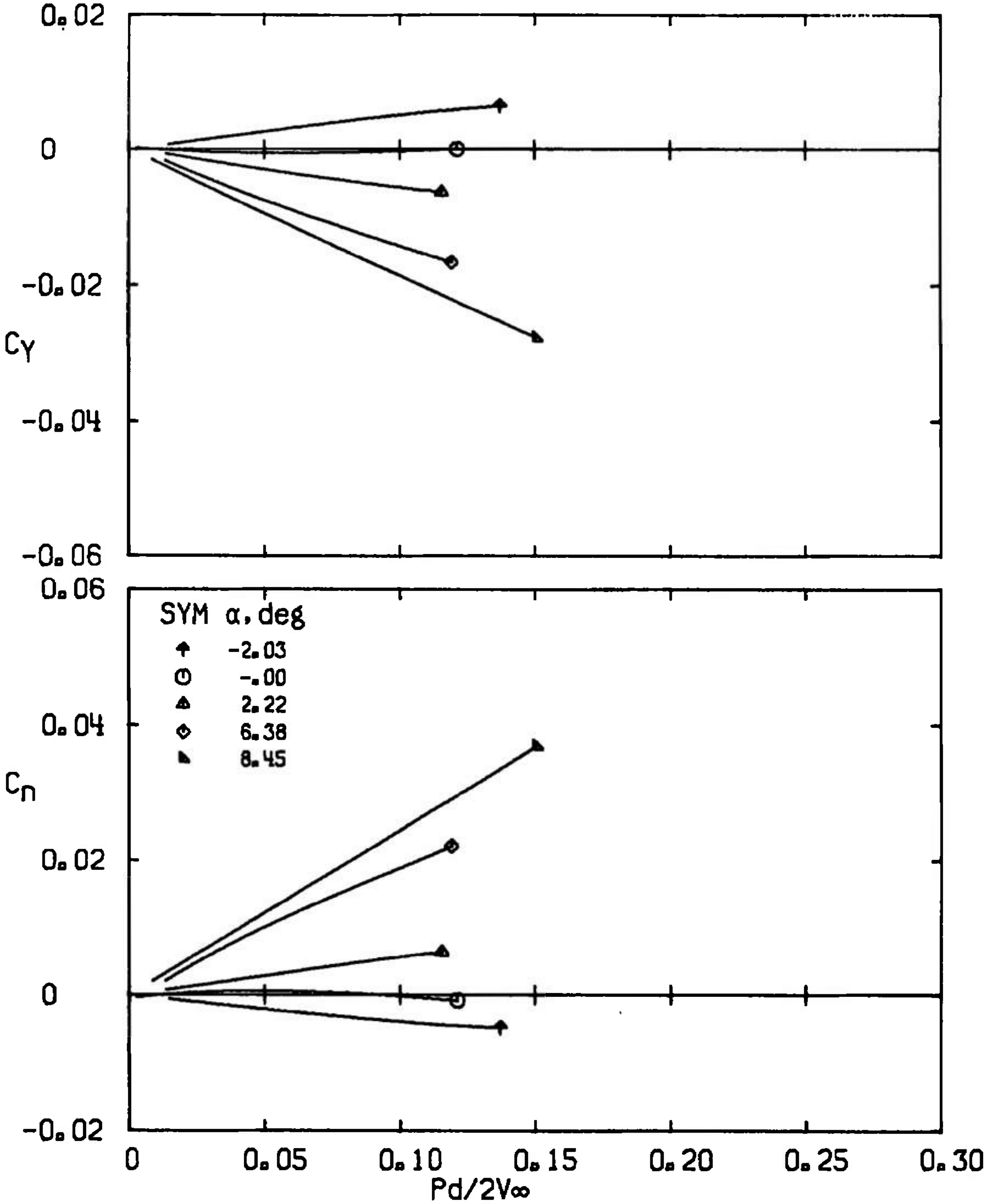

c. $M_\infty = 2.5$

Fig. 17 Concluded

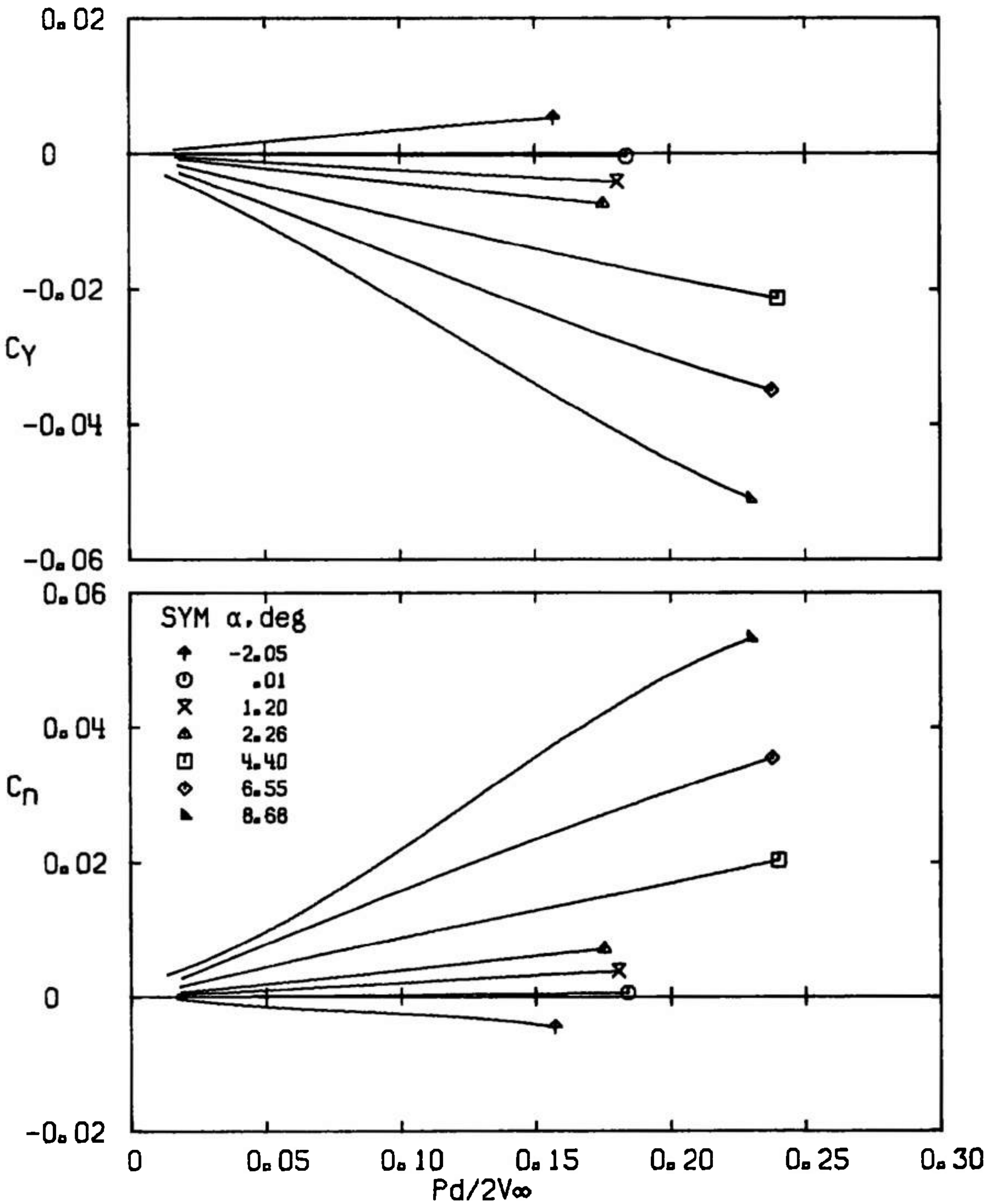

a. $M_\infty = 1.5$

Fig. 18 Variation of C_Y and C_n with $pd/2V_\infty$ for Configuration 4 without Vanes

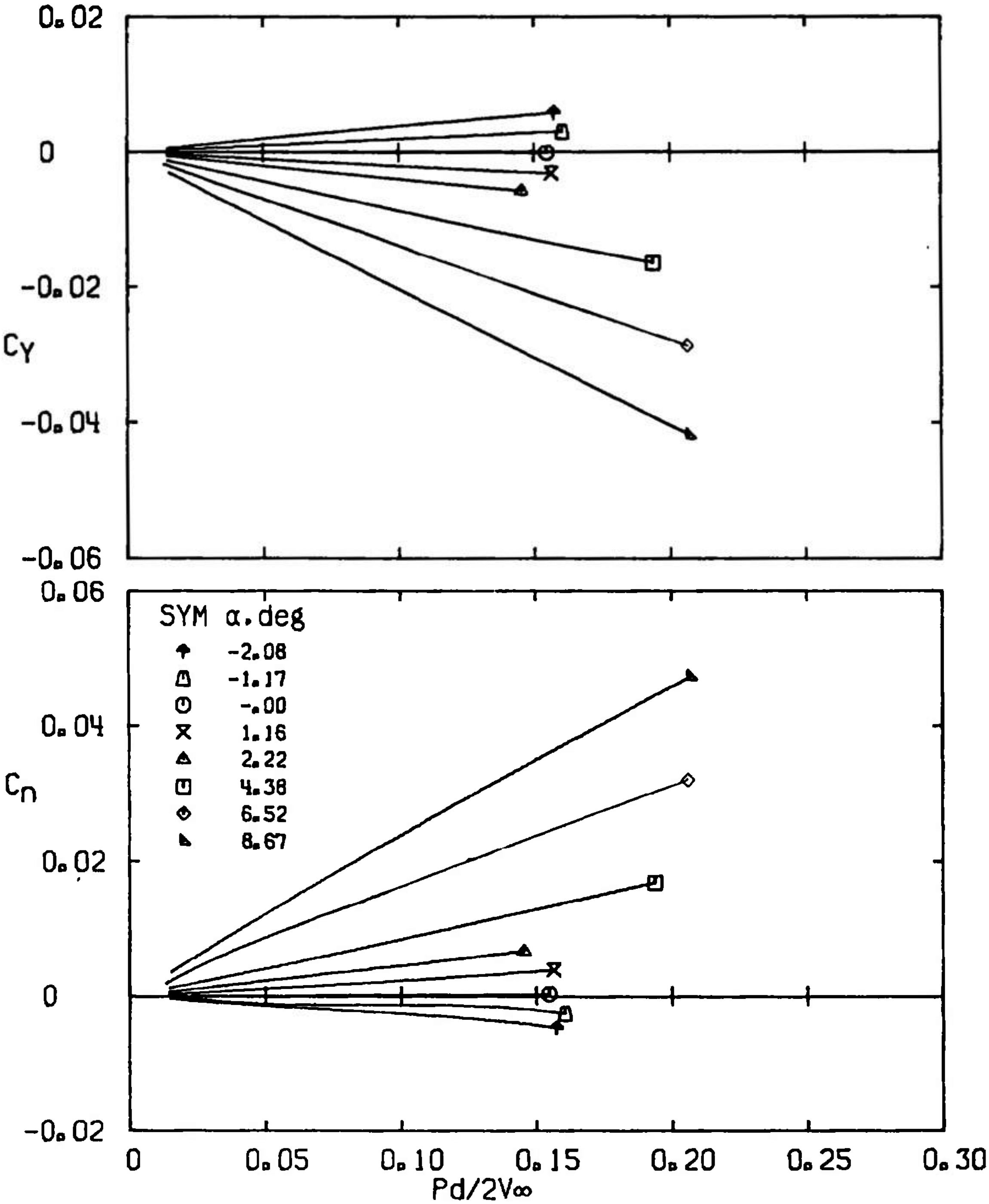

b. $M_\infty = 2.0$
Fig. 18 Continued

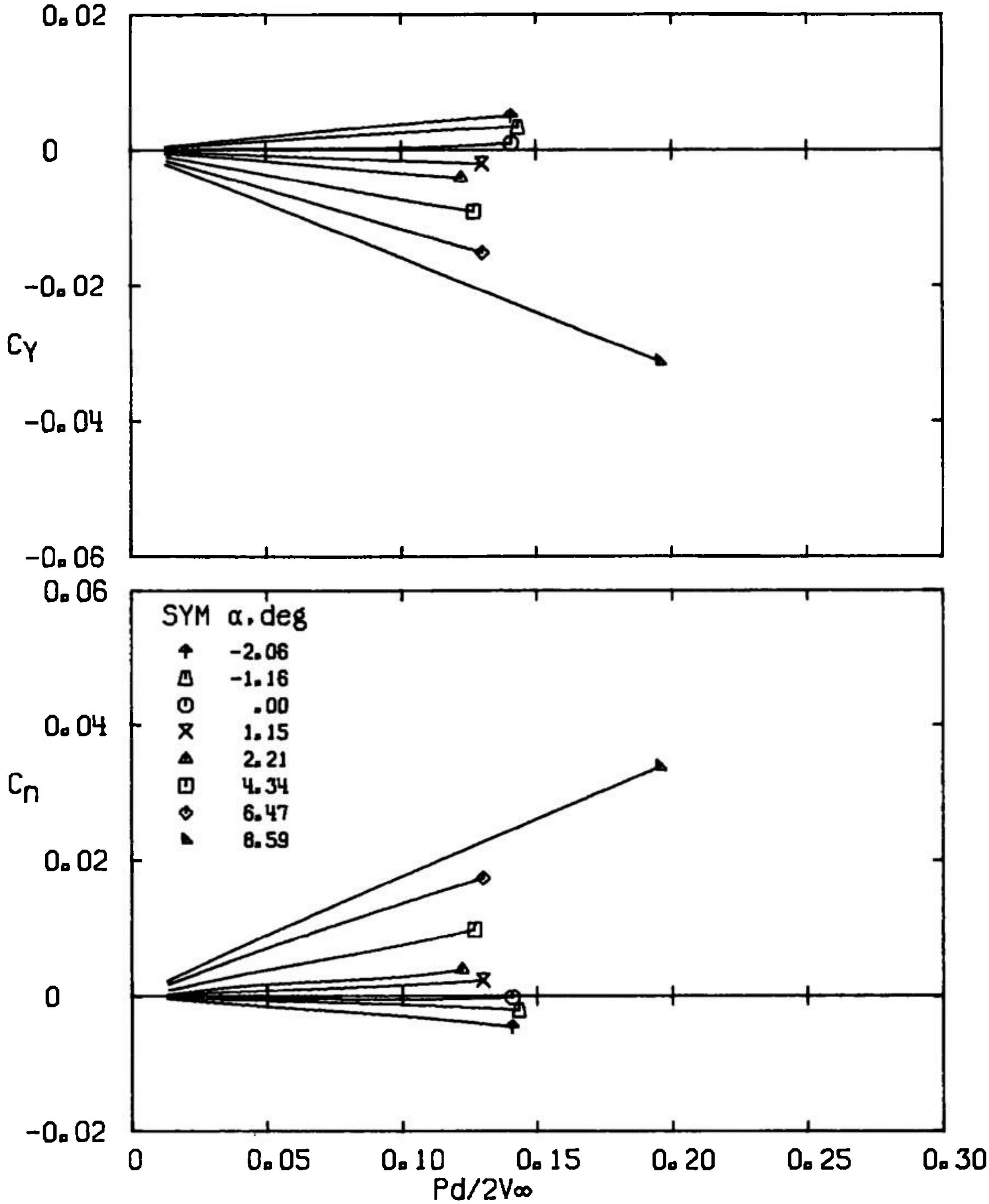

c. $M_\infty = 2.5$
Fig. 18 Concluded

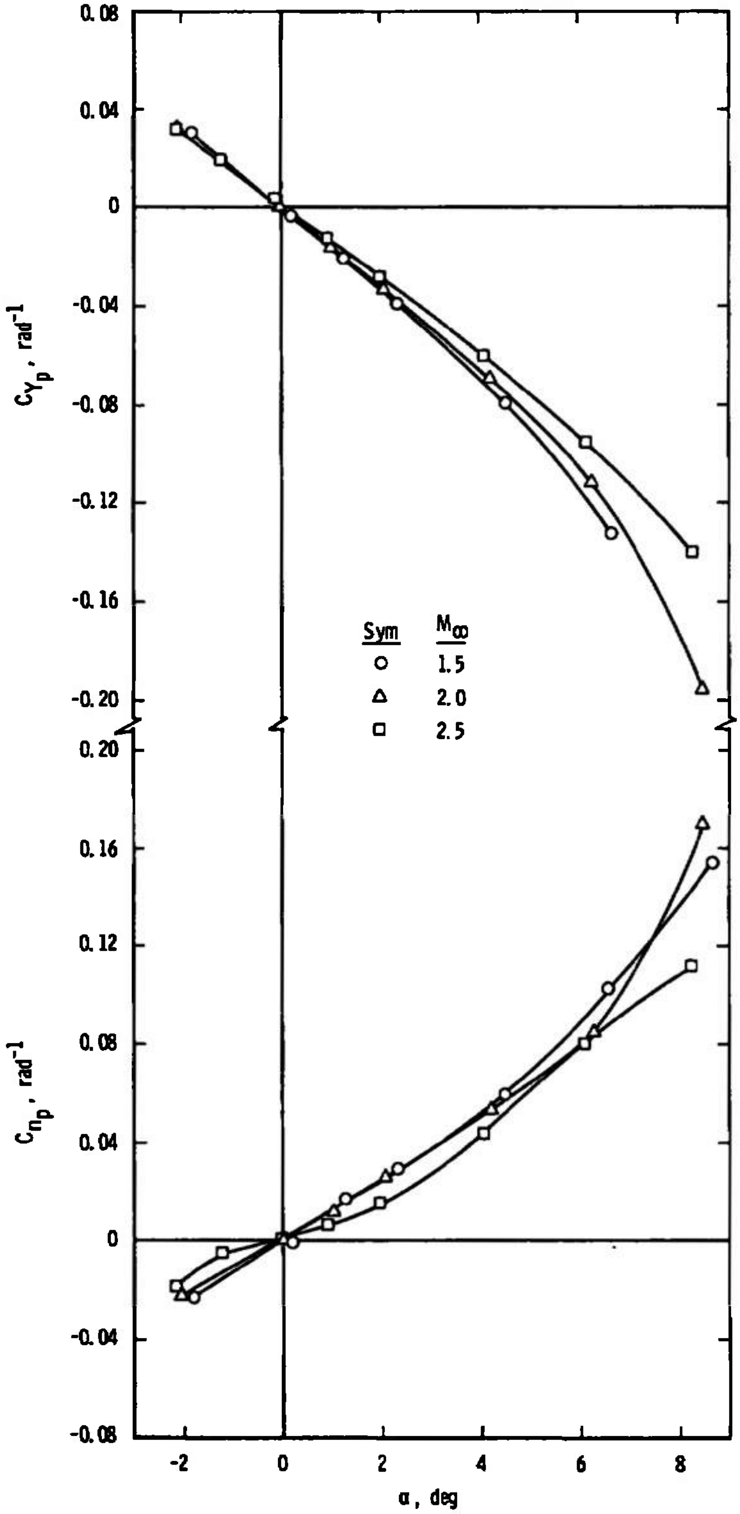

a. Without Vanes

Fig. 19 Variation of C_{Y_p} and C_{n_p} with Angle of Attack for Configuration 0

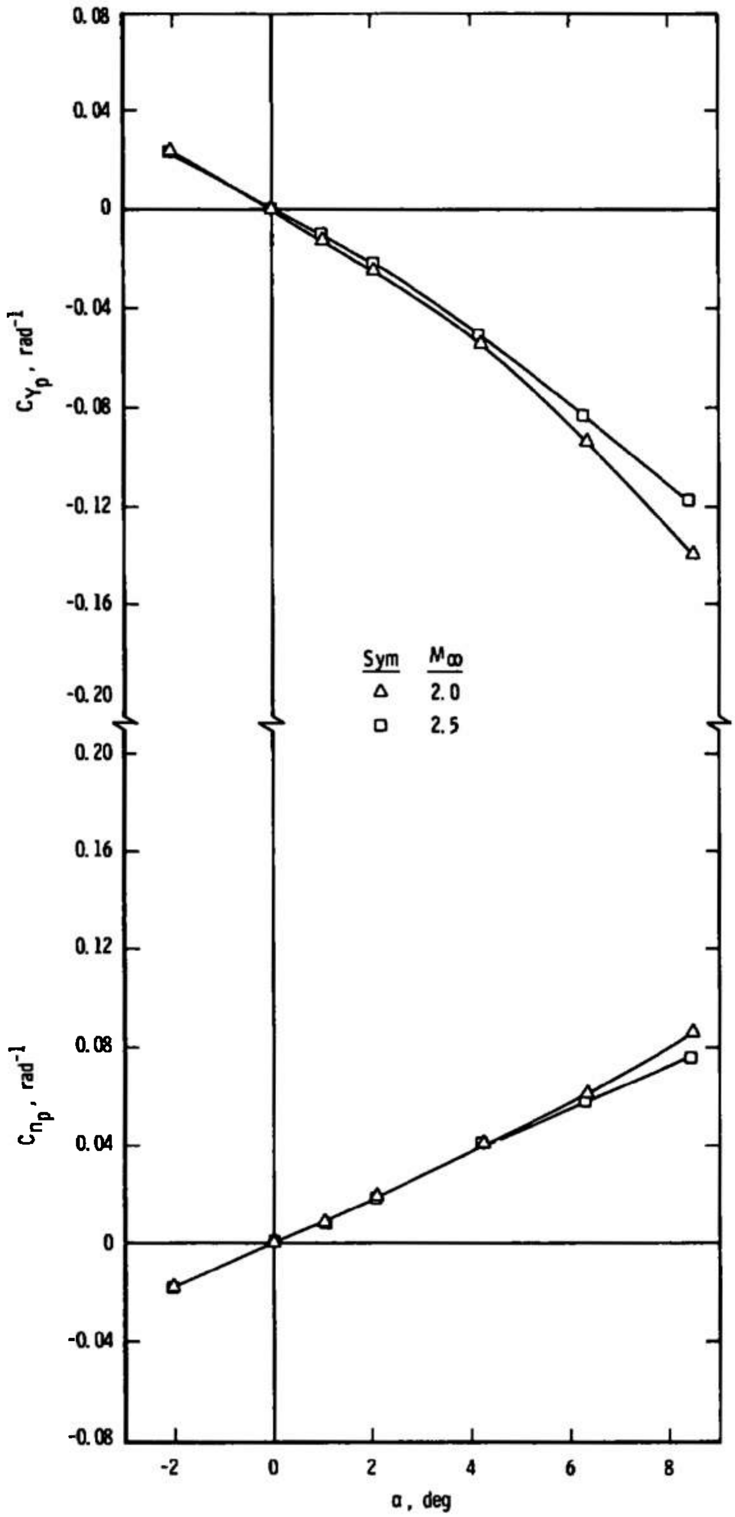

b. With Straight Vanes
Fig. 19 Continued

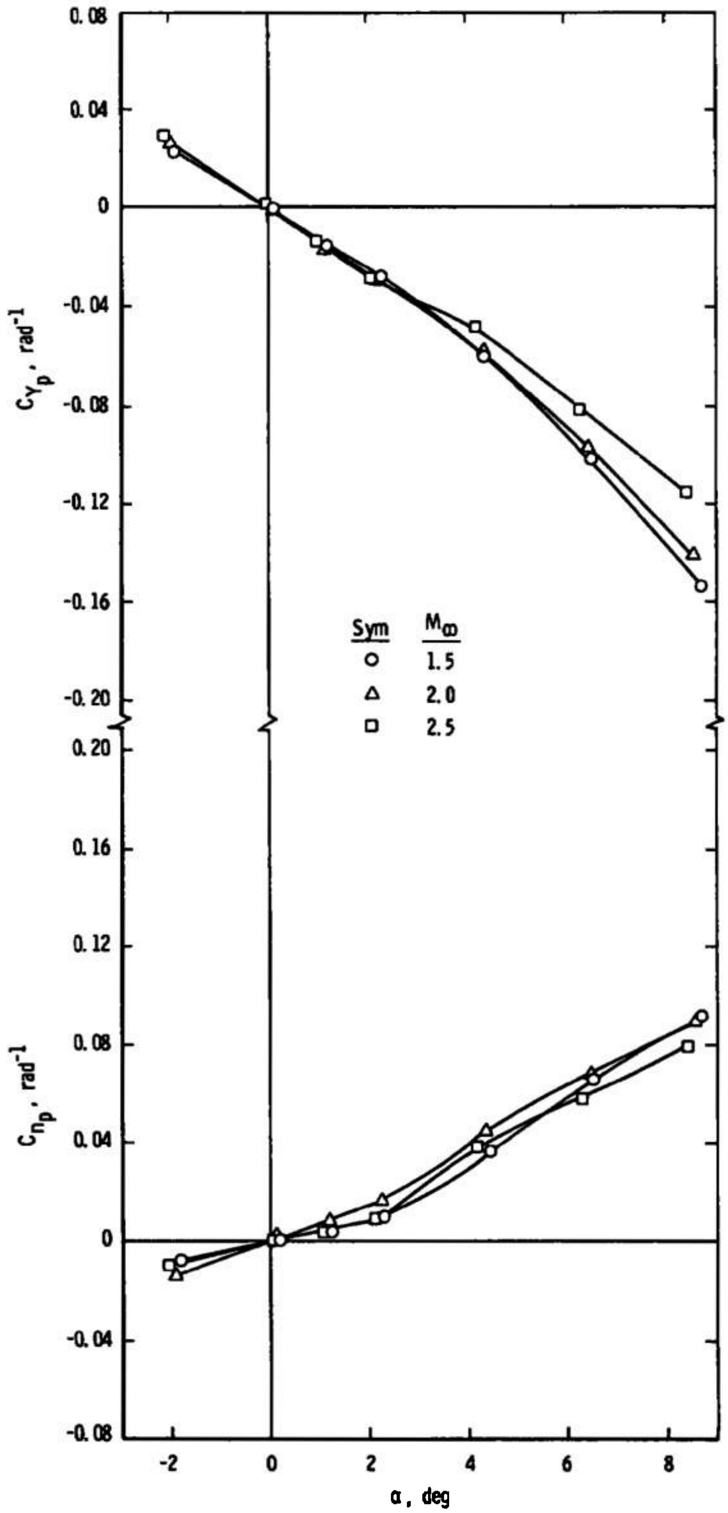

c. With Canted Vanes
Fig. 19 Concluded

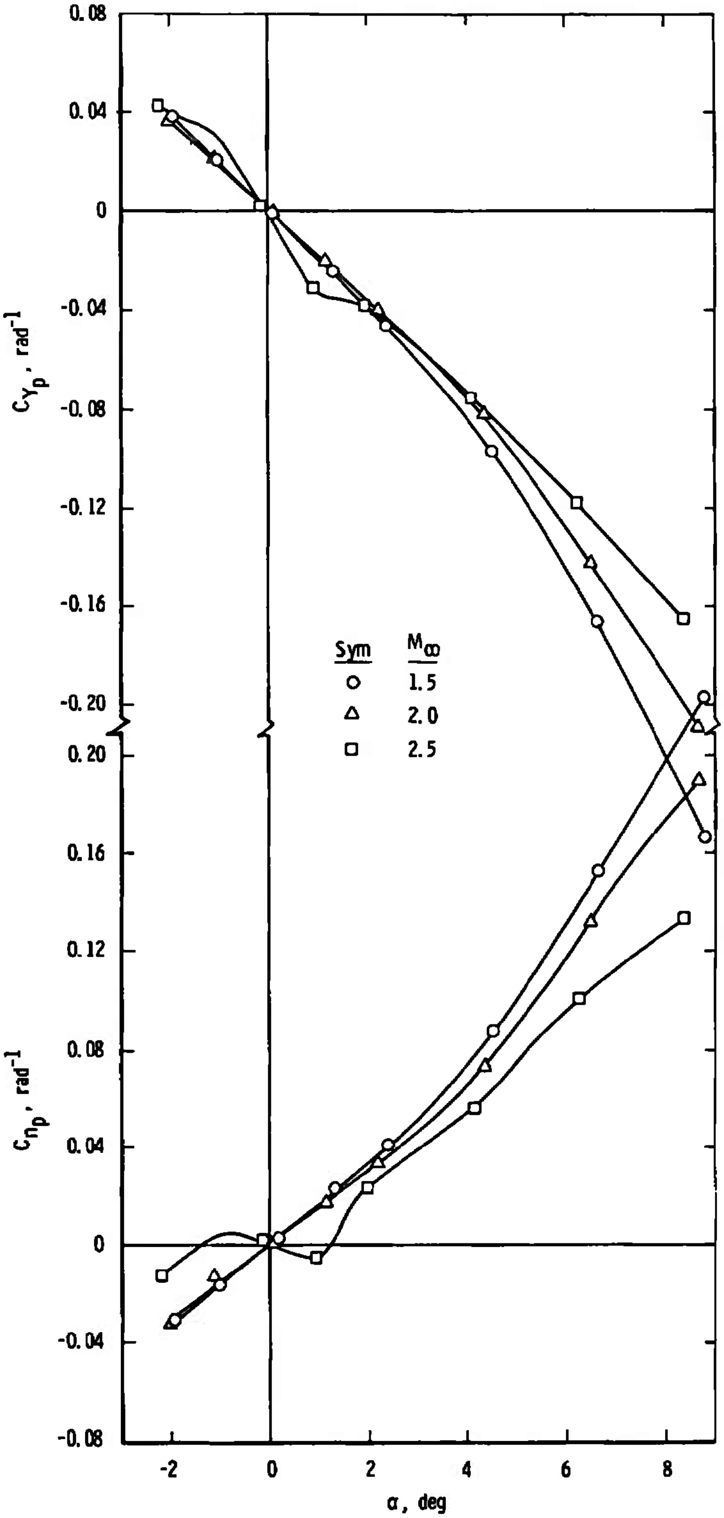

a. Without Vanes

Fig. 20 Variation of C_{Y_p} and C_{n_p} with Angle of Attack for Configuration 2

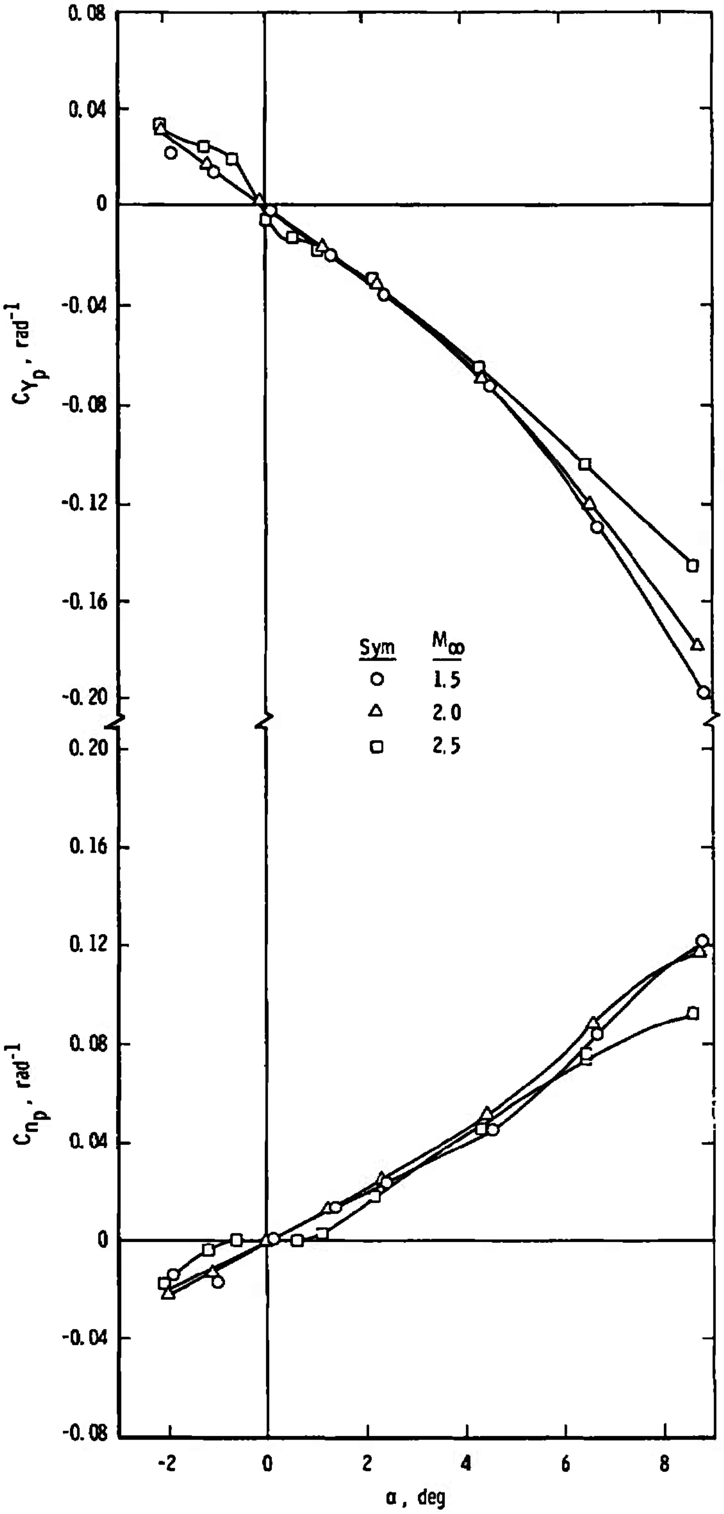

b. With Straight Vanes
Fig. 20 Continued

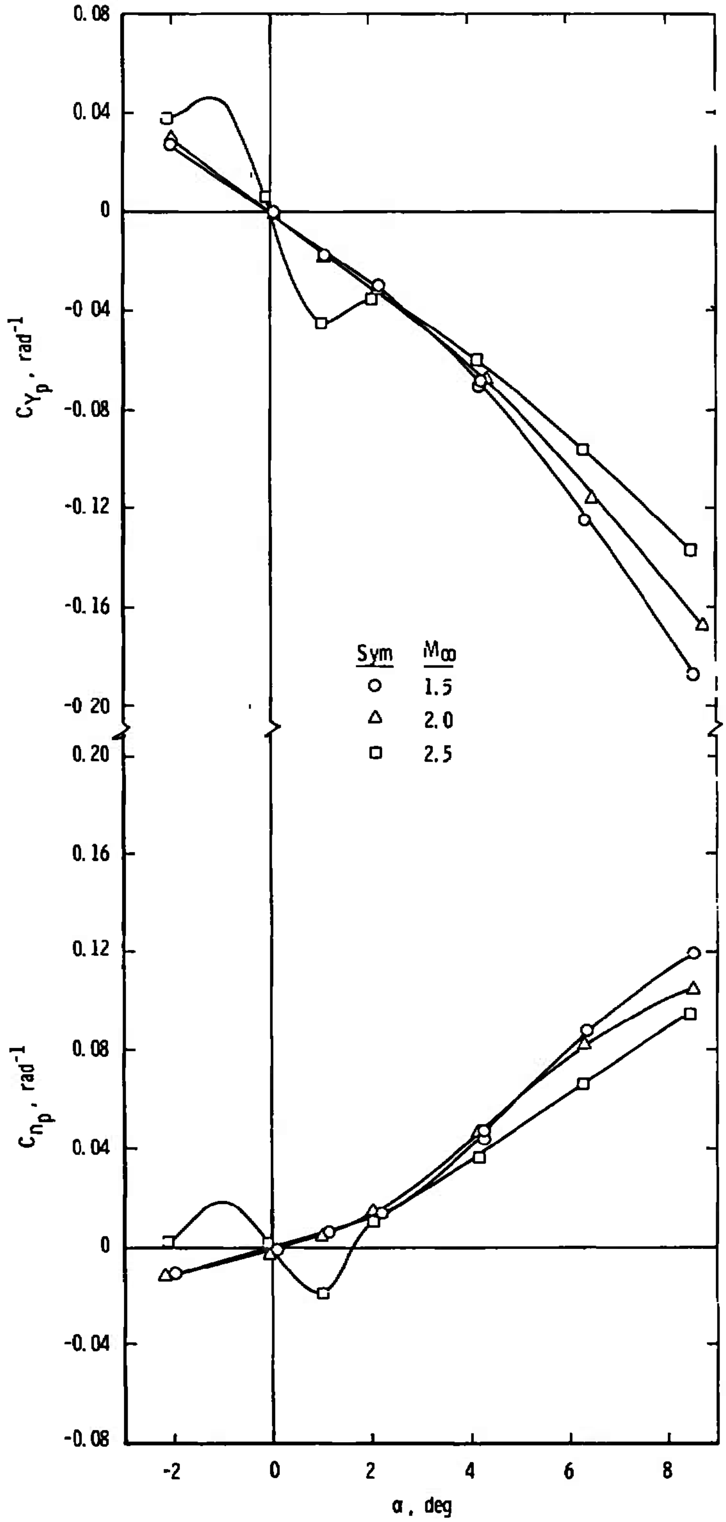

c. With Canted Vanes
Fig. 20 Concluded

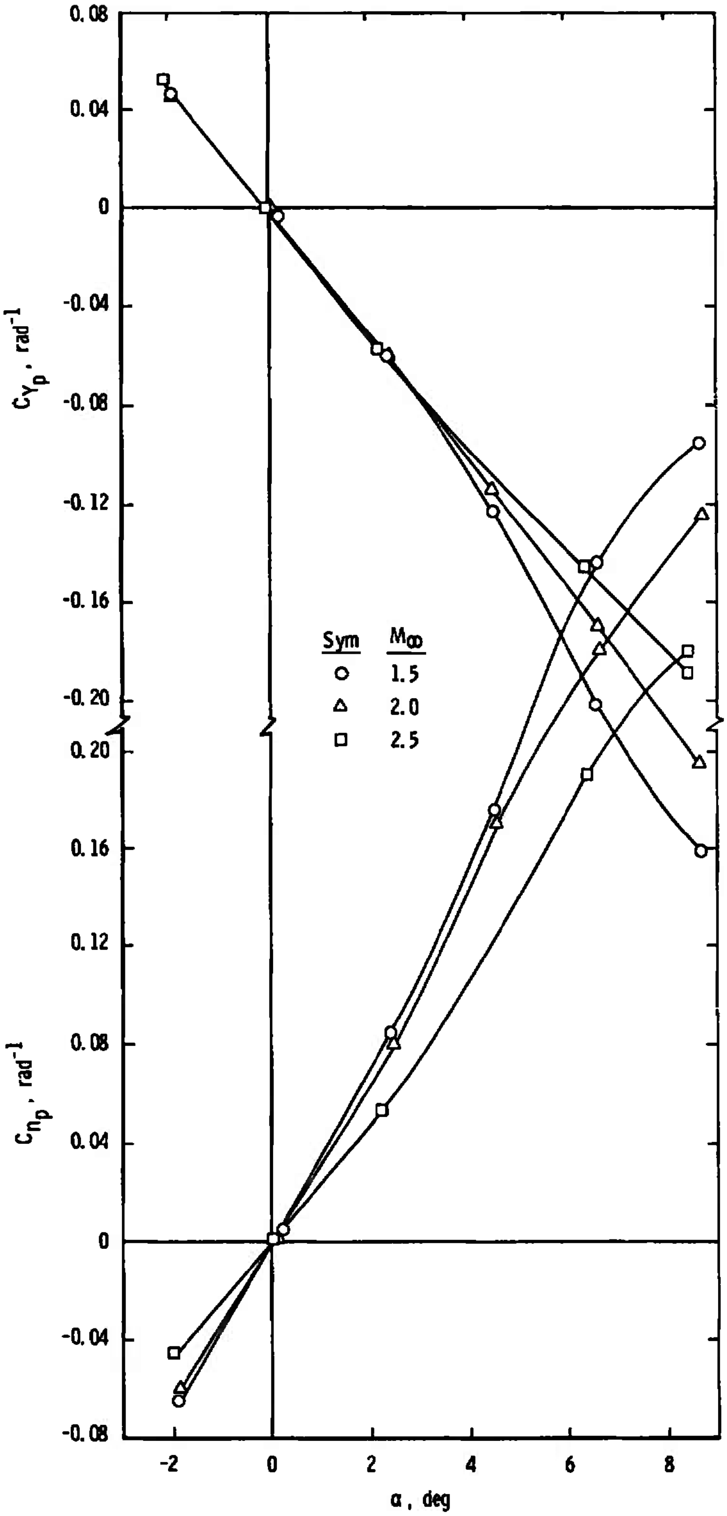

Fig. 21 Variation of C_{Y_p} and C_{n_p} with Angle of Attack for Configuration 3 without Vanes

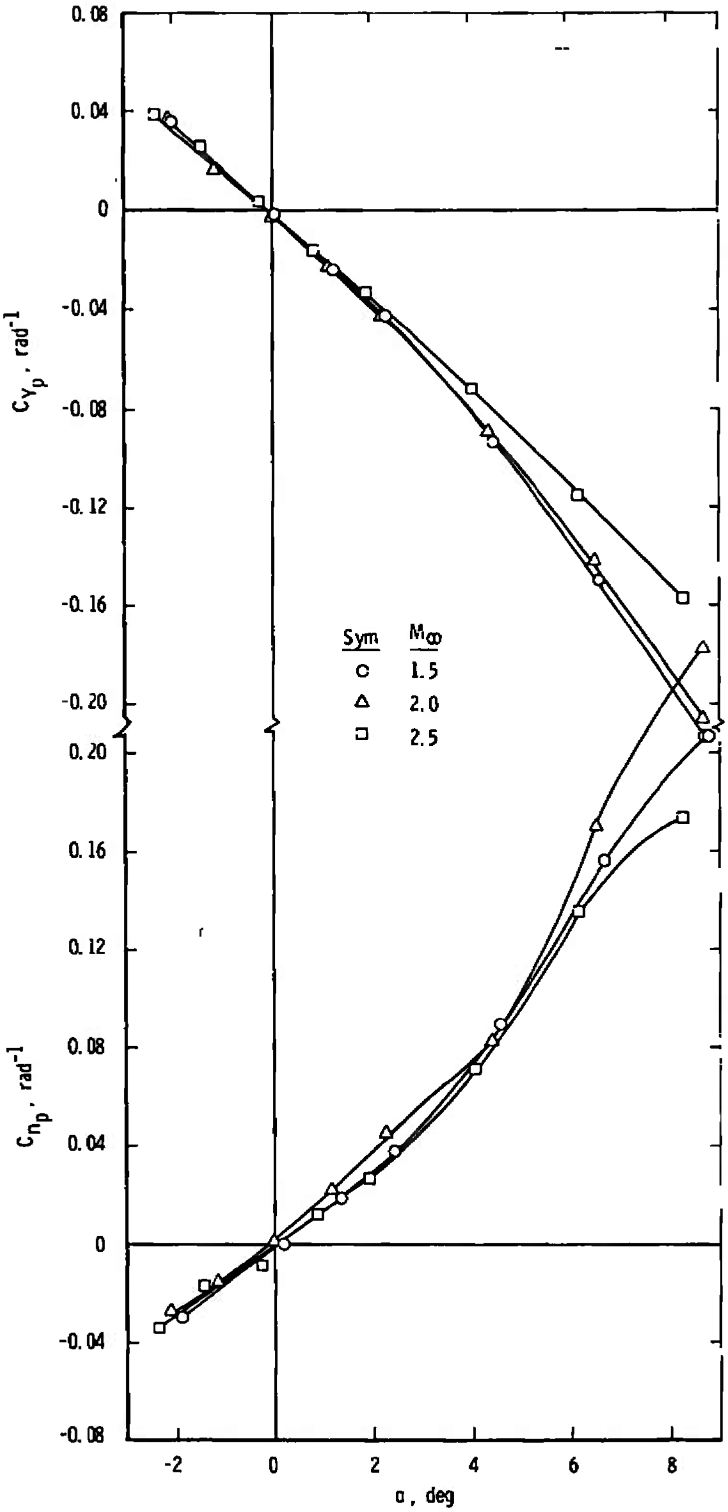

Fig. 22 Variation of C_{Y_p} and C_{n_p} with Angle of Attack for Configuration 4 without Vanes

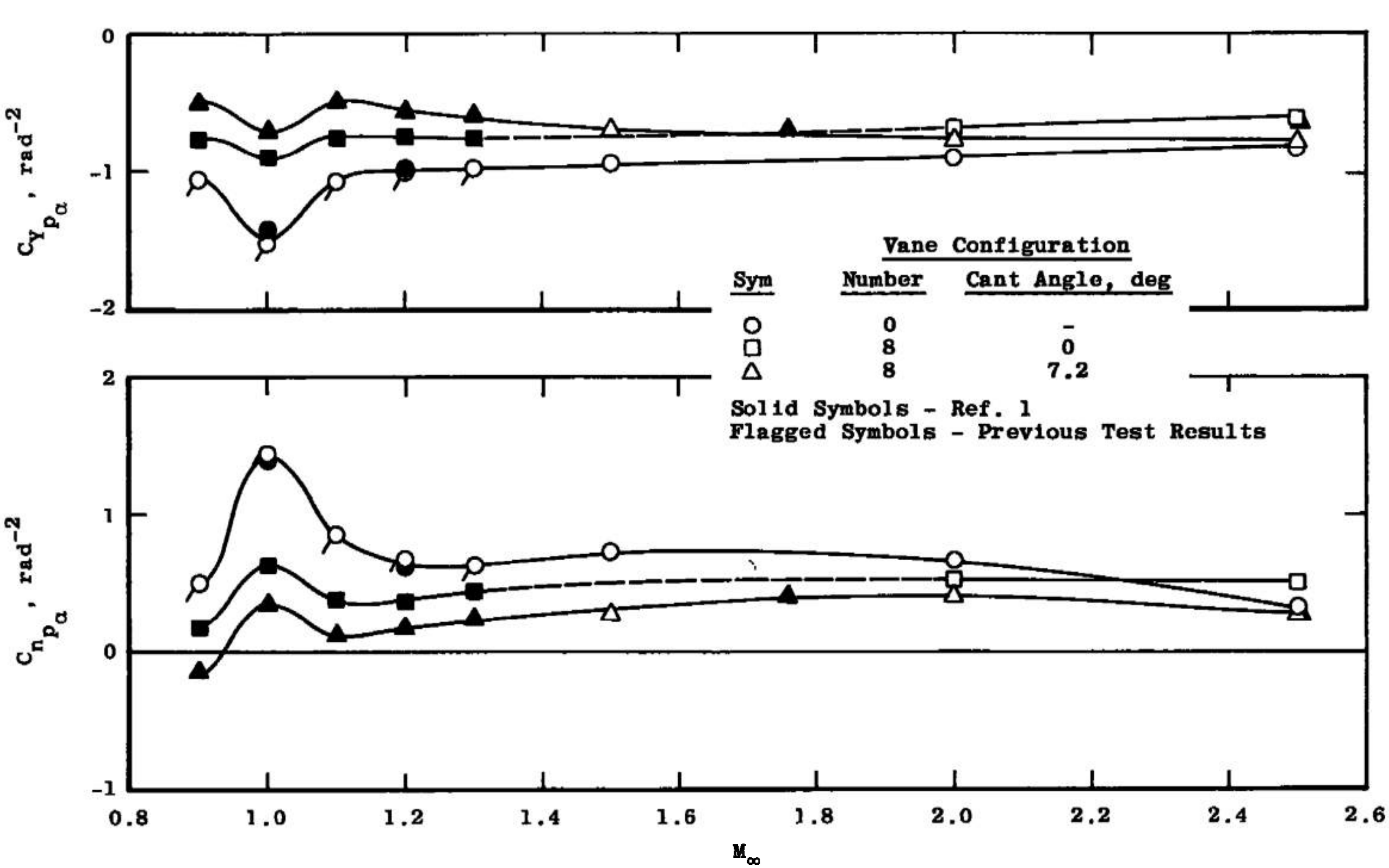

a. Configuration 0

Fig. 23 Variation of $C_{Y_{p_\alpha}}$ and $C_{n_{p_\alpha}}$ with Mach Number

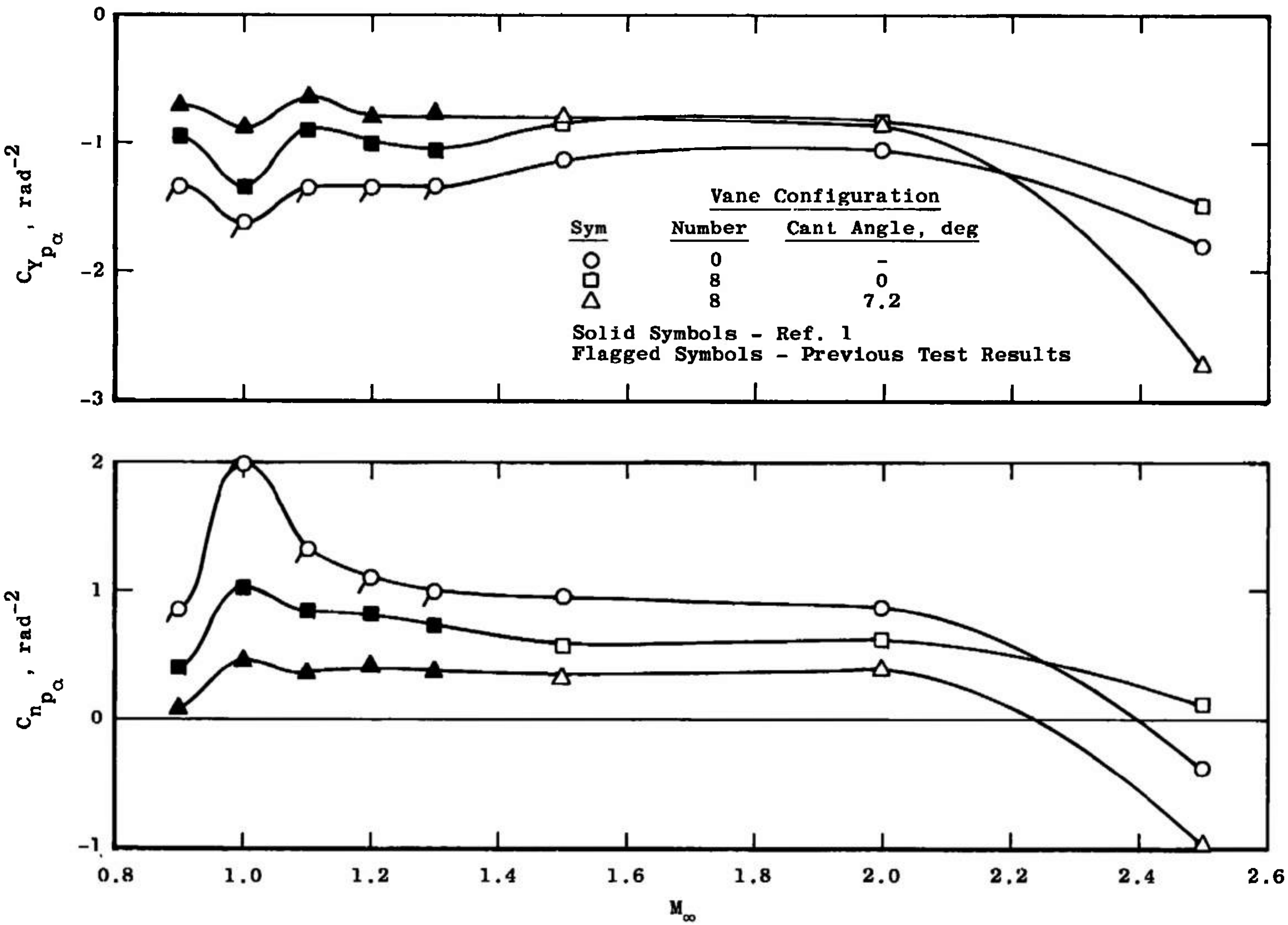

b. Configuration 2
Fig. 23 Continued

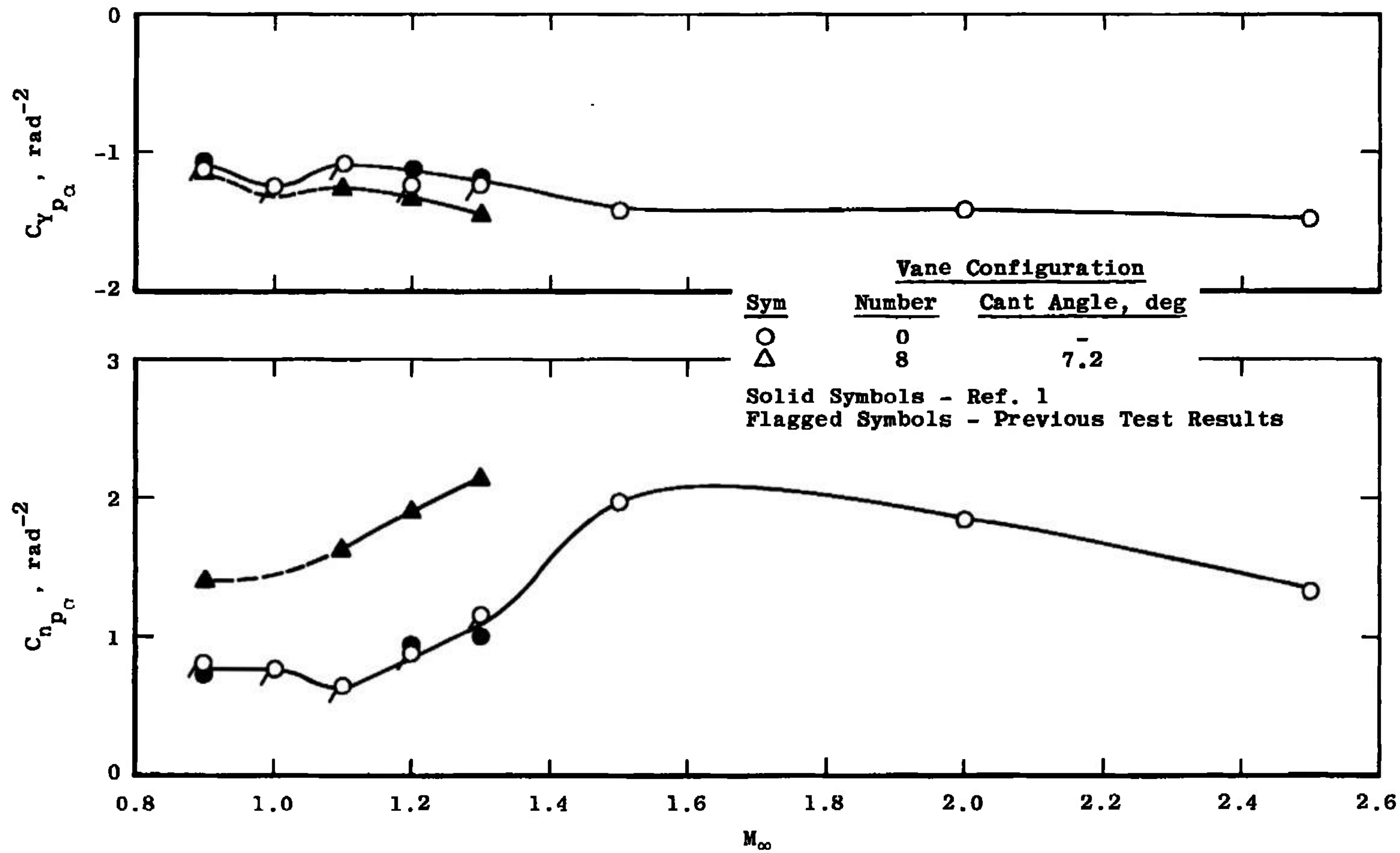

c. Configuration 3
Fig. 23 Continued

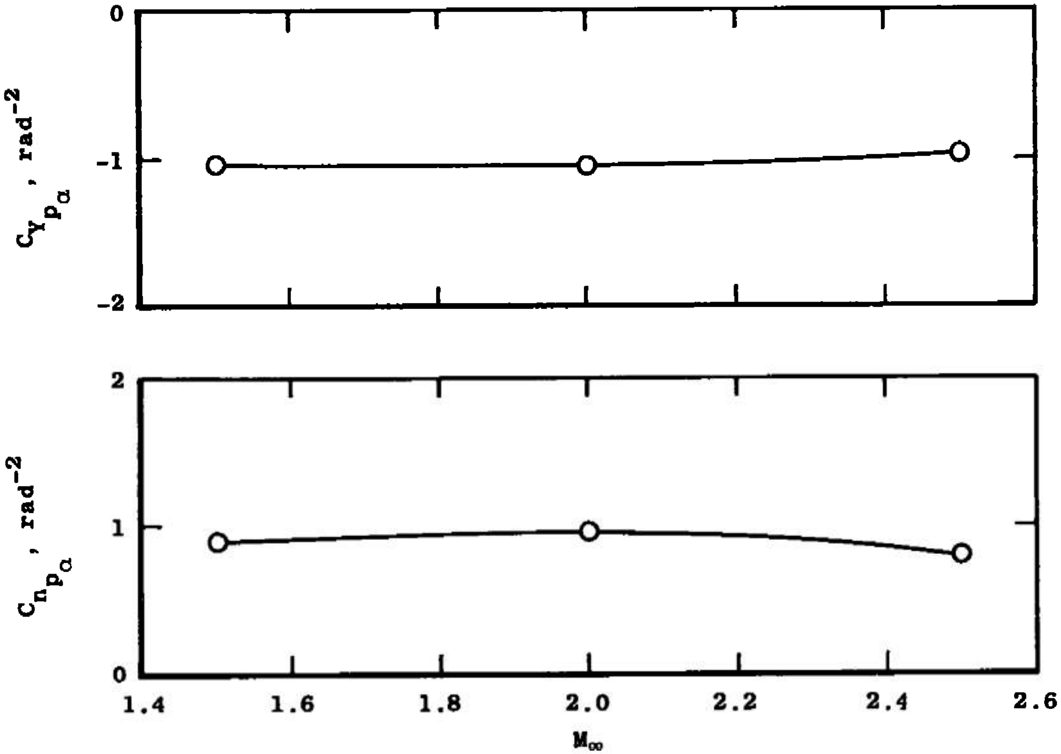

d. Configuration 4

Fig. 23 Concluded

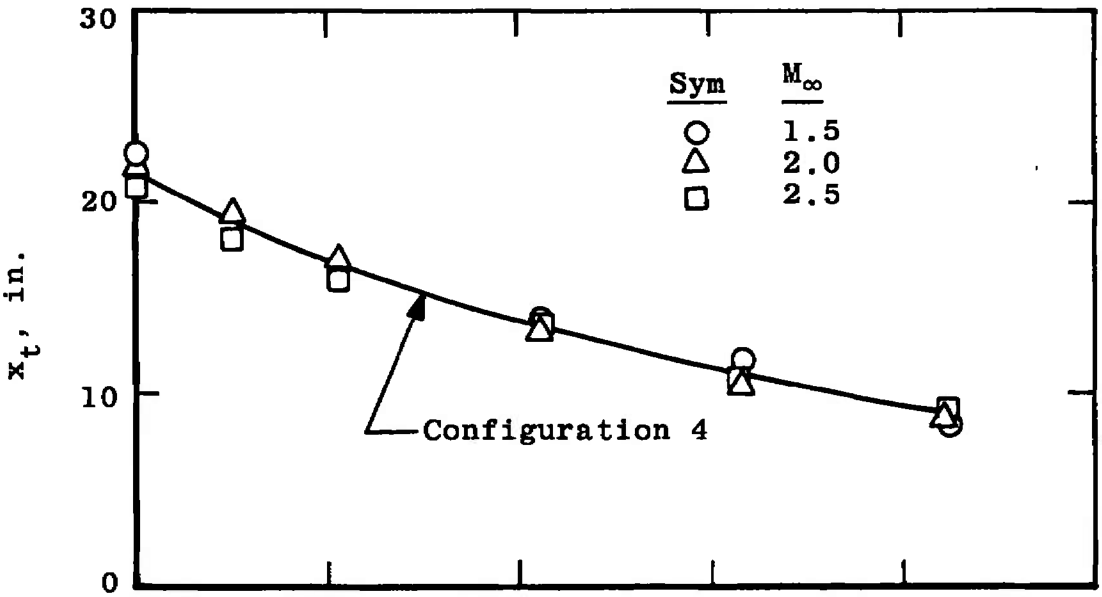

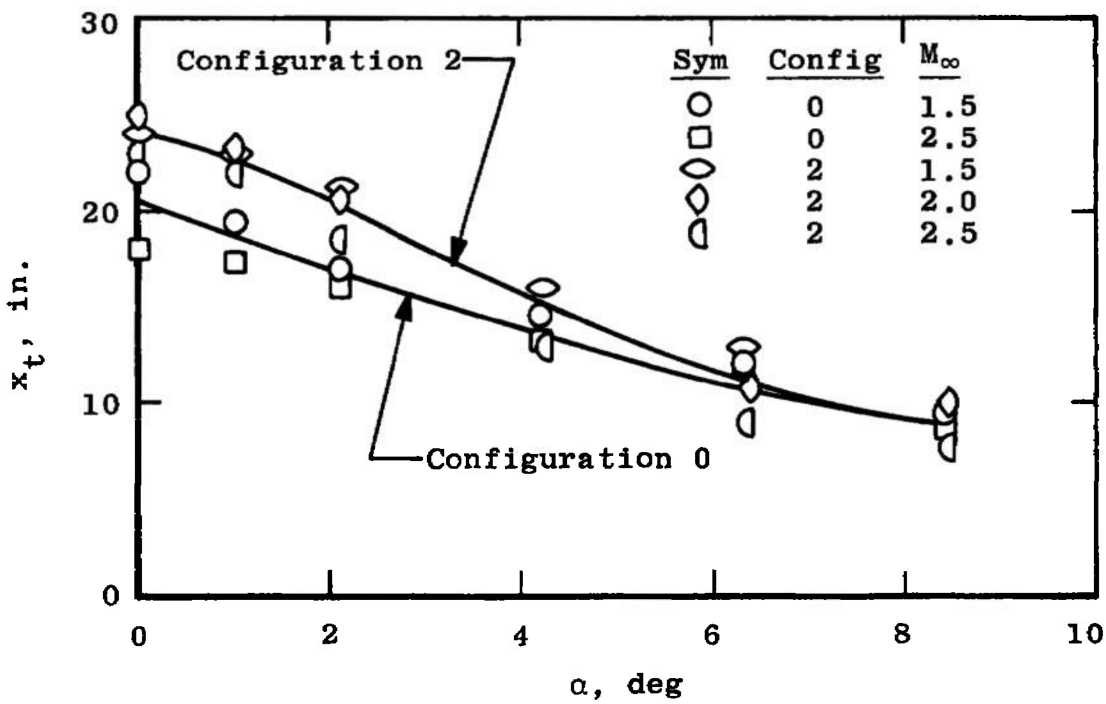

Fig. 24 Onset of Transition on the Leeward Surface of Configuration 0 at Supersonic Mach Numbers in Tunnel A

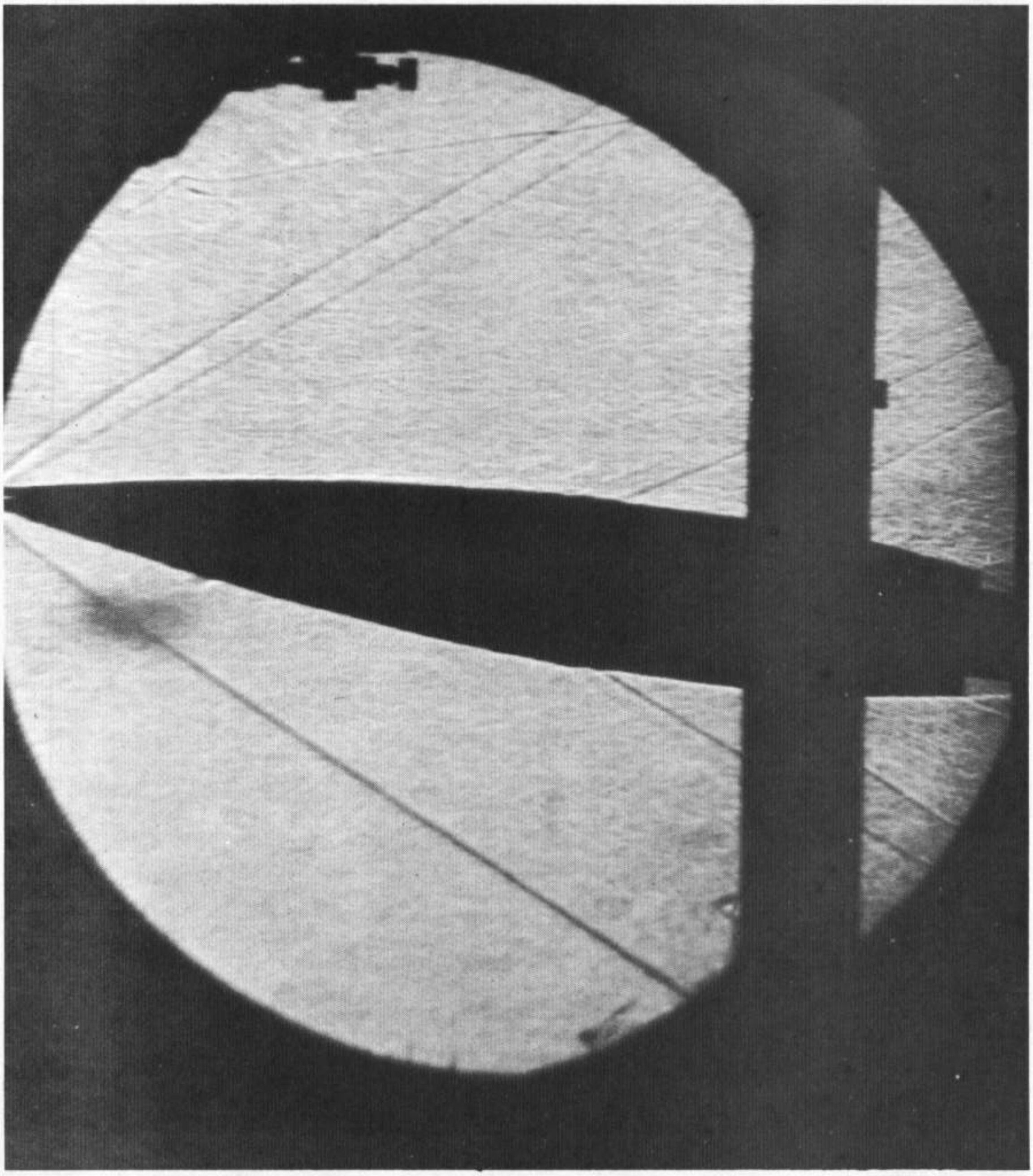

Fig. 25 Typical Shadowgraph of Configuration 2 at $M_\infty = 2.0$, $\alpha = 6.4$ deg (Tunnel A)

DOCUMENT CONTROL DATA - R & D

(Security classification of title, body of abstract and indexing annotation must be entered when the overall report is classified)

1 ORIGINATING ACTIVITY *(Corporate author)* Arnold Engineering Development Center Arnold Air Force Station, Tennessee 37389	2a. REPORT SECURITY CLASSIFICATION UNCLASSIFIED 2b. GROUP N/A

3 REPORT TITLE

EXPERIMENTAL CHARACTERISTICS OF BALLISTIC PROJECTILES WITH AND WITHOUT ANTI-MAGNUS VANES AT MACH NUMBERS 1.5 THROUGH 2.5

4 DESCRIPTIVE NOTES *(Type of report and inclusive dates)*
Final Report--May 24 through 25, 1973

5 AUTHOR(S) *(First name, middle initial, last name)*

Leroy M. Jenke, ARO, Inc.

6 REPORT DATE	7a. TOTAL NO OF PAGES	7b. NO. OF REFS
December 1973	79	4

8a. CONTRACT OR GRANT NO b. PROJECT NO 2547 c. Program Element 62602F d.	9a. ORIGINATOR'S REPORT NUMBER(S) AEDC-TR-73-162 AFATL-TR-73-188 9b. OTHER REPORT NO(S) *(Any other numbers that may be assigned this report)* ARO-VKF-TR-73-89

10 DISTRIBUTION STATEMENT

Approved for public release; distribution unlimited.

11 SUPPLEMENTARY NOTES Available in DDC.	12. SPONSORING MILITARY ACTIVITY Air Force Armament Laboratory (DLDL), Eglin AFB, FL 32542

13 ABSTRACT

An experimental investigation was conducted to determine static-stability and Magnus characteristics of four spin-stabilized ballistic shell configurations with and without small anti-Magnus vanes on the boattail. The models (slightly larger than full scale) were tested at Mach numbers 1.5, 2.0, and 2.5 over an angle-of-attack range from -2 to 8 deg. The Reynolds number, based on a model diameter of 5.2 in., was 1.7 x 10^6, and the spin parameter ($pd/2V_\infty$) ranged from 0 to 0.25 radians. Results are presented showing the effects of spin, Mach number, angle of attack, and anti-Magnus vanes. These results show that the vanes were effective in reducing both Magnus force and moment for two of the basic configurations and that the canted (7.2-deg) vanes were generally more effective than the straight vanes.

14. KEY WORDS	LINK A		LINK B		LINK C	
	ROLE	WT	ROLE	WT	ROLE	WT
ballistic trajectories						
spin-stabilized ammunition						
subsonic flow						
Magnus effects						
Reynolds number						
angle of attack						
static stability						

AFSC
Arnold AFB Tenn